ISTANBUL TECHNICAL UNIVERSITY ★ GRADUATE SCHOOL OF SCIENCE ENGINEERING AND TECHNOLOGY

EVALUATION OF THREE SEMI-EMPIRICAL SOIL MOISTURE ESTIMATION MODELS IN AGRICULTURE AREAS WITH RADARSAT-2 IMAGERY PROCESSING IN THE SOUTHEAST OF TURKEY

M.Sc. THESIS

Elnaz BEHNAM MAKOEI
(504091391)

Department of Electronic and Communication Engineering

Telecommunications Engineering Program

Thesis Advisor: Prof. Dr. Sedef KENT

MAY 2015

İSTANBUL TEKNİK ÜNİVERSİTESİ ★ FEN BİLİMLERİ ENSTİTÜSÜ

GÜNEYDOĞU TÜRKİYE TARIMSAL ALANLARINDA, RADARSAT-2 UYDU GÖRÜNTÜLERİNİN İŞLENMESİ İLE YARI-DENEYSEL, ÜÇ TOPRAK NEMİ TAHMİN MODELİNİN GELİŞTİRİLMESİ

YÜKSEK LİSANS TEZİ

Elnaz BEHNAM MAKOEI
(504091391)

Elektronik ve Haberlesme Mühendisliği Anabilim Dalı

Telekomünikasyon Mühendisliği Programı

Tez Danışmanı: Prof. Dr. Sedef KENT

MAYIS 2015

Elnaz Behnam Makoei, a **M.Sc** student of ITU **Institute of Electronic and Communication Engineering** student ID **504091391**, successfully defended the **thesis** entitled "**EVALUATION OF THREE SEMI-EMPIRICAL SOIL MOISTURE ESTIMATION MODELS IN AGRICULTURE AREAS WITH RADARSAT-2 IMAGERY PROCESSING IN THE SOUTHEAST OF TURKEY**", which she prepared after fulfilling the requirements specified in the associated legislations, before the jury whose signatures are below.

Thesis Advisor :	**Prof. Dr. Sedef Kent** İstanbul Technical University	....
Jury Members :	**Prof. Dr. Sedef Kent** İstanbul Technical University	....
	Doç.Dr. Mesut Kartal İstanbul Technical University	....
	Yrd.Doç.Dr. Serdar Kargın Beykent University	....

Date of Submission : 04 May 2015
Date of Defense : 28 May 2015

To my son Eran,

FOREWORD

I would like to thank all the people who contributed in some way to the work described in this thesis. First and foremost, I thank my academic advisor, Professor Sedef Kent, for accepting me into her group. During my study, she has contributed by giving me the intellectual freedom to perform my work, engaging me with new ideas, and demanding a high quality of work in all my endeavors. Additionally,I would like to thank Professor Ümit Aygölü who encouraged me to reenter the world of education, as well and Dr. Ibrahim Papila for his great interest in my work and his invaluable support.

I also want to thank the UHUZAM department of Istanbul Technical University for the RADARSAT-2 and ground measurements data support, the PCI Geomatica Company for their free software support of used for processing the RADARSAT-2 data, Dr. Uğur AVDAN from the Institute of Earth and Space Sciences in Anadolu University, for allowing me the use ofhis laboratory facilities and research support and alsoProfessor. Y.S. RaoCentre of Studies in Resources Engineering Indian Institute of Technology, Bombay, for his guidance.

In addition, I have been very privileged to get to know and to collaborate withmany other great people who have become good friends over the last several years. I have learned alot from them about life, research, ways to overcome new challenges and how to developtechniques to solve them.

Finally, I would like to express my gratitude to the friends and family who have supported me during the research process.First and foremost I would like to thank mom anddad, Manizhe and Ghanbar, for their constant love and support. Furthemore, I would like to mention that the completion of this thesis would not have been possible without thesupport and encouragement of my close friend and my great leader in life, Elchin, whose discipline, patience and enthusiasm. I admire, and express my sincere gratitude for having inspired me to pursue this path.

April 2015 Elnaz BEHNAM MAKOEI

TABLE OF CONTENTS

Page

ABBREVIATIONS

2D	**:**Two- Dimensional
3D	**:**Three- Dimensional
A/D	**:**Analog –to –Digital
CSA	**:**Canadian Space Agency
DC	**:**Direct Current
DEM	**:**Digital Elevation Model
DN	**:**Digital Number
DOP	**:**Degree Of Polarization
DOY	**:**Day Of Year
EM	**:**ElectroMagnetic
ENL	**:**Equivalent Number of Looks
ESA	**:**European Space Agency
FDR	**:**Frequency Domain Reflectometry
FFT	**:**Fast Fourier Transform
FM	**:**Frequency Modulated
GHZ	**:**Gigahertz
GPR	**:**Ground Penetrating Radar
GCP	**:**Ground control Point
HH	**:**Horizontal Horizontal
HV	**:**Horizontal Vertical
IEM	**:**Integral Equation Model
IFOV	**:**Instantaneous Field Of View
LIA	**:**Local Incidence Angle
M	**:**Mean
MC	**:** Moisture Content
MDA	**:**MacDonald Dettwiler Associates
MHz	**:**Megahertz
MN	**:**Normalized Mean
MPSSI	**:**Mean Preservation Speckle Suppression Index
NAN	**:** Not A Number
PALSAR	**:**Phased Array type L-band Synthetic Aparture Radar
PRF	**:**Pulse Repetition Frequency
QP	**:**Quad polarisation
RAR	**:**Real Aperture Radar
RCS	**:**Radar Cross Section

RMSE	**:**Remoot Mean Squared Error
RS	**:**Remote Sensing
RS-2	**:**RADARSAT-2
SAR	**:**Synthetic Aperture Radar
SDP	**:**Selective Dual Polarisation
SLC	**:**Single LookComplex
SP	**:**Single Polarisation
SSL	**:**Speckle Suppression Index
SSMPI	**:**Speckle Suppression and Mean Preservation Index
SSP	**:**Selective Single Polarisation
Std	**:**Standard Deviation
TARBİL	**:**Tarımsal İzleme ve Bilgi Sistemi
TDR	**:**Time Domain Reflectometry
UTM	**:**Universal Transverse Mercator
UHUZAM	**:**Uydu Haberleşmesi ve Uzaktan Algılama Merkezi
VV	**:**Vertical Vertical

LIST OF TABLES

Page

LIST OF FIGURES

EVALUATION OF THREE SEMI-EMPIRICAL SOIL MOISTURE ESTIMATION MODELS IN AGRICULTURE AREAS WITH RADARSAT-2 IMAGERY PROCESSING IN THE SOUTHEAST OF TURKEY

SUMMARY

Soil moisture or soil water content is an important factor and parameter for agricultural, hydrologicaland meteorological applications. Usually the soil moisture definition is, divided into two branches: deep or root zonesoil moisture, and surface soil moisture.Surface soil moisture is refers to the water that is in the upper 10 cm of soil and only constitutes 0.0012% of all water available on Earth(Verhoest et al., 2008). Whereas root zone soil moisture is the water that is available to plants, which is generally considered to be in the upper 200 cm of soil.

The water stored in the soil has different roles in the global water cycle. For instance, the growth of plants, irrigation scheduling management, good product, crisis management during drought, etc. Or, it controls the partitioning of rainfall into runoff and infiltration. Runoff commonly means both exporting fresh water to other areas and degradation of topsoil through leaching and erosion(surface moisture),infiltration mean filling underground aquifers (deep soil moisture) (Verhoest et al., 2008). It has been widely observed that soil moisture is also a key variable in flood forecasting.However, the measurement of soil moisture is very important in other branches of science. Methods for measuring the mass of soil water have been in use since the 15th Century. Today, the most common method is with regard to the mass, volume or saturation of the soil. There are various methods available to measure the soil moisture content both directly and indirectly (Stachder 1996, Prietzsch 1998, Marshall 1999). In principle, direct and indirect methods of measurement can be distinguished from one another. Direct methods include all measured processes in which the soil water is removed via evaporation, extraction, or chemical reactions and gravimetric method such as the FDR or TDR methods.

On the other hand, research in to the remote sensing of soil moisture began in the mid 1970's thanks to a surge in the development of satellite technology. Soil moisture measurement and estimation from remotely sensed data has come a long way due to its unique capability of monitoring large areas with long term repetitive coverage. Remote sensing is data acquisition with out direct contact with the object of interest by using of particular wavelength of electromagnetic spectrum. The omitted or reflected signals in remote sensing methods far from the Earth's surface contain information about soil properties and surface details in both optical and microwave remote sensing and have been put to use for soil moisture study.

Studies on backscattering coefficiencyhave beenpublished regarding many different models for surface soil moisture estimation; (i) the empirical model (EM) of Oh et al., 1994, (ii) the theoretical integral equation model (IEM) of Fung et al., 1992,X-Bragg model (2008), and (iii) the semi-empirical models of Oh et al., 1992, Oh et al., 2004 and the model of Dubois et al., 1995.

In this study by using performance of the Oh et al., 1992, Oh, 2004 and Dubois et al., 1995a, surface soil moisture estimation models was evaluated with two RADARSAT-2 scenes (FQ1, FQ19) on agricultural area over the Harran ,Sanliurfa of east south of Turkey.

The results was researched in soil moisture models that was used in thesis,analyzed by Lee, Enh_Lee, Forst and Kuan filters to reduce speckle noise and improve the models performance and the accuracy of RADARSAT-2 soil moisture maps.
In addetion, the optimal filter sizeby study about of statistical calculated indices for different kernel size was estimated . Highest agreement for optimal filter kind is Kuan,15×15, 5×5 kernel size for OH92, OH04 for 07.September.2012 RADARSAT-2 's data and 5×5,5×5,15×15 kernel size for OH92,OH04,DU95 models for 08.September.2012 ,RADARSAT-2 's data .
By using Pauli RGB image was estimated surface coverage. The surface coverage information was used to find estimated soil moisture values in study area. Finally, the local and estimated values werecompared.
This research supports the idea of incidence angle effect on the performance of models (Baghdadi et al. 2008 and Mo et al. 1984) and the idea of surface roughness as having animportant effect on the estimation ofsoil moisture values (Baghdadi et al.,2002; Verhoest et al., 2000; S.Khabazan et al., 2013; Zribi and Dechambre, 2003).

GÜNEYDOĞU TÜRKİYE TARIMSAL ALANLARINDA, RADARSAT-2 UYDU GÖRÜNTÜLERİNİN İŞLENMESİ İLE YARI-DENEYSEL, ÜÇ TOPRAK NEMİ TAHMİN MODELİNİN GELİŞTİRİLMESİ

ÖZET

Su yeryüzünde hayatın önemli bir kaynağıdır. Yaşadığımız küre üzerinde tüm canlılar hayatlarını devam ettirebilmeleri için mutlak suya muhtaçtırlar. Toprakta mevcut bulunan besin elementlerinin doğal döngüsünü tamamlayabilmeleri tamamen su döngüsüne bağlıdır. Toprak erozyonu, sel baskını, orman yangınları, küresel ısınma vesıcaklık değişimleri, bitki türlerinin dağılışını ve farklı hayatı etkileyen faktörlertopraktaki yüzey nem oranı miktarı ile yakın ilişki içerisindedir. Bu nedenle tarımsal, hidrolojik, ve meteorolojik uygulamalarda, toprak nemi ya da toprağın su içeriği önemli birer faktör ve parametredir. Toprak neminin tanımlanması genellikle iki dala ayrılır; derin toprak nemi (kök bölgesi nemi) ve yüzey toprak nemi. Yüzey toprak nemi, toprağın üsteki 10cm.lik kısmındaki su miktarını tanımlar ki, bu dünyadaki toplam su miktarının yalnızca %0.0012'sini içerir (Verhoest et al., 2008). Bununla birlikte, bitkiler için önemli olan ve kullanılabilen derin toprak nemi (kök bölgesi nemi), toprağın yüzeyden itibaren 200cm.lik kısmında tanımlanır.

Toprak nemi bilgisinin önemine rağmen, bu faktörün ölçülebilmesinin birçok bilim dalında çok önemli yer tuttuğu açıktır. 15. yüzyıldan bu yana toprağın su içeriğinin belirlenmesi ile ilgili olarak birçok metod uygulana gelmiştir. Günümüzde, toprağın neminin belirlenmesinde en çok kullanılan metodlar, topraktaki suyun kütlesi, hacmi ya da toprağın suya doygunluğunun ölçülmesidir.

Büyük bir uzay için, zaman ve maliyet sınırlamaları toprak nem ölçümü elde etmesi için dikkate alınmalıdır. Geleneksel çalışmada, prensipte toprak neminin doğrudan veya dolaylı olarak ölçülmlenmesi ile ilgili metodlar, birbirlerinden ayrılabilir. Doğrudan metodlar, toprak neminin buharlaştırılması, suyun topraktan alınması, ya da FDR ve TDR gibi kimyasal ve gravimetrik ölçüm metodlarını metodları içermektedir. Literatürde, toprak neminin ölçülmesiile ilgili olarak, doğrudan veya dolaylı, birçok ölçüm metodu tanımlanmıştır (Stachder 1996, Prietzsch 1998, Marshall 1999). Genel olarak toprak nemi; kuru ağırlık yüzdesi, hacim yüzdesi, derinlik ve tansiyon olmak üzere 4 farklı şekilde ifade edilmektedir. Bu çalışmada toprak nemi hacim yüzdesi şekilde ifade edilmektedir (vol.%).

Ek olarak, 1970'lerde uyduların kullanıma girmesiyle, toprak neminin uzaktan algılama metodlarıyla belirlenmesi araştırmaları da gündeme gelmiştir. Uydu verileriyle toprak neminin belirlenmesi, uyduların geniş alanları gözlemleme ve uzun sürelerce bu gözlemleri tekrar edebilmesi nedeniyle hemen uygulama alanı bulmuştur. Uzaktan algılama, ilgi konusu olan nesne ile doğrudan temas olmadan, elektromanyetik spektrumun belirli dalgaboylarını kullanarak, bilgi edinmek demektir. Uzaktan algılama metodleri, gündüz ve gece operasyonları için küresel ölçekte ve hava şartlarindanbağımsız çalışmalarda, yüksek çözünürlüklü izleme ssahibi olarak son on yılda,çok kullanmaktadır . Yeryüzü tarafından yayılan veya yansıtılan hem optik hem de mikrodalga elektromanyetik sinyaller, yüzey hakkında olduğu kadar toprağın nemi hakkında bilgiler de içermekte ve toprağın neminin belirlenmesi çalışmalarında kullanılmaktadır. Bu yöntemtoprağın elektriksel iletkenliğinin ölçülmesi esasına dayanmaktadır. Su dielektrik sabiti ‘80’ ve kuru toprak dielektrik sabiti ‘0’ dir . Budielektrik sabitleriarasındaki büyük farka dayanarak uzaktan algılama geri saçılması yönteminin toprak nemi ile ilgili

çalışmalar için iyi bir faktör olduğu gözükmektedir. Geri saçınım katsayısı çalışmasıyla birlikte birçok toprak nemi tahmin modeli yayınlanmıştır:

(i) Deneme modelleri: Oh (1994)
(ii) Fiziksel modelleri: teorik integrasyon denklemi metodu, Fung et al., 1992; XBragg Modeli (2008)
(iii) Yarı-Deneysel modelleri: Ohet al., (1992), Oh (2004), Duboiset al., (1995)

Yarı-Deneysel OH92 ve OH04 modelleri için RADAR geliş açısı 10 ve 70 dereceearalığında ve DU 95 modeli için 30 ve 65 dereceearalığındadır.
Bu çalışmada, Oh (1992), Oh (2004), Dubois (1995) Yarı-Deneysel yüzey toprak nemi modelleri olarak kullanılarak, Harran, Şanlıurfa ve Güneydoğu Anadolu'daki tarım alanlarında, iki RADARSAT-2 görüntüsü (FQ1, FQ19) ile bir yüzey toprak nemi tahmininde bulunulması amaçlanmış ve kullanılan modellerin performans verilerini değerlendirmek için bir çalışma yapılmıştır.
Uydu görüntülerinin kullanıldığı pek çok uygulamada koordinatlandırma işlemi gerekli ve önemli bir adımdır. Koordinatlandırmada, temelde görüntü ve nesne koordinat sistemleri arasında bir dönüşümün sağlanması söz konusudur.
Bu işlem sonucunda RADARSAT-2, den alınan dataların koordinatları UTM koordinatlarına dönüşürülür ve uygun bir örneklemeden sonra kullanılabilir bir veri elde edilir.
Yarı-Deneysel modelleri uygulamak için RADARSAT-2 den alınan verilerin dönüştürülmüş olan halini kullanarak (ENVI programı yardımıyla):

(i) Python 2.7 programı kullanarak PolSARproprogramı da olan modellere ait alt programları yürüterek ismi geçen Yarı-Deneysel modeller için sonuç elde edilmiş,
(ii) Kullanılan modellerden elde edilen sonuçlar, Lee, Enh-Lee, Forst ve Kuan filtreleri ile analiz edilerek, benek gürültüsü azaltılmış ve model performansı arttırılmıştır,
(iii) Farklı çekirdek boyutları (8 farklı boyut 3×3 - 15×15) için, istatistiksel olarak hesaplanmış indislerle (ortalama ve standart t sapma ağırlıklı olan miktarlar) optimal filtre boyutu tahmini yapılmıştır,
(iv) Elde edilen optimal filtrer sonuçları araştırma alanı üzerinde belirtilmiş 3 farklı bölgede topraktaki nem elde edilmiştir.Sonraki aşamada eldeedilen topraknemi ve yerel istasyonlar da hesaplanan toprak nemi karşılaştırarak hata miktarıbelirlenmiştir.

07 Eylül2012 RADARSAT-2 verilerinin yarı-deneysel modellemeleri uygulaması kısmında Dubois modellemesindeki bakış açısının sınır dışı olması nedeni ile (18.40 -20.40)bu modelleme yapılmamaktadır. OH92 ve OH04 modelleri için en yüksek uyuşma:

(i) OH92 modeli için: 15×15 boyutlu Kuan filtresi(SSMPI=0.5126 , SSI=0.5126) optimal filtre olarak seçilmiştir.
(ii) OH04 modeli için: 5×5 boyutlu Kuan filtresi SSMPI=1.000, SSI=0.7590<1) optimal filtre olarak seçilmiştir.

08 Eylül2012 RADARSAT-2 datasıiçin uygulanan DU95 ,OH92, OH04 modellerinde en yüksek uyuşma ve optimal filtre boyutlari aşağıda özetlenmiştir:

(i) DU95 modeli için : 15×15 boyutlu Kuan filtresi , (ENL = 0.2234, SSMPI= 0.4327) optimal filtre olarak seçilmiştir.

(ii) OH92 modeli için: 5×5 boyutlu Kuan filtresi, (SSMPI= 0.5629) optimal filtre olarak seçilmiştir.

(iii) OH04 modeli için: 5×5 boyutlu Kuan filtresi, (SSMPI=0.5004, SSI=0.7829<1) optimal filtre olarak seçilmiştir.

Pauli-RGB görüntüsü kullanılarak, yüzeyde bitki örtüsü yoğunluğu tahmin edilmiştir. Yüzey kapsama bilgisi, çalışma bölgesindeki tahmini toprak neminin hesaplanmasında kullanılmıştır. Son olarak yerel ve tahmini değerler karşılaştırılmıştır. Bu araştırma, geliş açısının modellerin performasına olan etkisini (Bagdadi, 2008 ve Mo, 1984) ve yüzey pürüzlülüğünün (yüzey dalgalılığı, şekilsizliği) tahmin edilen toprak nemi değerine etkilerini (Bagdadi, 2002; Verhoest, 2000; S.Kabazan, 2013; Zribi ve Dechambre, 2003) desteklemektedir.

1. INTRODUCTION

Soil moisture, or soil water content, is an important factor and parameter used for agricultural, hydrological and meteorological use. Without doubt, soil moisture can be regarded as one of the most essential life sustaining entities on our planet. In many studies on the subject, it is divided into two modes: deep soil moisture or root zone, and surface soil moisture, that only constitutes 0.0012% of all water available on earth (Verhoest et al., 2008).The water stored in the soil has various roles in the global water cycle. For instance, the growth of plants, irrigation scheduling management, good product, crisis management during drought, etc. Furthermore, it controls the partitioning of rainfall into runoff and infiltration. Runoff commonly means both exporting fresh water to other areas and degradation of topsoil through leaching and erosion(surface moisture),infiltration mean filling underground aquifers (deep soil moisture) (Verhoest et al., 2008). It is observed that soil moisture is also a key variable in the flood forecast.

The measurement of soil moisture in a large space, time and cost limitations must be considered.In the traditional study, to evaluate soil moisture one must rely on various point measurements for estimating the result (average for soil moisture for study area).Theoldest and most accurate is gravimetric measurement(Foody, 1991).Conventional methods for attaining a measure are specific to location and limited time, but soil moisture is a variation of time and spatial,in last decade for high resolution monitoring in global scale and weather independent studies, for day and night operations providing remote sensing technique. Remote sensing methods are non-destructive and don'tnecessitate disturbing the soil to assess it spatially. Studying soil moisture with using remote sensing methodswas a trend which began in the 1970s (Schugge et al., 1974).In the field of soil moisture estimation the use of passive and active remote sensing techniques have been used.

Backscatter signals from the bare soil depends on several factors:These includeradar properties as frequency and polarization,surface characteristics as surface roughness, dielectric constant,and the incidence angle from incoming pulse, which all hold equal weight in the process. Estimate soil moisture with peruse received pulse of land surface is possible in remote sensing method. In comparison to traditional methods they have many advantages,such as beingrapid process, large area cover, low cost, better spatial and temporal resolution, long-term dynamic monitoring. Therefore, using remotesensing techniques has been the main way to obtain top few centimeters soil moisture in large region or field (Xiao et al.,2005).

There exists several theoretical, empirical and semi-empirical methods in literature for estimation of volumetric soil moisture using microwave sensors (Mishra et al., 2013).Some limitations exist in methods. Theoretical methods can rarely be used to invert data measured from natural surfaces, mainly because of the restrictive assumptions made when deriving them (Sherwin et al., 1962). Empirical methods are easy to use and handle but are notaccurate, and may not be applicable to data sets other than those used to develop the model in the first place.Semi-empirical (The most widely used semi-empirical models arethe Oh et al., 1992; Oh, 2004; Dubois et al., 1995aand Dubois et al., 1995b). Modified Dubois Model (MDM) (Baghdadi andZribi., 2006; Sahebi and Angles., 2009) approaches are based on theoretical scattering modelsand extend or modify these according to empirical observations. They are generally valid only for specific soil conditions andthis may limit their use significantly (Mishra.Pet al., 2013).

1.1 Purpose of Thesis

The main objective of this research is to evaluate the changes in soil moisture with in the study area as caused byenvironmental changes by relying on theOH92, OH04and DU95semi-empirical models with RADARSAT-2data. The study area is specifically the Harran area, outside the city of Sanliurfa in the South-East of Turkey. The study will discuss themethodological quality and accuracy of the measurements taken, as well as informing on the surface backscattering of SAR, contents soil properties and details on roughness. But use some approximation and simplified assumptions for decrease have entered some what into the process, partly due to an error in the estimation.For this study, the intention was to evaluate the influence of the speckle filter selection and window size to improve the accuracy of the results.

The work is composed of six chapters organized in a hierarchical manner, with each chapter building upon the previous ones. Following this introduction, basic definitions, fundamental principles of SAR and RADARSAT-2 are given inChapter *2*.Essential surface properties in the field of radar remote sensing and backscatter analysis and surface roughness are given inChapter 3.Surface soil moisture and important soil moisture theories are discussed in Chapter 4.Description of the study area,field methodology and method for estimation soil moisture in a different time but the same place are given in Chapter 5. Result and Discussion of research and analysis data is contained in chapter 6. Finally, in the end, the conclusions is given.

1.2 Literature Review

The condition of moisture in the soil can be assessed in three ways: measurements using resources on ground, estimation from remotely sensed data and simulation from hydrological and land surface models. Each has its own advantages and disadvantages, none being perfect.Remote sensing methods are briefly reviewed in following section to give a broad idea to readers, about soil moisture estimation by using these methods.

1.2.1 Soil Moisture Through Remote Sensing

Soil moisture measurement and estimation from remotely sensed data has come way due to its unique capability of monitoring large areas with long-term repetitive coverage.Remote sensing is data acquisition without direct contact with the object of interest using particular wavelength of electromagnetic spectrum.The omitted or reflected signals in remote sensing methods from earth's surface contain information about soil properties and surface details in both optical and microwave remote sensing have been used for soil moisture study.In optical, studies have used visible and thermal infrared, but a lot of efforts have gone in to the microwave section, for both active and passive.Microwave Remote Sensing operates in the frequency range from 0.3 GHz to 300 GHz, wavelength of 1mm to 1m.The principle behind the use of microwave remote sensing for soil moisture content assessment is the contrast in dielectric properties of soil moisture of liquid water (~80) and dry soil (<4).Table 1.1shows some of advantages and disadvantagesofoptical sensors, passive microwave method, synthetic aperture radar (SAR) and real aperture radar (RAR).

Optical remote sensors, like Landsat and SPOT, detect the electromagneticradiation that comes from the sun and is reflected from the Earth's surface (Campbell, 2007). These instruments cannot operate under all atmospheric conditions (Heilman et al., 1977; Li et al., 2008).

Table 1.1 : Advantagesand disadvantagesof RSmethods for soil moisture study .

Method	Advantage	Disadvantage
Optical sensor	Large area coverage	Small penetration in soil, Require atmospheric and meteorological information
Passive RS	Large area coverage, Not affected by atmosphere	Need land cover and temperature information
SAR	High spatial resolution, Deep penetration in soil	High sensitive about vegetation and roughness ,limitation in swath width
RAR	High temporal resolution Deep penetration in soil	Affect by vegetation, Cross spatial resolution

On the other hand, radar sensors can operate under all atmospheric conditions, improving the potential for surface soil moisture estimation (Engman and Chauhan.(1995); Lakhankar et al., 2009; D'Urso and Minacapilli.,2006). Several studies have shown the potential for estimating surface soil moisture by using different radar sensors,like GPR systems (Huisman et al., 2001; Lunt et al.,2005), passive microwave (Mohanty and Skaggs. 2001; Schmugge., 1998), ENVISAR (Baup et al., 2007),ERS1 and 2 (Blumberg and Freilich., 2001); Quesney et al., 2000), RADARSAT-1 (Baghdadi et al. 2007); Sahebi et al., 2003); Jackson and Wood. 2001).

The sensitivity of the radar-backscattering coefficient (σ^0) to soil moisture at low microwave frequencies is well described in the literature (Ulaby et al., 1978; Ulaby et al., 1981b; Ulaby et al., 1982a; Ulaby et al., 1982b; Hallikainen et al., 1985; Dobson et al., 1985; Dobson and Ulaby., 1986; Oh et al., 1992). On the other hand in many studies, considerable effort has been researched on the retrieval of soil moisture from C-band radar data (Cognard et al., 1995; Altese et al., 1996; Rombach and Mauser,1997; Schneider and Oppelt., 1998; Quesnay et al., 2000; Verhoest et al., 2000; Le Hégarat-Muscle et al., 2002; Leconte et al., 2004; Paloscia et al., 2008), which is operational today on earth observation platforms such as ERS-2 (ESA), RADARSAT-1 (CSA), ENVISAT (ESA) and RADARSAT-2 (CSA). Besides the surface roughness,a major impediment of soil moisture is the presence of a vegetation cover.In different kinds of areas like bare area or agricultural fields, forest covered places there are differences between the method and their performance. Thus, the estimation of spatial soil moisture patterns that is accurate enough and thus suitablefor application requires the use of correction procedures for vegetation and roughness effects (Jackson et al., 1997; Satalino et al., 2001; Loew et al., 2006; Mattia et al., 2006).

Gherboudj et al. in 2011 have studied soil moisture estimation by using semi-empirical soil moisture estimation models(near Saskatoon, Saskatchewan, Canada during the summer of 2008, the area covered by different crops like wheat,peas, lentil,fallow,pasture and canola). The originality of this study is that the proposed empirical relationships are independent of crop type, contrary to those found in the literature. Soil moisture is estimated over various crop fields with an average relative error of 32% (Gherboudj et al., 2011).

The most common methods for estimation of soil moisture by using active remote sensing are the Integral Equation Model (IEM) (Fung et al., 1992), the Oh Model (Oh et al., 2002; Oh., 2004), and the Dubuois Model (Dubois et al., 1995).

Rao et al. (2010) in West Bengal and Andhra Pradesh by using ALOS-PALSAR fully polarimetric data have tested soil moisture in diffrent dates.In this research Dubois et al, Oh et al. (1992) and X-Bragg methods was used.The local measurement is not available and in this study, the researcher intends to compare different models. They have also studied the various inversion models and found that the Dubois et al. model over estimates soil moisture as compared to Oh et al. models. The soil moisture difference between Oh et al. (1992) and X-Bragg model estimations fail to invert soil moisture for several fields. They have shown that fully polarimetric and compact polarimetric mode give better accuracy than other combinations (Rao and Venkataraman., 2010).

In agricultural fields in Harran area on a Sanliurfa, southeast of Turkey, a comparison among the spatial distribution of retrieved soil moisture changes from SAR images was done. The correlations between the soil moisture content and backscattering of ASAR, RADARSAT-1 and PALSAR images were found 76%, 81% and 86 % respectively. Although the resolution of RADARSAT-1 fine beam image (6.25m × 6.25m) is closer to the resolution of PALSAR image (6.25m × 6.25m), PALSAR gives better correlation than RADARSAT-1 image. Although the resolution of RADARSAT-1 and PALSAR images is far higher than that of the ASAR image (30m × 30m), the significance of the results produced is almost similar in such flat areas (Sanli et al., 2008).

On the other hand, there have beenmany studies and data analysis on modifying methods in semi-empirical models.In these studies; the main aim has beento increase the performance of models.

Evaluation of the Dubois, Oh, and IEM radar backscatter models over agricultural fields (two agricultural areas in Canada)using C-band RADARSAT-2 SAR image data was studied by Merzouki et al., 2010.They have shown that the Dubois and Oh models overestimate the backscatter coefficient in HH and VV polarizations and systematically produced significant biases that are largely associated with measurement of soil moisture and surface roughness in the field. The error has similar patterns of variation in HH and VV polarizations for both models. Correction factors were estimated through a trial and error analysis to correct this discrepancy.In addition,results have shown that the IEM simulations did not accurately reproduce measured backscatter coefficients. To correct this discrepancy, the semi-empirical calibration of the model was implemented and evaluated to improve the correlation between simulated and measured data.

Rao et al., 2013, modified the Dubois model for estimating soil moisture with dual polarized SAR data.In this study, the semi empirical model derived by Dubois et al., 1995, was modified to work using σ_{HH} instead of two like polarization equation σ_{HH},σ_{VV} so that soil moisture can be obtained for the larger area frequency.The field derived roughness correlated with the cross polarization ratio (HV/HH) to replace the one unknown parameter 's' in the Dubois model and hence the dielectric conestant was derived by inverting the Dubois model equation (HH).

Zribi and Dechambre, (2003)have suggested a new empirical model to retrieve soil moisture and roughness from C-band radar data;they have introduced new parameter that was named as Z_s($Zs = S^2/l$).

Baghdadi et al., 2006 and Baghdadi et al., 2004, proposed an empirical calibration of the IEM for HH and VV polarizations. It is based on large experimental data composed of SAR images and ground measurments of soil moisture and surface roughness. In this calibration, the discrepancies observed between the IEM and the SAR data were related both to the shape of the correlation function and the accuracy of the correlation length measurements. The order physical input parameters used in the IEM standard deviation of height and soil moisture are assumed to be relatively accurate. The approach consists of replacing the measured correlation length, for SAR configuration (radar wavelengths, incidence angle, and polarization), by a fitting/calibration parameter (L_{opt}), so that the IEM model reproduces better radar backscattering coefficient.In the end, the IEM model presentedoptimal correlation length. The results have shown that the calibration parameter was found to be dependent on rms surface height and radar incidence angle.Moreover, the simulation produced by the calibrated IEM fit correctly SAR measurements (bias and standard deviation of the error were reduced).With this calibration, bare agriculture soils can be characterized by two surface parameters (rms height and soil moisture), instead of four(height,correlation length, correlation function and soil moisture) (Baghdadi et al., 2011).

1.3 Objectives and Hypotheses

As shown in section 1.1 the main objective in this study is evaluate soil moisture by using OH92, OH04 and DU95, semi-empirical models.More specifically, the objectives are:

- RADARSAT-2 data was used for estimated the soil moisture values during the study. ENVI Classic 5.0.6 was used for raw data process.It was hypothesized that:

    - In preparing raw data, due to study area is agricultural area, DEM and GCP points estimation was emitted.
- Reduce the speckle noise and improve accuracy of soil moisture maps. Optimal filter type and window size was found by using statistical values.
- The semi-empirical methods, that was presented in this study, are suitable for bare surface. It was hypothesized that:
    - Pauli RGB image was used on the study area to estimate surface coverage. However, Pauli RGB image only has information about vegetation dense. There are not any detail about crops type, crops height and tillage methods in this image.Then moderate coverage area was used for estimation.
- For finding the soil moisture values in the surface layer (0-5cm) at ground measurements,it was hypothesized that:
    - Soil composition (only loam)
    - Infiltration direction (vertical direction)
    - Tillage method (i.e. conventional, minimal, no-till)

2. GENERAL BACKGROUND OF SYNTHETIC APERTURE RADAR

2.1 Purpose

Nowadays,activeand passive remote sensing is one of the most important instruments for soil surface, deep and layer study.One of the most known techniques in active remote sensing (active sensor in remote sensing is a sensor that does not rely on the natural emissions from object.Instead, it illuminates the objects and then measures the reflected wave.) is Synthetic Aperture Radar (SAR) imaging, operating in the microwave region of the electromagnetic wave spectrum, generally between P-band and Ka-band (Figure 2.1).

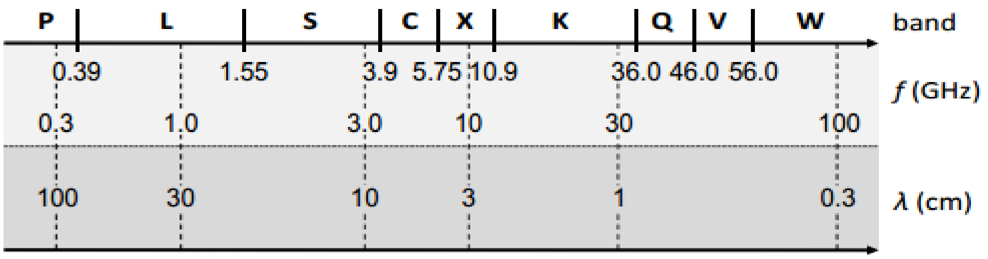

Figure 2.1 : Microwave section of the electromagnetic spectrum.

SAR sensors are independent of solar illumination and thus capable of day and night time acquisitions.SAR systems, allow all weather conditions, then it is suitable to global scale Earth monitoring.In addition,SAR has the advantage of providing control over such factor as,frequency, phase,polarization, incident angle, spatial resolution and swath width, all of which important when designing and operating a system for the extraction of quantitative information.In SAR, the forward motion of the actual antenna is used to 'synthesize' a very long antenna. At each position a pulse is transmitted, the return echoes pass through the receiver and recorded in an 'echo store'. The Doppler frequency variation for each point on the ground is a unique signature. SAR processing involves matching the Doppler frequency variations and demodulating by adjusting the frequency variation in the return echoes from each point on the ground. Result of this matched filter is a high-resolution image.(Figure 2.2).The main scope of this chapter is to provide a brief overview of the basic concepts of Synthetic Aperture Radar. More detailed information can be found in the dedicated literaturelike (Cumming and Wong, 2005; Henderson and Lewis, 1998;Chan and Koo, 2008).

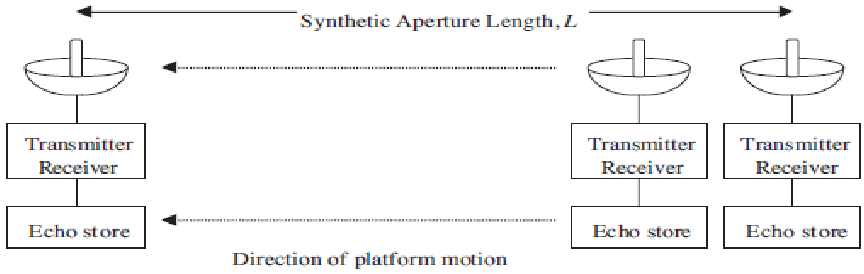

Figure 2.2 : Synthetic aperturescheme.

2.2 Principles of Synthetic Aperture Radar

In the early 1950s, an engineer named Carl Wiley, while employed at the Goodyear Aircraft Corp, worked on the idea of using platform movement and signal coherenceto reconstruct a large antenna. The synthetic aperture concept was first introduced by him.Wiley was the first to observe a one-to-one correspondence between the along-track coordinate of a reflecting object (being linearly traversed by a radar beam) and the instantaneous Doppler shift of the signal reflected to the radar from that object. He concluded that a frequency analysis of the reflected signals could enable higher along-track resolutions than that permitted by the along-track width of the physical beam itself.The development of his ideas is retracted in a paper by Sherwin el al. (1962).

SAR is based on the generation of an effective long antenna by signal processing means rather than by the actual use of a long physical antenna. As the radars moves between two pulse transmissions, it is indeed possible to combine in phases all of the echoes and synthesize a very large antenna array. This is the principle of synthetic aperture radar.SAR mostly uses airborne or space borne side-looking radar system. Nowadays P, L, S, C, and X band with different kind of polarization are commonly used.

2.3 SAR Imaging Geometry

Radar imaging provides a two-dimensional image(2-D).There are two scenarios for radar imaging operation. The first one has used the same sensor for transmitting and receiving, that is, transmitter and receiver.This scenario is known as monostatic configuration. According to the second scenario, known as bistatic and multistatic configuration, transmitter and receiver are separated.

A monostatic SAR imaging systemis mounted on a moving platform operating in sidelookinggeometry as illustrated in Figure 2.3(a).The length of the antenna is given by coordinates (L_x, L_y), range resolution is represented in the X-axis direction and azimuth resolution in the Y.

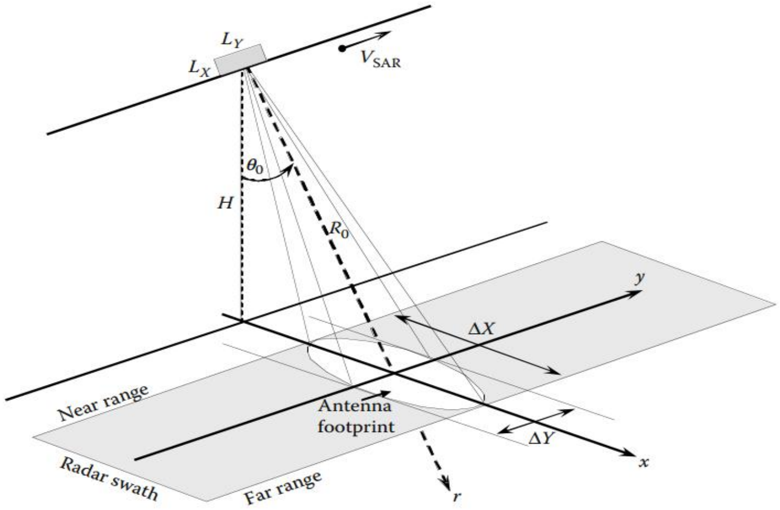

(a)

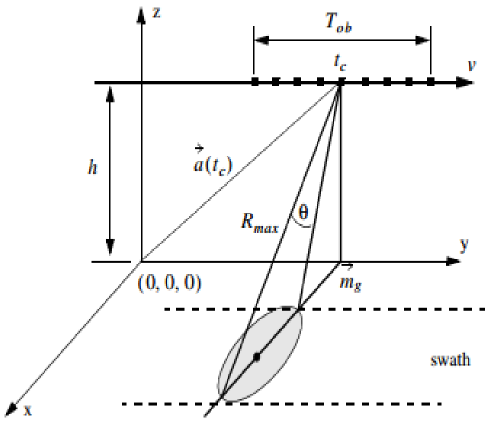

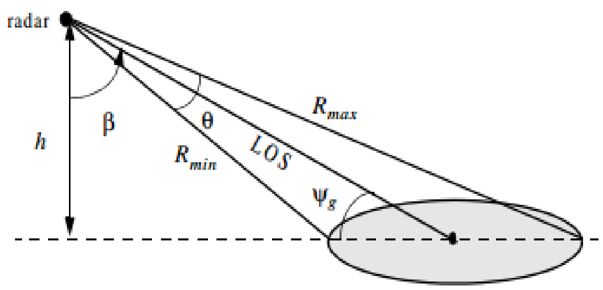

(b) (c)

Figure 2.3 : (a) SAR imaging geometry in strip-map mode (Lee et al.,2009),(b) Length of antenna , Maximum slant range R_{max}, (c) Grazing Angle (ψ_g).

In the SAR system with a velocity (V),altitudeor Nadir (H), incidence angles(θ_0) (the angle between theradar beam and the vertical where the beam meets the surface)was shown inFigure 2.3(a),the area scanned by the antenna beam is known as the radar swath andthe area covered by the antenna beam in the ground range (x) and azimuth (y) directions is the so-called antenna footprint.The size of the footprint is a function of thegrazingangle (ψ_g),Figure 2.3(b).The antenna footprint is defined from theantenna apertures (θ_X, θ_Y)given by:

$$\theta_X = \frac{\lambda}{L_X} \quad \text{and} \quad \theta_y = \frac{\lambda}{L_y} \qquad \textbf{(2.1)}$$

WhereL_X and L_Y correspond to the physical dimensions of the antenna,λ is the wavelength corresponding to the carrier frequency of the transmittedsignal.By using theFigure 2.3(b)for Δx and Δy :

$$\Delta x = \frac{R_0\theta_x}{cos_{\theta_0}} \quad \text{and} \quad \Delta y = R_0\theta_y \qquad \textbf{(2.2)}$$

Where R_0 is the distance between the radar and the antenna footprint center (Lee et al.,2009).

The minimum slant range to the swath is R_{min}, and the maximumslant range is R_{max} depicted at Figure 2.3(b)and denoted as:

$$R_{min} = h / cos(\beta - \theta/2) \qquad \textbf{(2.3)}$$

$$R_{max} = h / cos(\beta + \theta/2) \qquad \textbf{(2.4)}$$

Notice that the elevation angle β is equal to:

$$\beta = 90 - \psi_g \qquad \textbf{(2.5)}$$

2.4 SAR Complex Images

Target analysis isone of the most important applications in remote sensing instruments and techniques. But in target analysis in SAR it is necessary that SAR is not only imaging sensor, it is a very good active coherent device, which works on the principleoftransmitting coherent electromagnetic pulses and recording the amplitude as well as phase information of backscattered signal. SAR instrument emits radar pulses and records the time, frequency and phase of the scattered return. The Doppler history of returns is used to determine the position in the azimuth (along path)direction, and the echo time to determine the range (across track) position.Then SAR image has information about phase and amplitude, bi- dimensional and complex value data. Thecomplex image can be redefined as a local descriptor of the scatterers and structured scatterers to detect and recognize objects and regions. Texture descriptors can be computed for an image using many approaches like statistical, structural or spectral approaches(Singh et al.,2010).

Due to the side-looking operation, the geo-location error caused by incident angle is inevitable.The effect of terrain height causes the foreshortening when the slope of the local terrain is less than the incidence angle. Similarly, a layover condition exists for steep terrain where the incidence angle is less than the slope of the local terrain; and an image distortion related to the layover effect is radar shadow. Shadowing occurs when the local terrain slopes away from the radar at an angle whose magnitude is greater than or equal to the incidence angle of the transmitted wave(Rho et al. ,2011). For solving this kind of error readers may refer to proposed algorithm using the GCP in (Rho et al. ,2011).

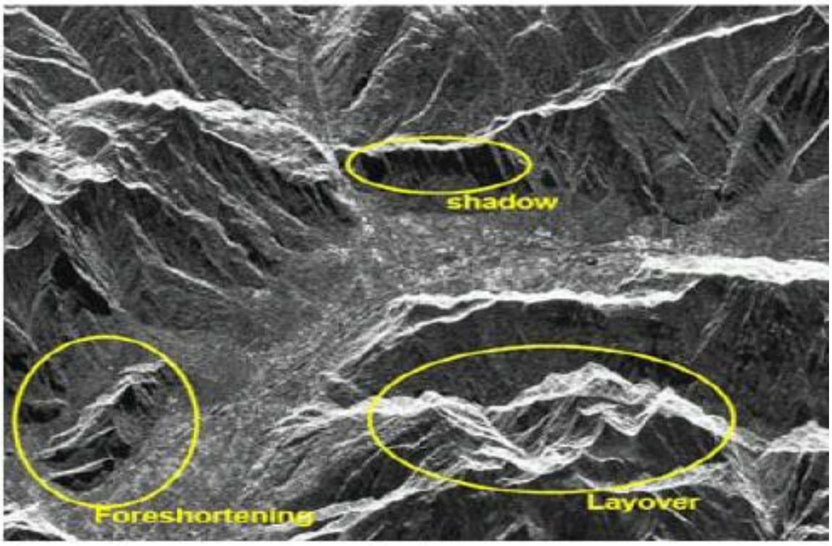

Figure 2.4 : Multiple target distortion example image(Rho et al., 2011).

2.5 SAR Resolution

By precisely measuring the time difference between the transmitted pulse and receipt of the reflected energy, radar is able to determine the distance of the reflection object (named range or slant range). The range resolution of radar system is its ability to distinguish two objects separated by some minimum distance. If the objects are adequately separated, each will be complex combination of the reflected energy from the two objects.

Spatial resolution in the range direction is not the range of directly wavelength dependent, but is instead a function of the effective (processed) pulse–width (τ) multiplied by speed of light (c) and divided by two. Range resolution can also be expressed as the reciprocal of the effective pulse –width (the pulse bandwidth (β) multiplied the speed of light.

$$\text{Range Resolution} = \frac{c\tau}{2} = \frac{c}{2\beta} \qquad \textbf{(2.6)}$$

As the range resolution becomes finer, the pulse bandwidth and data grows accordingly. Most modern radars like SAR transmit a pulse called linear frequency modulated (FM) ‘chirp’. The transmitter varies the frequency of the radar pulse linearly over a particular frequency range (an increase in frequency is called an up – chirp).The chirp length and slope are based on the radar hardware capabilities (RF pulse power, pulse repetition frequency (PRF), Analog –to –Digital (A/D) sampling conversion) and the range resolution requirement. Both real aperture radar (RAR) and SAR achieve their spatial range in this way.

As seen in the previous section azimuth resolution is presented along the Y-axis. $\mathbf{\Delta Y}$ was used to Showing the change in azimuth direction in Equation 2.2. Hence, it can be seen that high resolution in azimuth direction requires large antennas. The maximum length for the synthetic aperture is the length of the flight path from which a target is illuminated and is equal to the size of the antenna footprint on the ground ($\Delta \boldsymbol{Y}$). If a scattering target, at a given range R_0, is coherently integrated along the flight track, the azimuth resolution is equal to:

$$\text{Azimuth Resolution} = \frac{L}{2} \qquad \textbf{(2.7)}$$

Where, L is length of antenna.

The corresponding azimuthal resolution expression for an orbital SAR imaging system is given by (Schuler et al., 1996):

$$\text{Corresponding Azimuth Resolution} = \frac{R_E}{R_E+H}\frac{L}{2} \qquad \textbf{(2.8)}$$

Where,R_E is the earth's radius,H is the platform altitude.

2.6 Synthetic Aperture Radar Specific Parameters

2.6.1 Wavelength

Most radar satellites uses of the microwave portion of the electromagnetic spectrum, from a frequency of 0.3 GHz to 300 GHz(Figure 2.1) and wavelengths range is between 0.5 cm and 75 cm .

The penetration capability of microwaves into material media is one of the importantaspects in the soil and soil moisture research. Shorter wavelengths (i.e. X- or C-band) interact predominantly with its upper layer and thus the obtained radar image contains information only about this part of the illuminated medium(suitable for dry soil or surface study). In contrast, by using radars operating at lower frequencies (L-band or P-band), the incident waves penetrate further into the medium, and the obtained images may contain information about deeper layers.Aschematic illustration of the relation between penetration depth and wavelength is shown in Figure 2.5. It can be seen that the longer wavelength at L-band penetrates much clearer than the shorter wavelength at C-band.

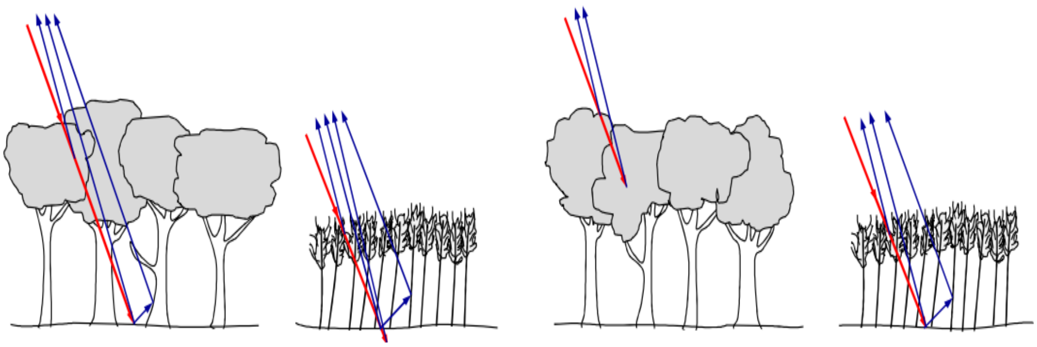

Figure 2.5 : Schematic representation of radar penetration in to vegetation and soil at L-band and C-band (redrawn after Ulaby et al., 1981b).

2.6.2 Incidence Angle and Look Direction

The incidence angle is the angle between the incidence radar signal and the directionperpendicular to the ground surface that the signal strikes (Campbell, 2002).In high incidence angle of smooth surface backscatter is less than low ones (Srivastava et al., 2009).Topography may be affected the incidence angle.Look direction is the direction in which the radar antenna is pointing when transmittingsignals and receiving backscatter from the ground surface.

2.6.3 Polarization

Polarization is an important property of a plane electromagnetic (EM) wave. It refers to the alignment and regularity of the electric field component of the wave, in a plane perpendicular to the direction of propagation. The electric field of a plane wave can be described by the sum of two orthogonal horizontal(H) and vertical (V) components (Bornand Wolf , 1999).Signals can transmit horizontal (H) or vertical (V) electrified vectors, and receive either horizontal (H) or vertical (V) return signals, or both.Polarization can belinear, circular, or elliptic.Diffrent types of polarization are:

(i) Single polarization: The radar system operates with the same polarization for transmitting and receiving the signal.

(ii) Cross polarization**:**A different polarization is used to transmit and receive the signal.

(iii)Dual polarization: The radar system operates with one polarization to transmit the signal and both polarizations simultaneously to receive the signal(HH and HV, VV and VH, or HH and VV).

(iv)Quad polarizationorFour polarizations**:** H and V polarizations are used for alternate pulses to transmit the signal and with both simultaneously to receive the signal(HH, VV, HV, and VH).

A quadrature polarized (i.e. polarimetric) radar uses these four polarizations, and measures the phase difference between the channels as well as the magnitudes. Some dual polarized radars also measure the phase difference between channels, as this phase plays an important role in polarimetric information extraction [Url-1].By using Stokes parameters parameters the degree of polarization of wave can be obtained by (Huynen, 1970; Huynen,1990):

$$\mathrm{DoP} = \frac{\sqrt{g_1{}^2+g_2{}^2+g_3{}^2}}{g_0} \tag{2.9}$$

For ful -polarization DoP =1 and partially -polarization wave 0<DoP<1.For many details about polarization found in(Boerner et al.,1981;Stratton,1941;Kostinski and Boerner,1981).

The electric field vector of a monochromatic plane electromagnetic with constant amplitudeE_0propagatingin the directionzof orthogonal three dimensional coordinate(Lee et al.,2009):

$$\mathrm{E(z,t)} = \begin{bmatrix} E_{0x} cos(\omega t - kz + \delta_x) \\ E_{0y} cos\left(\omega t - kz + \delta_y\right) \\ o \end{bmatrix} \tag{2.10}$$

An the other hand by using Jones vector for incident and scattered waves E_I and E_S we can write :

$$E_S = \frac{e^{jk\,r_R}}{r_R} S\, E_I = \frac{e^{jk\,r_R}}{r_R} \begin{bmatrix} S_{hh} & S_{hv} \\ S_{vh} & S_{vv} \end{bmatrix} E_I \tag{2.11}$$

S is called scatter matrix and r is distance between object and receiver(m).In this matris $\boldsymbol{S_{vv}}$, $\boldsymbol{S_{hh}}$are coherent polarization elements and $\boldsymbol{S_{vh}}$,$\boldsymbol{S_{hv}}$ are non- coherent polarization elements.Because the response answer in the mono statics radar system ,and the non-chorenet elements are equal and in process it is enough to find six independent phases and amplitude parameters.

For a reciprocal target matrix, in the monostatic backscattering case, the reciprocity constrains the Sinclair scattering matrix to be symmetrical, that is,$S_{XY} = S_{YX}$**,**the 4-D polarimetric coherency T_4 and covariance C_4 matrices reduce to 3-D polarimetric coherency T_3 and covariance C_3 matrices with:

$$\overrightarrow{k_p} = \frac{1}{\sqrt{2}}[S_{HH} + S_{VV} \quad S_{HH} - S_{VV} \quad 2S_{HV}]^T \qquad \textbf{(2.12)}$$

$$[T]=<\overrightarrow{k_p}.\overrightarrow{k_p}^{+}> = \frac{1}{2}\begin{bmatrix} <|S_{HH}+S_{VV}|^2> & <(S_{HH}+S_{VV})(S_{HH}-S_{VV})^*> & 2<(S_{HH}+S_{VV})S_{HV}{}^*> \\ <(S_{HH}-S_{VV})(S_{HH}+S_{VV})^*> & <|S_{HH}-S_{VV}|^2> & 2<(S_{HH}-S_{VV})S_{HV}{}^*> \\ 2<S_{HV}(S_{HH}+S_{VV})^*> & 2<S_{HV}(S_{HH}-S_{VV})^*> & 4<|S_{HV}|^2> \end{bmatrix} \qquad \textbf{(2.13)}$$

$$[C]=\begin{bmatrix} <|S_{HH}|^2> & \sqrt{2}<(S_{HH})(S_{HV})^*> & <(S_{HH})(S_{HV})^*> \\ \sqrt{2}<(S_{HV})(S_{HH})^*> & 2<|S_{HV}|^2> & \sqrt{2}<(S_{HV})S_{VV}{}^*> \\ <S_{VV}(S_{HH})^*> & \sqrt{2}<S_{VV}(S_{HV})^*> & <|S_{VV}|^2> \end{bmatrix} \qquad \textbf{(2.14)}$$

2.7 Radar Backscattering Coefficient

The SAR image is a grey scale image that the intensity of each pixelrepresenting the amountof energy returned from that area on the ground (Liew, 1997).Low backscatter or little energy returned from SAR,was indicated in dark area (Freeman, 1996).A rough surface scatters the radar pulse in all directions while part of the radar energy is scattered back to the radar sensor. The nature of backscattering from an area depends upon the SAR system and the environmental conditions. System parameters include the frequency and polarization of the radar pulses, the incidence angle of the radar beam and the look direction. Environmental variations comprise the types, sizes and shapes of features, the types of land cover (i.e. soil, vegetation or manmade features), the moisture content and geometric factors (i.e. roughness and slopes). Thus, when different frequencies are used, backscatter also tends to differ. The interaction between radar signals and the ground surface depends on the incidence angle of the radar pulse on the surface (Lillesand et al., 2004). Backscatter variations may result from the interaction of various roughnesses and incidence angles.

As shown in the previous paragraph, the targets scatter the energy transmitted by the radar in all directions. The energy scattered in the backward direction is what the radar records. The intensity of each pixel in a radar image is proportional to the ratio between the density of energy scattered and the density of energy transmitted from the targets in the Earth’s land surface (Waring et al. 1995).

The energy backscattered is related to the variable referred as radar cross-section (σ), and is the amount of transmitted power absorbed and reflected by the target. The backscatter coefficient ($\sigma°$) is the amount of radar cross-section per unit area (A) on the ground (Jensen, 2000). $\sigma°$ is a characteristic of the scattering behaviour of all targets within a pixel and because it varies over several orders of magnitude, it is expressed as a logarithm with decibel units (Waring et al., 1995).

Backscatter coefficient is a function of wavelength, polarisation and incidence angle, as well as target characteristics such as roughness, geometry and dielectric properties. (Waring et al., 1995). The backscatter is measured as a complex number, which contains information about the amplitude (easily converted to $\sigma°$ by specific equations) and the phase of the backscatter (Baltzer, 2001).

Backscattering coefficient can be defined as average radar cross section per unit:

$$\sigma° = \frac{\sigma}{A_0} = \frac{4\pi {r_R}^2}{A_0} \frac{|E_S|^2}{|E_I|^2} \quad \textbf{(2.15)}$$

The backscattering coefficient is the quantity employed as the SAR observation is the most of the SAR -based scattering models.As mentioned before,the RCS,and thus, the backscattering coefficient depends on the polarization of the incident and bacscatter wave.Therefore, backscattering coefficient can be rewrittenfollows:

$$\sigma_{qp}^0 = \frac{\sigma}{A_0} = \frac{\boldsymbol{4\pi {r_R}^2}}{A_0} \frac{|\mathbf{E_{Sq}}|^2}{|\mathbf{E_{Ip}}|^2} \quad \textbf{(2.16)}$$

q,p denotes of the polarization state of the incident and scattered fields,respectively. Element of the scattering matrix are related to backscattering coefficient as:

$$\sigma_{qp}^0 = 4\pi |S_{qp}| \quad \textbf{(2.17)}$$

The backscattering coffient $\sigma°(\theta)$ of vegetation covered soil can be written in the form (Mo et al.,1984):

$$\sigma°(\theta) = \sigma°_v(\theta) + \sigma°_s(\theta) \exp\left({-2\tau}/{cos\theta} \right) \quad \textbf{(2.18)}$$

$\sigma°_v(\theta)$ is vegetation coffient and $\sigma°_s(\theta)$ is soil coffient ,τ is optical thinckness of the vagetation layer. Folowing the Mo et.al,1984, $\sigma°_s(\theta)$ on the roughest surface involvest two parts:(i) coherent backscatter, and(ii) incoherent backscatter.

$$\sigma°_s(\theta) = \sigma°_{coh}(\theta) + \sigma°_{inc}(\theta) \quad \textbf{(2.19)}$$

β^0, is a radar brightness coefficient. The reflectivity per unit area in slant range is dimensionless and corresponds to the average radar cross section (RCS) per unit image area (Wang et al, .2006). The pixel or resolution cell, in dB is the standard radiometric product for uncelebrated radar images. It is a direct result of the amplitude of the received signal expressed in terms of the digital number *DN* as:

$$\beta^0 = 10(log\frac{DN^2}{k}) \tag{2.20}$$

K is the so-called absolute calibration constant. The radar backscattering coefficient σ°is defined as the average RCS per unit ground area in dB. Hence, σ°can be obtained by normalizing $\beta^0$to the ground patch corresponding to the projection of each pixel onto the ground with.

$$\sigma° = \beta^0 \times \sin\theta \tag{2.21}$$

Finally,a function of soil texture, structure, density, roughness (RMS height), soil moisture, and soil surface conditions described by the autocorrelation function of a random surface height and correlation length.

2.8 Speckle

The major problem with processing SAR images is that the coherent nature of the microwave signal gives rise to a phenomenon called speckle(Singh et al.,2010).Speckle noise in radar data is assumed to involve a multiplicative error model which must be reduced before the data can be utilized otherwise the noise is incorporated into and degrades the image quality. Multi-look processing or spatial filtering (Raney, 1998) can reduce speckle noise (A´ lvarez-Mozos et al., 2005).

On the other hand, speckle significantly affects the accuracy of the extractedtarget decomposition parameters. Several studies have been reported to investigate the speckled effect on target decomposition (Touzi, 2004;Lopez- Martinez et al.,2005;Touzi, 2007). Lopez- Martinez et al.,2005, showed that the PolSAR speckle noise has a big impact on quantitative physical parameter estimation, especially in high entropy environments. They showed that the sample eingenvalues are biased, with bias that decreases with an increase in the number of independent samples.

The removal of speckle noise in SAR image is an important problem. There are many studies about removal speckle in SAR image. In most of removal speckle algorithm the image in small window is assumed to be uniform (constant gray) or texture (regions where about intensity changes) (Eom, 2008).Touzi, 2007, showed that the processing window size significantly influences the accuracy of the estimates derived from the incoherent decomposition parameters. The results indicated that for unbiased estimation of the incoherent target decomposition parameters, the coherency matrix has to be estimated within a moving window that includes a minimum of 60 independent samples. However, coherent decomposition should be limited to coherent targets with sufficiently high signal to clutter ratios. It was also evidenced that the averaged parameters derived from coherent decomposition in application that involve extended natural targets may be significantly biased.

The SAR image y(s) is modeled by unobservable original image representing ζ(s),representing the reflectivity of target area, corrupted by white multiplicative noise v(s):

$$y\,(s)= \zeta(s)\ v(s),\ \{(s_1,s_2);0\leq s_1,\ s_2 \leq N - 1)\} \qquad \textbf{(2.22)}$$

The multiplicative noise V (S) in Equation 2.22 can be modeled as:

$$V = 1 + \beta\omega(S) \qquad \textbf{(2.23)}$$

β is the strength of noise, | β |<1,and ω(S)is a 2-D white noise with zero mean and unit variance.

$$\mathrm{Log}y(s) = X_1(s) + X_2(s) + \log u(s) \qquad \textbf{(2.24)}$$

$X_1(s)$: Represents the global structure of the image, and is assumed to be locally near-invariant for a small window (say W×W) . $X_2(s)$:Represents local features such as edges or lines, and is assumed to follow a low-order polynomial model (Eom, 2008; and A´ lvarez-Mozos et al., 2005).

Assuming $x\widehat{1(s)}, x\widehat{2(s)}$ be the estimates of $x_1(s)$ and $x_2(s)$, respectively, then the speckle-filtered image $\widehat{\zeta(s)}$ is:

$$\widehat{\zeta(s)} = \exp\,(\widehat{X1(}s) + X\widehat{2(s)}) \qquad \textbf{(2.25)}$$

The structural component $x_1(s)$ is estimated by removing the effect of detailed component and noise by applying low-pass filtering to logarithm of the observed image y(s).

$$X_1(s) = h(s)*\log y(s) \qquad \textbf{(2.26)}$$

The spatial filters are categorized into two different groups:

(i) Non-adaptive: Filters take the parameters of the whole image signal into consideration and leave out the local properties of the terrain backscatter or the nature of the sensor. These kinds of filters are not appropriate for non-stationary scene signals. Fast Fourier Transform (FFT) is an example of such filters.

(ii) Adaptive: Adaptive filters accommodate changes in local properties of the terrain backscatter as well as the nature of the sensor. In these types of filters, the speckle noise is considered as being stationary but the changes in the mean backscatters due to changes in the type of target are taken into consideration (A´ lvarez-Mozos et al., 2005).

2.9 Image Georefrencing and Resampling

It is a process of transforming an uncorrected, raw image from an arbitrary coordinate system into a geographic or map projection coordinate system. Namely, image pixels are positioned and rectified to align and fit into real-world map coordinates.Geocoding and rectification can achieve two objectives: relate the image to a known map coordinate system when combining the image with other geo-spatial data, and correct geometric distortions in the images to improve the accuracy when making measurements on the image.Geo-referencing is also known as geocoding, rectification, ortho-rectification, registration, coregistration, or geometric transformation in different contexts (Jensen ,1996).

When geocoding and rectification is performed, the output image will commonly have different pixel size, orientation, and coordinates from those in the input image. To determine the DN values for pixels in output image, the resampling process is required. Resampling is the process of determining new values for output pixels after geometric transformation of input image.It is based on the original image. Three commonly used resampling techniques are

(i) Nearest neighbor resampling : The nearest neighbor assignment will identify the location of the closest input pixel, then will assign the value of the nearest input pixel to the output pixel. Nearest neighbor sampling has the least apparent impact, copying actual data values to the output image. However, this technique may induce high frequency artifacts, causing edges to appear in the direction of sampling. Nearest neighbor resampling should be used for multi-band images. During processing, the relationship between bands is preserved, allowing more accurate crossband operations(Jensen ,1996).

(ii) Bilinear resampling : Bilinear interpolation identifies the four nearest input pixels to the location of an output pixel. The new value for the output pixel is a weighted average determined by the value of the four nearest input pixels and their relative position or weighted distance from the location of the center of the output pixel in the input image. The bilinear interpolation reduces the high frequency component of the image, blurring sharp edges. It is preferred for continuous surfaces and smoothly varying images. Elevation, temperature, air pressure, gravitational or magnetic field can be represented as continuous smooth images, and are most appropriately resampled using bilinear interpolation. Bilinear resampling is not suitable for crossband processing. During 2dimensional interpolation the relationship between the two bands can be altered undesirably(Jensen ,1996).

(iii)Cubic convolution resampling : Cubic convolution uses the 16 nearest input pixels to determine the output pixel value. A smooth surface specified by a two dimensional (2-D) third order polynomial equation is fitted through the input pixels to find the value at the output pixel center. Cubic convolution tends to smooth the data more than bilinear resampling method. Cubic convolution may considerably distort the original data, and is not recommended for rigorous calculations. But it can be used to enhance data for visual display (Jensen ,1996).

2.10 RADARSAT-2 (RS-2)

SEASAT SAR observed the earth only 105 days and L-band one polarization (HH) 23.5 in wavelength has opened the door for using satellite for imaging radar and earth study. SIR-A in 1981 and SIR-B in 1984, the European ERS-1 and 2 in 1992 and 1995, the Japanese JERS-1 in 1992, as well as the Canadian RADARSAT-1 in 1995 and Japanese ALOS, the Canadian RADARSAT-2 in 2007, and the German TanDEM-X are the other satelliteswhich were used. In this thesis, RADARSAT-2 data for soil moisture measurements is investigated.

RADARSAT-2 is Canada's(CSA :Canadian Space Agency) and MDA (MacDonald Dettwiler Associates Ltd. of Richmond,BC)second-generation commercial Synthetic Aperture Radar (SAR) satellite and was designed with powerful technical advancementsthat provide enhanced information for applications such as environmental monitoring, ice mapping, resource mapping disaster management, and marine surveillance.Radarsat-2 left- and rightlooking modes provide more revisits and up-to-date information which reduce planning lead times for data acquisition (CSA, 2007).The various advances in Radarsat-2 technology allow many earth observation applications such as disaster management, agriculture, cartography, forestry, geology, hydrology, marine surveillance, ice studies and coastal monitoring (CSA, 2007). Data from Radarsat-2 has been used in disaster responses such as floods, earthquakes, tsunamis, landslides, and forest fires**.**

Radarsat-2 has a sun-synchronous orbit (a dawn-dusk orbit) with the ascending mode at 18:00 hours ±15 min local mean time and completes 14 orbits per day with a repeat cycle of 24 days. The average altitude of the orbit is 798 km with an inclination of 98.6° (CSA, 2007; Morena et al., 2004). Table 2.2 shows the orbit characteristics of Radarsat-2.New-generation RADARSAT-2 satellite was put into orbit on December 14, 2007 on the Russian Soyuz-FG carrier vehicle from the Baikonur launch site in Kazakhstan. RADARSAT-2 ensures the continuity of all RADARSAT-2 imaging modes. It has an extensive range of new features that improve resolution, polarization selection, tasking and data delivery. Significant improvements include a state-of-the-art phased array SAR antenna composed of hundreds of miniature transmit-receive modules. The antenna can be steered electronically over the full range of a swath and switched instantaneously between operating modes.The radar transmitter and receiver operate through an electrically steerable antenna(MDA, 2009). The transmitted pulses generated by the antenna are of constant amplitude and phase modulated waveforms for each range resolution and up-converted to 5.405 MHz are sent to the Antenna subsystem for transmission (Livingstone et al.,2005). Polarization can be controlled on H orVpolarization(Table 2.2).

Table 2.1: Satellite orbit parameter for RADARSAT-2.

Satellite Orbit Parameter	
Orbit type	Polar sun-synchronous
Altitude	798km
Inclination	98.6 degrees
Rotation period	100.7 min
Repetivity	24 days

Table 2.4 : SAR operation mode for RADARSAT-2.

Satellite Operation Parameter	
Frequency range	C-band (5.405 GHz)
Channel bandwidth	11.6, 17.3, 30, 50 ,100 MHz
Channel polarization	HH, HV, VH, VV
SAR antenna dimensions	15m x 1.5m

There are different types of files included within RADARSAT-2 products. The basic product as generated by the RADARSAT-2 processor contains a Product Information File(ASCII file) and one or more Image Pixel Data Files. The composition of RADARSAT-2 products is shown in **Figure 2.6**.

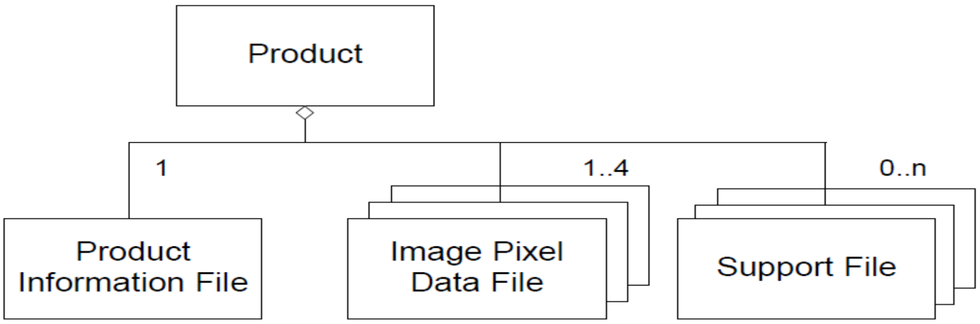

Figure 2.6 : File format in RADARSAT-2.

The product file is organized in hierarchical layers, with the basic product layers being supplied by the RADARSAT-2 processor. The product file is hierarchy mod and contain source attributes (Radar parameters, raw data attributes, orbit and attitude),image generation parameters(slant range to ground range, Doppler centroid ,Doppler rate values ,..), image attributes (raster attributes,geographic information) information. Product files of RADARSAT-2 data that was used in this study was shown in Appendix D and Appendix E.

The RADARSAT-2 SAR instrument may be operated in one of three mods: Single beam, Scan SAR, SpotlightFigure 2.7 (Url-3).It obtains data in three polarization configurations: single,dual and quad polarization,Table 2.4(Url-3).

Table 2.5 : Radarsat-2 beam modes and products (MDA, 2009).

Beam Mode	Resolution (m)	Scene size (kmxkm)	Incidence Angle(^{0})	Number of looks	polarization
Spotlight	1	18x8	20-49	1x1	SSP
Ultrafine	3	20x20	20-49	1	SSP
Multi-look fine	8	50x50	30-50	2x2	SSP
Fine	8	50x50	30-50	1x1	SSP or SDP
Standard	25	100x100	20-49	1x4	SSP or SDP
Wide	30	150x150	20-45	1x4	SSP or SDP
Scan SAR Narrow	50	300x300	20-46	2x2	SSP or SDP
Scan SAR wide	100	500x500	20-49	4x2	SSP or SDP
Extended high	25	75x75	49-60	1x4	SP
Extended low	25	170x170	10x23	1x4	SP
Fine quad-pol.	8	25x25	18-49	1x1	QP
Standard quad-pol	25	25x25	18-49	1x4	QP

Note:

1. SP: Single polarisation - HH.
2. SSP: Selective single polarisation - HH or HV or VV or VH.
3. SDP: Selective dual polarisation - HH+HV or VV+VH.
4. QP: Quad polarisation - HH+HV+VV+VH acquired (full polarimetric).

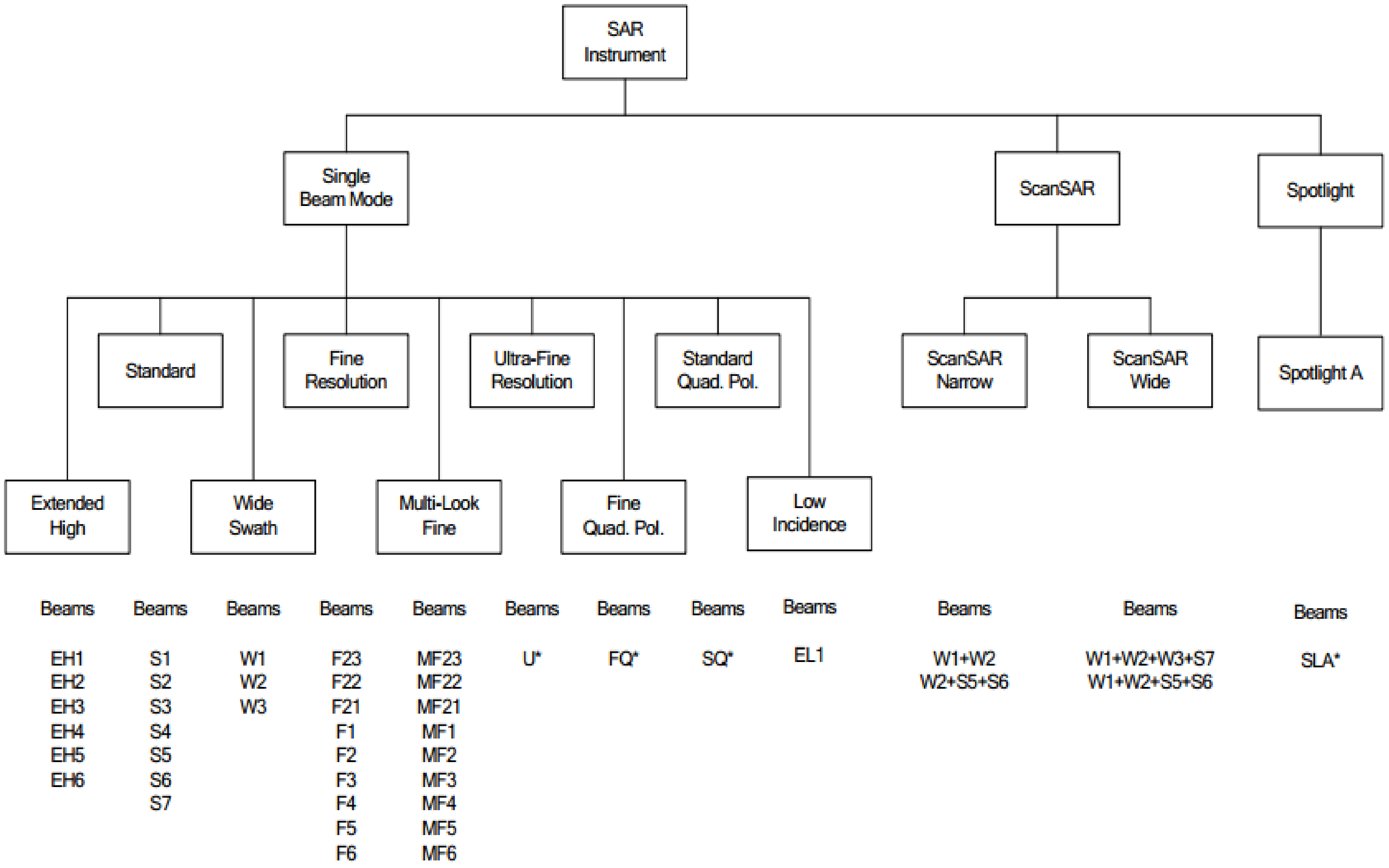

Figure 2.7 :RADARSAT-2 SAR instrument modes.

3. SOIL SURFACE PHYSICALPROPERTIES

3.1 Purpose

Estimating soil moisture is dependent on many parameters. These parameters generally have been divided into two major categories: the parameters of the survey instrument that includes wavelength effect, incidence angles,polarization methods and the parameters of surface.

Active sensors measure, particularly Synthetic Aperture Radar (SAR) offering high resolution images (<100 m), the backscattering coefficient σ^0 of soil surfaces which depends on both roughness and moisture characteristics(the geometrical and the dielectric properties).The influence of surface roughness on the scattering process limits the ability to correctly estimate volumetric soil moisture values unless detailed roughness measurements are acquired(A´ lvarez-Mozos etal.,2005). Roughness is most frequently characterized by three parameters: RMS height, correlation length and an autocorrelation function.Using these parameters about the soil, types of soil are estimateddue, first of all, to the fact that it is important to define what soil is.As will be shown after, obtained parameters from soil roughness study will be used as measurements of soil moisture.

Surface roughness and vegetation reduce the ability of instruments to accurately determine soil moisture values.The effect of surface roughness and vegetation in soil moisture estimation from passive microwave radiometers is much lower than that of active radar. However, the spatial resolution of the microwave radiometers is also much lower than SAR system's resolution.

In various studies, soil surface was defined in different scales like the top 2.5, 5, 10 or 15 cm (Snell et al., 1950; Bond and Willis, 1971; Shaver et al., 2002).In Radar studies soil surface scale is function of the given radar band (Ulaby et al., 1982b).

The purpose of this chapter is to outline the main parameters that characterize the dielectric and geometric behavior of natural soil surfaces,and to review briefly the physical and chemical processes.

3.2 Soil Water Content

In soil studies, soil is detined as a heterogeneous multiphase porous system with three natural phases. Soil particles are one of these phases and classified according to grain size ,sand, silt and clay. Soil texture triangles are used to show sand, silt and clay percent in the selected soil, Figure 3.1. The percentageof soil particles is important to estimate of soil type. Soil water and soil air are another phases of soil matrix. The amountof soil water to soil air are measured in relation to soil texture.

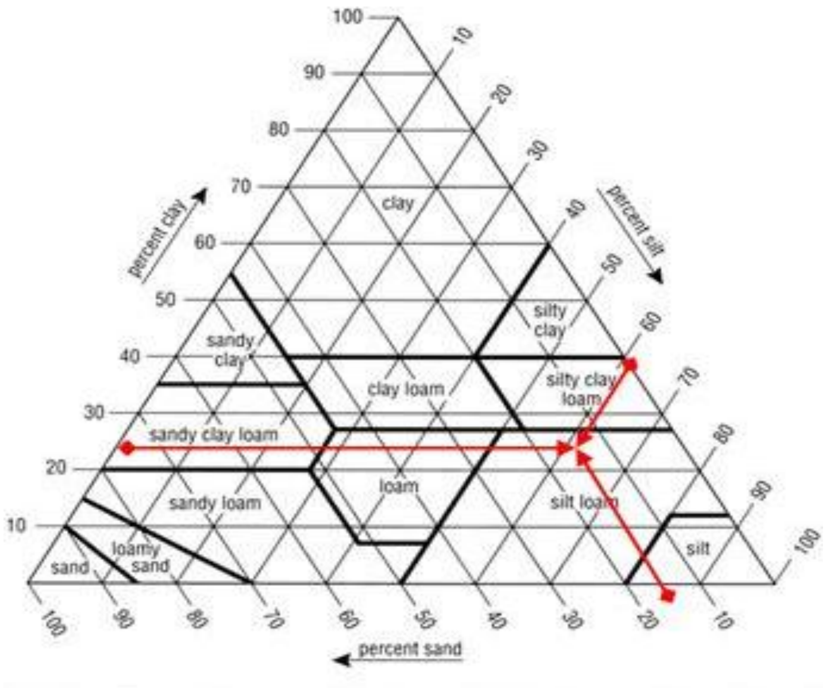

Figure 3.1 : Soil texture tiangle(sand17%, silt 61%, clay24%: slit loam).

In the soil matrix, the water amount within the soil is represented by the volume and mass fraction as presented in Equation 3. and Equation 3.2.:

Water content, volume fraction $m_v = V_w / V_t$ **(3.1)**

Water content, mass basis $R_m = M_w / M_s$ **(3.2)**

Where V_w is the volume of water in soil , V_t is the total volume of soil,Figure 3.2, m_v is the volumetric soil moisture and R_m is the dry mass of the soil.

If all soil pores are filled with water the soil is said to be saturated. There is no air left in the soil .Water saturation is the ratio of water volume to pore volume. This factor is on another definition to explain water amount within soil matrix. It is given by :

$$\text{Degree of saturation} S = V_w / V_v \qquad \textbf{(3.3)}$$

By combining Equation(3.1) and Equation(3.2)is obtained by the new equation (Equation (3.4).That was useful in the field study,by following this equation, conversion from the mass basis to the volume fraction is possible.

$$Rv = Rm\rho_b / \rho_w \qquad \textbf{(3.4)}$$

In Equation(3.4),it is assumed that the density of water is unaffected by being adsorbed in soil so that m_v / V_l is equal to ρ_w, the density of pure free water. The volume fraction, R, is equivalent to a depth fraction representing the ratio of the depth of water to the depth of the soil profile that contains it. This form is used when examining gains and loss of water in the field, because precipitation and evaporation are also expressed as depth of waters (Gardner, 1986).

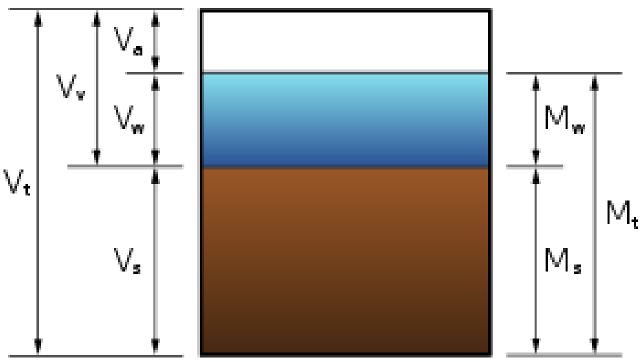

Figure 3.2 : Soil composition by phase: s-soil (dry), v-void (pores filled with water or air), w-water, a-air. V is volume, M is mass.

The moisture content as a volume fraction ranges between zero at oven dryness and a maximum value at pore space saturation. In agronomic and hydrological applications, two intermediate stages are commonly recognized during the drying of wet soils. (i) The wetter stage is known as the field capacity expressing the water content found when a thoroughly wet soil has drained for about 2 days. (ii) The so-called permanent wilting point, constituting the dryer stage, expresses the moisture content found when plants wilt and do not recover (Scheffer and Schachtschabel, 2002).

3.2.1 Properties of water

The molecule of water contain two hydrogen and one oxygen atoms. The connection of single electron of each hydrogen to the oxygen atomscausing a positive charge on bothhydrogen atoms. Because the two hydrogen atoms are arranged towards one side of theoxygen atom, water acts as an electrical dipole with a positive pole at the hydrogen atomsand a negative pole at the oxygen atom. Furthermore, a molecule of water can connect with another water molecule through hydrogen. Because of its strongly polarized molecular structure, water usually has unusual properties and becomes a the special liquid.

In a review on the structure of water,Némethy (1966) shows that, the effect of hydrostatic pressure on the viscosity of a liquid should increase with pressure. However, in water, it first decreases and only after applying sufficient pressure it reaches normal values.This is because of the fact that the clusters of hydrogen-bonded molecules are progressively eliminated by increased the pressure up to the point that water behaves like a normal liquid. In addition, among the various unique properties of water, is its high surface tension and its heat capacity.Another unusual properties of water are boiling point and freezing point ,surface tension, heat of vaporization, and vapor pressure ,viscosity and cohesion. More details are in Cracolic at el.,2006 paper.

Another one of the unique properties of water is known as electrostriction. Since the centers of positive and negative charges are separated in the molecule, water molecules are attracted and oriented by the electrostatic field of a charged ion resulting in the hydration of solute ions. As evidence of the rearrangement of water molecules accompanying hydration, it can be observed that the overall volume is commonly reduced when adding salt to the water.The phenomenon of hydration can also occur in soils.Hydration of ions in soil build cations.Polarized water molecules are interact with these cotions and it is a major mechanism in water absorption at the first stage of soil wetting(Marshall et al.,1999).

3.2.2 Complex dielectric constant

At first time, in the 1820s ,Michael Faraday, observed that non-conductive materials can also be influenced by electrical fields. The main parameter used in describing non-conducting materials in electrical field is called complex dielectric constant. Charged particles, under the impact of an external electrical field, are getting out of balance, while the free electrons of a conductor move until the electrical field inside the conductor vanishes. This only partially happens in dielectric, where the free charges are moving until the back force in the solid body equalizes the force affected by the external electrical field. Since, positive and negative particles are contrarily linked, they form electric dipoles. This process is also called dielectric polarization (Marshal*et al*. 1999). In other words, the dielectric constant shows the ability of the material in getting polarized when exposed to an electric field (Chudinova, 2009). When time elapses, the electric field changes and the dipole moment must align with the electric field again. However, loss of energy in the material causes a phase difference between the applied field and the dipole. In other words, the polarization does not happen immediately. For dielectric polarization some of energy is loss and some of them is reflected, because of these values usually the dielectric constant is treated as a complex number .

On other word when microwaves are incident on the surface of the earth, part of the energy is reflected, part is transmitted through the surface and rest is absorbed. Snellius law in the electromagnetic wave theory defines the real part of the complex dielectric constant as reflection of microwaves.Another part of the wave that is referred to dielectric loss (dielectric attenuation of a material) is noted by imaginary part at complex dielectric constant(Stratton, 1941; von Hippel, 1995b; Fannin et al., 2002).The dielectric constant and dielectric loss (complex dielectric constant parts) of a soildependent on numerous parameters, such as frequency, texture, temperature ,ferromagnetic substances and salinity of the soil. Complex dielectric constant ε is given by:

$$\varepsilon = \varepsilon' - j\varepsilon'' \qquad \textbf{(3.5)}$$

Where denotes the permittivity of material, while is show dielectric loss. Values for the dielectric constant typically range from 0 to 80.For microwave frequencies dielectric constant of free water is high (about 80) comparing to the water in soil (Ulaby et al., 1986). The imagery part of complex dielectric equation is factor of attenuation, assuming that the propagating electromagnetic energy has exponential attenuation,with depth, the penetration depth σ_p of the wave into a medium is denoted as the skin depth given by (Rees, 2001):

$$\sigma_p = \frac{\lambda\sqrt{\varepsilon'}}{2\pi\varepsilon''} \qquad \textbf{(3.6)}$$

For pure water the frequency dependency of thedielectric constant is given by the Debye equation as (Wang & Schmugge, 1980):

$$\varepsilon_{\omega} = \varepsilon_{\omega\infty} + \frac{\varepsilon\omega 0 - \varepsilon\omega\infty}{1 + j2\pi f_{\tau\omega\infty}} \quad \textbf{(3.7)}$$

Where ε_{w0} is a static dielectric constant of pure water and represents a high-frequency (oroptical) limit of ε_{w}. Both formulations are dimensionless. $\tau_{w}$is the relaxation time and is defined as the finite time (1/e) it takes a dipole to reach equilibrium when a field is applied or removed.. This parameter is measured in seconds and the electromagnetic frequency f is given in Hz (Debye,1929).

In many soil moisture measurement methods, such as empirical, theoretical or semi-empirical, dielectric constant plays an important part in the estimation process.

Several studies have shown that the sensitivity of the real part of the dielectric constantto changes in soil moisture is much higher than the imaginary part(Schmugge, 1985; Hallikainenet al., 1985; Ulaby et al., 1986).

There are several empirical and semi-empirical dielectric mixing models thatdescribe the ε ' dependence, based only on the volumetric water content, ortaking also into account the textural characteristic of the soil.Wensink model (Wensink,1993); Topp et al. (1980) are famous empirical models often used in many studies.In this study, the developed polynomial relation by Topp et al. (1980) of the third order was used for the conversion from the volumetric soil water content $m_v$to the real part of the dielectric constant $\varepsilon'$was used .

3.2.3 Soil mosture measurment

Methods for measuring the mass of the soil water have been already applied since the 15^{th} Century. There are many methods have beenpreferred in theestimation and evaluation of soil moisture but in soil moisture studies, all of the methods were divided into main groups, direct and Indirect methods (Stacheder, 1996; Marshall, 1999).

The direct methods include all measured processes in which the soil water is removed with evaporation, extraction, or chemical reactions.Gravimetric Soil Moisture is the most usual direct method to evaluate the water content of a soil sample and to estimate the mass difference before and after drying it in an oven at 150° C until a constant mass is reached.The mass difference $m_v$corresponds to the water loss of the sample during the drying process.

Indirect methods use the functional relations existing between the physical or chemical properties of the soil matrix and the moisture of the soil.Frequency Domain Reflectometry (FDR) and Time Domain Reflectometry(TDR) are two famous indirect method models.In TDR ,the electric capacitance in between two conductors, with the length of 15 cm, placed in the soil depends upon the water content of the soil because the dielectric constant of water (ε' ≈ 80) is electromagnetically muchlarger than that of the dry soil (ε' ≈ 3 to 5) or the air (ε' ≈ 1), which replaces the water as the soildries.The impedance of the rod array affectsthe reflection of the 100 MHz signal, and these reflections combine with the applied signal toform a voltage standing wave along the transmission line. The output of the probe is ananalogue voltage proportional to the difference in amplitude of this standing wave at twopoints forming a sensitive and precise measure of the soil water content (Gaskin and Miller, 1996). The output signal is 0 to 1 [V] DC for a range of soil dielectric constant between 1 and32, what corresponds to a moisture content of approx. 50 Vol.-%. Studies published overmany years by Topp et al. (1980), Heimovaara etal. (1996) show almost linear correlation between the square root of the dielectric constantand the volumetric moisture content for a wide range of soil types.

When rain or irrigation water is supplied to a field, it seeps into the soil. This process is called infiltration. Infiltration is related by soil texture in direct mode. The infiltration rate of a soil is the velocity at which water can seep into it. It is commonly measured by the depth (in mm) of the water layer that the soil can absorb in an hour. A range of values for infiltration rates is given as: Low infiltration rate (less than 15 mm/hour), medium infiltration rate (15 to 50 mm/hour) and high infiltration rate (more than 50 mm/hour).Soil temperature,soil depth, transpiration, soil topology and pattern of vegetation,wind direction and velocity, tillage kinds,soil water fallow direction (horizontal or vertical direction), and method are important factors that influenced infiltration and soil moisture content in different layers of soil (Tromp-van Meerveld and McDonnell, 2005).When soil moisture is plotted as a function of depth, there is normally a sharp discontinuity in the curve at the boundary between layers (see Figure 3.3).However in agricultural soil kind like loam,loam sandy soil moisture has inverse ratio in non- liner equation with soil depth. Steady state water flow in these kind of soil always to influence in depth layers .Water in these area try to go groundwater resource level (Hanks and Aahcroft, 1980).

However, water infiltration can be described by Darcy's law. The flow rate ($m.s^{-1}$) across a unit cross section (m^{-2}) of soil is:

$$q_x = -K_h.\ d(z+ p/\gamma_w)dx = -K_h.[dz/dx + d\ (p/\gamma_w)/dx] \quad \textbf{(3.8)}$$

$$q_z = -K_h.\ d(z+ p/\gamma w)dz = -K_h.[1 + d\ (p/\gamma_w)/dz] \quad \textbf{(3.9)}$$

Where q_x and q_z are the flow rates ($m.s^{-1}$) in the horizontal (x) and vertical (z) directions (z is taken here to increase upwards), respectively, $-K_h$ is the hydraulic conductivity ($m.s^{-1}$), p is the soil water pressure ($F.m^{-2}$, where F is force) and γ_w is the weight density of liquid water ($F.m^{-3}$). The weight density of water ($kg.ag.m^{-3}$, where ag is gravitational acceleration) is approximately a constant(Vincent at el., 2014).

In this study, for local measurement parameter for soil moisture,TARBİL measurement data were used directly, not using any of soil moisture measurements in practice.

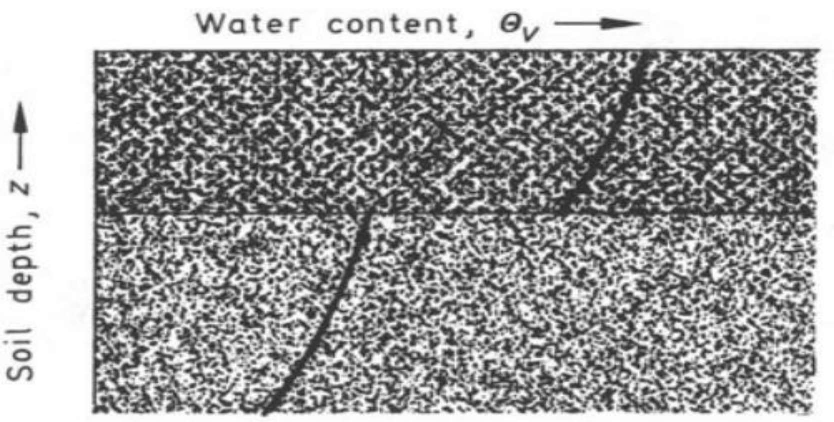

Figure 3.3 : The water contentcurve , the water contentcurve has a discontinuity at the boundry(Hanks and Aahcroft .1980).

3.2.4 Vegetation effect on soil moisture estimation

Several successful algorithms have been developed to estimate soil moisture of bare surfaces.When vegetation is present, soil moisture is typically underestimated by bare surfacealgorithms. The height and density of vegetation in the area also has direct influence in soil moisture estimation and sometime soil moisture estimation modelsfail in their accuracy and affect the estimation values if the flora is particularly dense in the subject area.

There are several method to estimate density of green on patch of land.NormalizedDifference Vegetation Index (NDVI) is a proportion that uses the visible and near-infrared bands of the electromagnetic spectrum, and is adopted to analyze remote sensing measurements and assess whether the target being observed contains live green vegetation or not(Moran et al., 2004). It has valid range between −1 to +1. In this range bare soil has values less than 0.2, moderate cover has values between 0.2 to 0.4.

$$NDVI = (REF\_nir - REF\_red)/(REF\_nir + REF\ red) \qquad \textbf{(3.10)}$$

This index is not suitable for RADARSAT-2 data. For RADARSAT-2 data usually RVI (Radar Vegetation Indices) is used. RVI generally ranges between 0 and 1 and is a measure of the randomness of the scattering. RVI is near zero for a smooth bare surface and increases as a crop grows (up to a point in the growth cycle), Equation 3.9.

$$RVI = \frac{8\,\sigma_{HV}}{2\,\sigma_{HV} + \sigma_{HH} + \sigma_{VV}} \qquad \textbf{(3.11)}$$

The Pauli RGB image can help to estimate covered area types.The Pauli color coding is based on a vector representation of linear combinations of scattering matrix elements. The resulting polarimetric channels HH+VV, HH-VV, HV are then associated to the blue, red and green colors respectively.

3.3 Surface Roughness

3.3.1 Statistical description of rough surfaces

In the geometric properties of a soil surface, it is important to understand thatthe solid phase of soils is composed of particles with various shapes and sizes (Figure 3.1). These particles are packed together in different ways, and this packing may be dense or open. The soil structure may then be defined as the arrangement of the solid particles and of the pore space between them (Low, 1954).

In surface backscattering models, geometry of the object is described using the parameters of the roughness of the soil surface .Therefore , characterization of the roughness is an important factor in modeling the backscatter wave from the soil .Soil surface roughness also affects the estimation of a soil moisture.

Randomly rough surfaces are usually described in terms of their deviation from a smooth 'reference surface'. There are essentially two aspects describing the nature of a randomly rough surface: the spread of heights about the reference surface and the variation of these heights along the surface. A variety of equivalent statistical distributions and parameters may be used to parameterise these two surface properties. In these investigations, the parameter set of the root mean square height RMS, *s* and the surface correlation length, *l*, associated to the surface correlation function are considered the best for the parametric description of the natural surfaces. The RMS height, *s*, is used to describe the vertical surface roughness and is defined as the standard deviation of the surface height variation in cm.

$$\text{RMS}_{\text{height}} = s = \sqrt{\frac{1}{N-1}\left[\left(\sum_{i=1}^{N} \text{Zi}^2\right) - \text{N}\bar{\text{Z}}^2\right]} \qquad \textbf{(3.12)}$$

Where N is f discrete steps along the transect, Zi is a single measurement, and $\bar{\text{Z}}$ is the mean of measurements. If $\text{RMS}_{\text{height}}$ = S> λ in result will be shown as rough surface and $\text{RMS}_{\text{height}}$ =S <λ in result will be shown as slightly rough surface.

On the other hand, the surface correlation function *ρ (x)* and the associated correlation length, *l,* are parameters used for the horizontal description of the surface roughness. In the discrete case, the normalised surface correlation function for a spatial displacement h=j$\Delta x$is given by:

$$\rho(h) = \frac{\sum_{i=1}^{N-j} \text{Zi Zi+j}}{\sum_{i=1}^{N} \text{Zi}^2} \qquad \textbf{(3.13)}$$

Where $\text{Zi} + \text{j}$is a point with the spatial displacement from the point *xi* (Fung 1994). The surface correlation length is defined as the displacement h for which$\rho(h)$between two points inhibits values smaller than 1/e (Euler's Value ≈ 2.7183).

$$\rho(l) = \frac{1}{e} \qquad \textbf{(3.14)}$$

In many studies, correlation parameter l is always neglected and it was made an error in results,Zribi and Dechambre,(2003). The proposed parameter Zs is include of h and l parameter:

$$Zs = S^2/l \quad \textbf{(3.15)}$$

Small values of Zs correspond to small values of s and/or large values of l. Large values of Zs correspond to large values of s or small values of l. A smooth soil surface corresponds generally to a small value of s and a large value of l and thus to a small Zs. A ploughed soil corresponds often to a large s and a medium to large l, and then to a medium to large Zs. A cloddy soil, even with a small s, corresponds to a small l and thus to a large Zs (Zribi and Dechambre,2003).

In many studies,for scattered EM was shown as a function that actually depend onwavelength λ.However, k is new factor k define as:

$$k = \frac{2\pi}{\lambda} \quad \textbf{(3.16)}$$

Ks (s, RMS $_{height}$ factor) and kl (surface correlation length,l) have compensatory effect in surface roughness studies .

Surface roughnessmeasurement techniques can be classified by measurement dimension and sensing type. The former includes two- dimensional (2D) profile measurements and three-dimensional(3D)measurements(usually elevation points in a regular raster).2D measurements facilitate quick data acquisition with simple means like a roller chain. Therefore, they are widely used in field investigations, although surface characterization is limited to indices with little physical meaning. 3D measurements give amore realistic surface representation, and allow the calculation of physical surface parameters. Concerning the surface sensing procedure, essentially two types of measurement techniques exist – contact and noncontact.More data about technics are featured in a paper by Werner and Klik, 2005.

3.3.2 Electromagnetic scattering from rough surfaces

All natural surfaces can be considered as rough, and this roughness is considered as the dominant factor for the scattering behavior of an EM wave from this surface (Stratton,1941). Soil surface roughness is not an intrinsic value.However, the soil surface roughness is defined by the amount of reflected electromagnetic waves on the surface.Both the frequency and the local incidence angle (LIA) of the incoming plane wave determine how smooth or rough a surface appears to be. The roughness term in radar science depends on the given wavelength, so that its appearance changes with the various frequencies. That is, at lower frequencies, the surface of an illuminated target appears smoother than at higher frequencies.To compensate for the effect of this factor, the RMS height 's' is scaled to the actual wavelength using the wavenumber k (2π/λ) with the following equation:

$$KS = S \times (2\pi/\lambda) \quad \textbf{(3.17)}$$

For smooth, unforestedsoil, reactivity can be related todielectric constant through Fresnel equationsΓ (Engman et al., 1995; Zheng et al., 2010;Ulaby et al., 1981b). Fresnel's equations describe the reflection and transmission of electromagnetic waves at an interface. That is, they give the reflection and transmission coefficients for waves parallel and perpendicular to the plane of incidence. For a dielectric medium where Snell's Law can be used to relate the incident and transmitted angles, Fresnel's Equations can be stated in terms of the angles of incidence and transmission.Fresnel's equations give the reflection coefficients as shown in Equation 3.18andEquation 3.19.

$$R_{||} = \frac{\mu \cos\theta - \sqrt{\mu\varepsilon - \sin^2\theta}}{\mu \cos\theta + \sqrt{\mu\varepsilon - \sin^2\theta}} \quad \textbf{(3.18)}$$

$$R_{\perp} = \frac{\varepsilon \cos\theta - \sqrt{\mu\varepsilon - \sin^2\theta}}{\varepsilon \cos\theta + \sqrt{\mu\varepsilon - \sin^2\theta}} \quad \textbf{(3.19)}$$

Where $R_{||}$ and $R_{\perp}$ represent thevertical and horizontal polarizations of the EM wave, ε' is the dielectric constant and θ is incidence angle (Wang, 2008). The variable μ is always equal to one for non-ferromagnetic media. The response of the horizontal polarization increases with increasing LIA, while the vertical polarization decreases to zero at a certain incidence angle. At this angle, known as Brewster angle, the transmitted wave is absorbed completely by the illuminated dielectric medium. With further increased LIA, however,$R_{||}$ suddenly increases again (Fung, 1994).

In constant wavelength at a fixed LIA, tested incoming wave from differently rough surfaces it is shown that the Fresnel reflectivity is valid only for a perfectly smooth surface boundary.

Qualitatively, the relationship between surface roughness and surface scattering can be illustrated through the example shown in Figure 3.4.As shown in Figure 3.4 parts the angular radiation pattern consists of two components: a reflected component and a scattered component. For the specular surface, the angular radiation pattern of the reflected wave is a delta function centered around the specular direction as shown in Figure 4.3 (a). But in the slightly rough surface the reflected component is the specular direction again. As shown in Figure 3.4 (b) in this surface magnitude power is smaller than for smooth surface.This specular component is often referred to as the coherent scattering component. The scattered component, also known as the diffuse or incoherent component, consists of power scattered in all directions, but its magnitude is smaller than that of the coherent component. As the surface becomes rougher, the coherent component gets poorer (Ticconi at el., 2011).

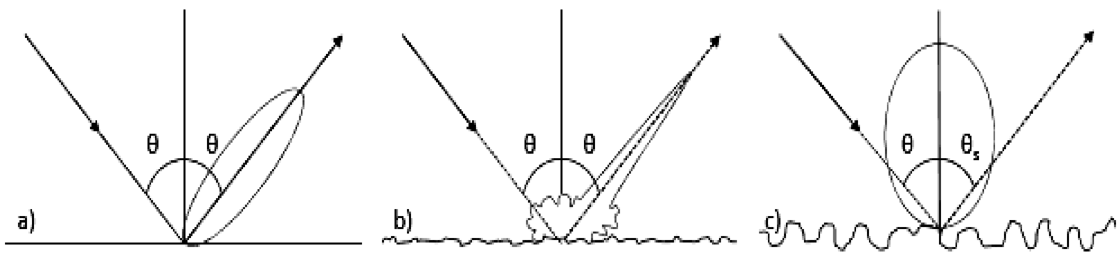

Figure 3.4 : Characterization of roughness components: (a) smooth, (b) slightly rough, and (c) very rough surfaces.

As shown in section2.3, the degree of roughness or smoothness of soil surface depends on wavelength of the wave which is used to sense the soil and on incidence angle. Same surface roughness mode, is variable in different wavelength. In the case of a plane monochromatic wave impinging at some angle θ upon a rough surface (Figure. 3.5), the phase difference $\Delta\varphi$ between two rays scattered from separate points on the surface can be calculated in a simple manner with(Ulaby et al., 1982b):

$$\Delta\varphi = 2h\frac{2\pi}{\lambda}\cos\theta \qquad \textbf{(3.20)}$$

Where h is the standard deviation of the roughness height from a reference height and θ is the local incidence angle .

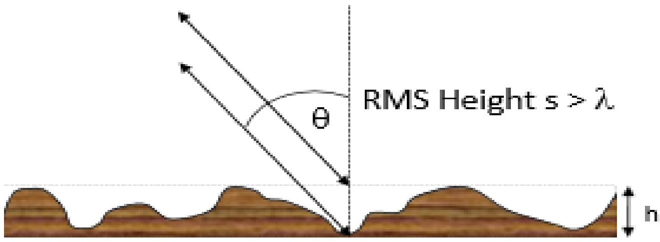

Figure 3.5 : Scheme for the determination of the phase difference between two parallel EM waves scattered from different points on a rough surface.

The Rayleigh criterion defines that a surface can be given by:

$$\Delta\varphi < \frac{\lambda}{\cos\theta} \qquad \textbf{(3.21)}$$

where λ is the wavelength and θ is the incidence angle.This criterion is considered as a useful first-order classifier of surface roughness or smoothness.

However, there is also a stricter criteria called the Fraunhofer criterion which is stated as (Ulaby et al., 1982):

$$\Delta\varphi < \frac{\lambda}{32\cos\theta} \qquad \textbf{(3.22)}$$

According to these criteria, waves with longer wavelengths are more tolerant of changes in surface height.An the other hand, surface roughness is amore serious factor in soil moisture study then using L-band is the better and more suitable.

4. SEMI-EMPRICAL MODELS FOR SOIL MOISTURE ESTIMATION

4.1 Purpose

A many new models for estimate and evaluation soil moisture by using remote sensing instruments data have been developed in the last decades.In this chapter, will give data about semi-empirical models that was used in study.In this chapter was used PolSARpro help formatto explain the models.

4.2 Semi-Empirical and Empirical Models

Semi-empirical models are based on theoretical scattering models and extend or modify these according to empirical observations.Numerous semi empirical models have been reported in different study .Here,Oh et al. (1992),Oh et al. (2004) and Dubois et al. (1995)will be explained .

4.2.1 Semi-empirical model using Oh et al. (1992)

4.2.1.1 Model description

Y. OH, K. Sarbandi, and F.T. Ulaby developed this semi-empirical model at the University of Michigan, in 1992. The radar measurements used for its development were obtained by a truck-mounted scatterometer (LCX POLARSCAT) operating at three frequencies (1.5, 4.5 and9.5 GHz) in a fully polarimetric mode with an incidence angle range from 10° to 70°. On the basis of the scatterometermeasurements and ground measurements, an empirically determined function for theco- and cross-polarised backscatter ratios was proposed (OH *et al*. 1992).

According to the Ohstudy, the relationship between selected fields measurements and scatterometer data as an empirically determined function for the co- and cross polarized backscattering ratios was proposed.Cross –polarization ratio was given by:

$$q=\frac{\sigma_{hv}^{0}}{\sigma_{vv}^{0}}= = 0.23\sqrt{\Gamma_0}[1-exp(-ks)] \qquad \textbf{(4.1)}$$

The cross-polarized ratio q << 1, shows – as compared to the co-polarized ratio - a stronger sensitivity to ks variations and a weaker dependency to soil moisture variations. q increases with increasing ks up to ≅1 and converges slowly to a value, which depends on the soil moisture content and finally reaches it for ks > 3. A significant sensitivity of the quotient q to surface roughness and no dependency on the incidence angle can be observed, respectively. Cross –polarizatin ratio was given by:

$$\sqrt{p}= \frac{\sigma_{hh}^{0}}{\sigma_{vv}^{0}}= 1-\left(\frac{2\theta}{\pi}\right)^{\left(\frac{1}{3\Gamma_0}\right)} exp(-ks) \qquad \textbf{(4.2)}$$

The co-polarized ratio p is always lower than one for all local incidence angles. It increases monotonically with increasing ks up to ks ≅ 1 and converges slowly to one, which finally reaches for ks > 3. On the other hand, for ks < 3, p decreases with increasing local incidence angle and/or with increasing soil moisture content. A significant sensitivity to soil moisture and incidence angle variations can be observed.

Γ_0 is the Fresnel reflectity of the surface at nadir (i.e. θ = 0).

$$\Gamma_0 =\left|\frac{1-\sqrt{\varepsilon'}}{1+\sqrt{\varepsilon'}}\right|^2 \qquad \textbf{(4.3)}$$

Validity Range of the Oh Model is, incidence angle is limited (10≤ θ ≤70), surface roughness parameter ks is limited 0≤ks ≤2.01 and 9% ≤m_v≤ 31%.

4.2.1.2 Model inversion

The inversion of the Oh-Model is based on the solution of Equation (4.1) and Equation (4.2) for ks and ε′,Equation (4.4). In the absence of an analytic solution, ks and ε′ have to be estimated by an iterative procedure. In a first step, Γ° is evaluated from p and q after eliminating ks.

$$\left(\frac{2\theta}{\pi}\right)^{\left(\frac{1}{3\Gamma_0}\right)} [1-\frac{q}{0.23\sqrt{\Gamma 0}}]+\sqrt{p}-1 = 0 \ , \qquad \textbf{(4.4)}$$

Where by using Equation (4.4):

$$\varepsilon' = \left|\frac{1-\sqrt{\Gamma 0}}{1+\sqrt{\Gamma 0}}\right|^2 \quad \textbf{(4.5)}$$

The obtained values for ε′ are converted into m_v values after TOPP *et al*. (1980), Equation (4.6).

$$m_v = -5.3\times10^{-2} + 2.99\times10^{-2}\varepsilon' - 5.5\times10^{-4}\varepsilon'^2 + 4.3\times10^{-6}\varepsilon'^3 \quad \textbf{(4.6)}$$

4.2.2 Semi-empirical model uing Oh et al. (2004)

4.2.2.1 Model description

OH at 2004 suggested new expression for p and q and the cross-polarized backscattering coefficient (Oh et al., 2004):

$$p = 1 - \left(\frac{2\theta}{\pi}\right)^{0.35 m_v{}^{-0.65}} e^{-0.4(ks)^{1.4}} \quad \textbf{(4.7)}$$

$$q = 0\cdot095\ (0.13 + sin1.5)^{1.4}\left[1 - exp[-1\cdot3(ks)^{0\cdot9}]\right] \quad \textbf{(4.8)}$$

$$\sigma^0_{vh} = 0.11 m_v{}^{0.7}\,(cos\,\theta)^{2.2}\left(1 - e^{-0.32(ks)^{1.8}}\right) \quad \textbf{(4.9)}$$

Where *p* and *q* indicate the co- and cross polarized backscatter ratios, respectively; is the local incidence angle, is the RMS height normalized to the wavelength, *ks* and m_v is the volumetric water content.

Validity Range of the Oh Model is, incidence angle is limited (10≤ θ ≤70), surface roughness parameter ks is limited 0.13< ks <6.98 and $4 \le m_v \le 29.1$

4.2.2.2 Model inversion

An inversion diagram is generated combining Equation (4.7) and Equation (4.9) for a frequency and an incidence angle to retrieve and from measured *s*, m_v, σ^0_{vh} and *p*. In the absence of analytic solution, and have to be estimated by an iterative procedure. In a first step, Equation (4.9) is solved for the estimate of ks.

$$Ks(\theta, m_v, \sigma^0_{vhm}) = [-3.125\ln\{1 - \frac{\sigma^0_{vhm}}{0.11 m_v{}^{0.7}(cos\theta)^{2.2}}\}]^{0.556} \quad \textbf{(4.10)}$$

Where σ^0_{vhm} is the measurement of the vh-polarized backscattering coefficient and m_v is the estimate of the soil moisture content to be determined.

By substituting Equation (4.10) to Equation (4.7), we obtain the following nonlinear equation for m_v

$$1-\left(\frac{2\theta}{\pi}\right)^{0.35m_v{}^{-0.65}} e^{-0.4}\,[\mathrm{Ks}(\theta, \mathrm{mv}\,, \sigma^0_{vhm})]^{1.4} - p = 0 \qquad \textbf{(4.11)}$$

The initial value of m_v can be set to 0.5, which is reasonable and give good results.

After solving Equation (4.11**)** using iterative method, m_v can be obtained, and the rms height s can also be obtained subsequently.

In a second step, the cross-polarized ratio q in the form of Equation (4.8) can contribute to finer accuracy of this inversion technique as follows. After obtaining estimate ks of from Equation (4.8),$m_v$can be computed either from Equation (4.7) and Equation (4.9).

A detailed block diagram in the figure shows the inversion algorithm. Only themeasurements satisfying $p<p_{\max}$are selected for the inversion, where$p_{\max}$ is computed with maximum s (5.5cm) and minimumm_v (0.01cm^3/cm^3).

Finally, the multiple estimates of the rms height and the volumetric water contentcan be averaged as:

$$s = \frac{(w_1\, s_1 + w_1 s_2\,)}{(w_1 + w_2)} \qquad \textbf{(4.12)}$$

$$m_v \;=\; \frac{(w_3\, m_{v1}\; + w_4\, m_{v2} + w_5\, m_{v3}\,)}{(w_3 + w_4 + w_5)} \qquad \textbf{(4.13)}$$

The values of weights, which give the best inversion results, are$w_1\,, w_2\,, w_3\,, w_4\,, w_5$ 1, 1.4,1,1,1, respectively.

4.2.3 Semi-empirical model using dubois et al. (1995)

4.2.3.1 Model description

The empirical model developed by P. C. Dubois, J. Van Zyl, and T. Engman in 1995 is considering only the two co-polarized backscatter coefficients. The data used in the original study, were collected with the scatterometer from the University of Michigan LCX as well as with the University of Bern scatterometer (RASAM) operating at six frequencies between 2.5 GHz and 11 GHz. In later investigations the algorithm was applied to SAR data (AIRSAR and SIR-C) in order to prove the robustness of the algorithm. In a first elaborative step, the dependence of the backscattering coefficient ratio on different soil moisture conditions and the local incidence angle was investigated. It was found that the relationship resembles most closely a tangent of the incidence angle. In a second step, the deviation caused by surface roughness was accounted for by an empirically derived expression for the roughness term log (ks ·sinθ). The resulting expressions are given by:

$$\sigma^0_{hh,} = 10^{-2\cdot75}\frac{cos^{1.5}\theta}{sin\theta^5}10^{o.028\varepsilon tan\theta}\,(kssin\theta)^{1.4}\lambda^{-0.7} \quad \textbf{(4.13)}$$

$$\sigma^0_{vv} = 10^{-2\cdot35}\frac{cos^{1.5}\theta}{sin\theta}10^{o.046\varepsilon tan\theta}\,(kssin\theta)^{1.1}\lambda^{-0.7} \quad \textbf{(4.14)}$$

Where θ is the incidence angle, ε is the real part of the dielectric constant, h is the RMS height of the surface, k is the wave number and λis the wavelength in cm. These two relations 1.5 <f <11 GHz, 30 <θ< 65 ,surfaces with roughness ranging from 0.3<ks<3 cm . Dubois et al. (1995) estimated the validity range for the surface parameters to bem$_v$<35 Vol.% and ks < 2.5. Their accuracy is stated as 4.2 Vol.-% for the soil moisture estimates and as ks of 0.4 for the surface roughness over bare soil. However, there are some important aspects, which are not considered by the Dubois model, such as the influence of the surface correlation length on the fields, or the influence of topographic variations on the accuracy of the estimates.

4.2.3.2 Model inversion

The inversion of the empirical algorithm addressed by DUBOIS *et al*. (1995) directly retrieves the dielectric constant and the surface roughness from the model using the co-polarised backscatter coefficient and the local incidence angle by using the following two stepinversion algorithm. The first step is to retrieve the surface roughness.

$$ks = \frac{\sigma^{0\ \ 1.3691}_{hh}}{\sigma^{0\ \ 0.8334}_{vv}}10^{1.79}(cos\theta)^{0.4465}(sin\theta)^{3.3454}\lambda^{-0.375} \quad \textbf{(4.14)}$$

$$\varepsilon' = \frac{log(\sigma^0_{hh})10^{2.75}(cos\theta)^{-1.5}(sin\theta)^5(kssin\theta)^{1.4}\lambda^{-0.7}}{0.028tan\theta} \quad \textbf{(4.15)}$$

For the discrimination of vegetated areas the VH/HH ratio may be used as a good vegetation indication. Ratio values of VH/VV > 0.079343282 (-11 dB) indicate the presence of vegetation, and such areas are masked out and remain unconsidered by the inversion. Asvery well pointed out in Dubois et al. (1995); this condition mask out very rough surface areas too, (***ks*** > 3), which leads to them being mistaken for vegetated areas, although such fields aretoo rough to be accounted for by the model and have to be excluded. The algorithm wasapplied only on areas where HH/VV < 1 and HV/VV < 0.079343282 (-11 dB) in order to consider only areas lying within the validity range of the model. For the estimation of thesoil moisture content the polynomial relation Topp*et al*. (1980) for the conversion from ε to mvis used.

5. STUDY AREA, METHODS AND MATERIALS

5.1 Purpose

In this chapter, the study area location and properties were shown; in addition, the methods and material used in different parts of research for obtaining acceptable results in the thesis were explained.

5.2 Study Area

The research was performed in the Harran in Sanliurfa, South-East of Turkey, A: 37° 6'7.53"N, 38°32'1.02"E, B: 36°38'43.87"N,38°39'5.07"E,C: 36°44'32.51"N, 39°14'39.64"E, D: 37°12'31.18"N, 39° 8'5.18"E (Figure 5.1).The area is composed of agricultural land.The cultivated agricultural area distribution is 99.6% of Harran region.In Sanliurfa agriculture map,the Harran region is irrigated area (Figure 5.2).The crops planted in the study area included wheat,barley, cotton, lentils, sesame, peas, watermelon, cumin, pepper, corn, tomatoes andeggplant, under a variety of tillage conditions .Wheat ,barley and cotton were the mains product in the study area.Cotton in aqueous conditions and wheat and barley products are cultivated mainly in dry conditions by using various methods of tillage.Farmlands were prepared in April.Most of the fields were seeded inMay and harvested in September. Researching about the study area was done in September (7^{th} and 8^{th} of September,2012);it means that during the study in most areas for the study, it was simultaneous harvest timeand this mean that farmlands were covered by different types of crops.

According to the T.C OrmanVe Su İşleri Bakanı Meteorolojy Genel Mudurlugu's report in 2013 reports, usually summers are hot and dry, while winters are relatively mild. The hottest period is July and August (sometimes temperature exceeds 40 degrees), while the months of December and January are generally the coldest. In thesemonths thedaytime temperatures range between12-14 degrees on some nights, thus rarely (0) can be reduced to the extent received. The region's rainfall is most abundant in the period October-April months. During September 2012, rainfall was generally less than normal. Monthly average rainfall is 13.1 mm, normal is 27.6 mm. Compared to the normal range, 52.6% is considered as a decrease in the precipitation observed(Figure 5.3). The soiltype in the Harran region is clay in most areas, and others are composed of a mixture of clay and sand.These kinds of soil types are more suitable to agriculture and shown as first level area in the classification of grade agricultural lands in the province of Şanlıurfa map (Figure 5.4). Finally, the amount of rainfall and temperature at different times of the 7th and 8th of September, 2012 was shown (Figure 5.5).

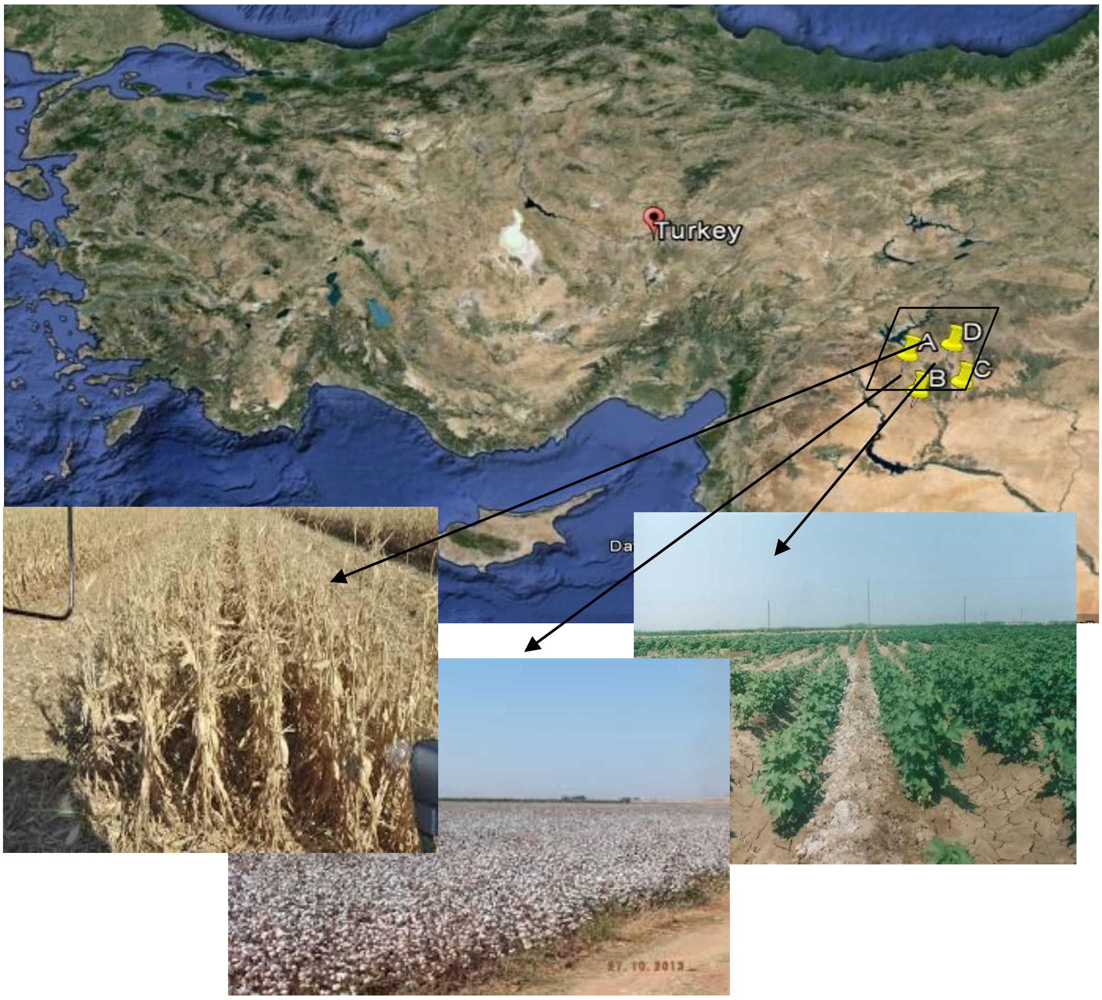

Figure 5.1 : Map of study area the Harran in Sanliurfa, South-East of Turkey location,and methods of tillage, types of crops.

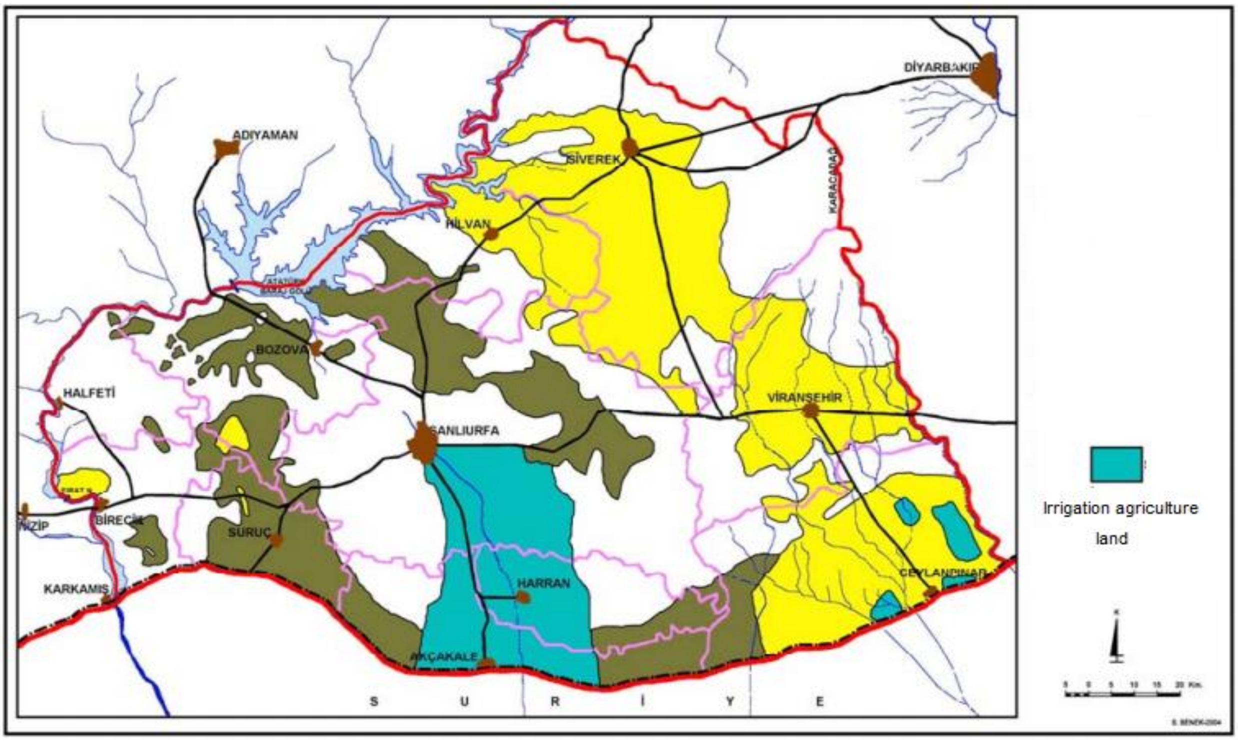

Figure 5.2 : Agricultural irrigation map in Sanliurfa.

Figure 5.3 : Precipitation anomaly map (September 2012).

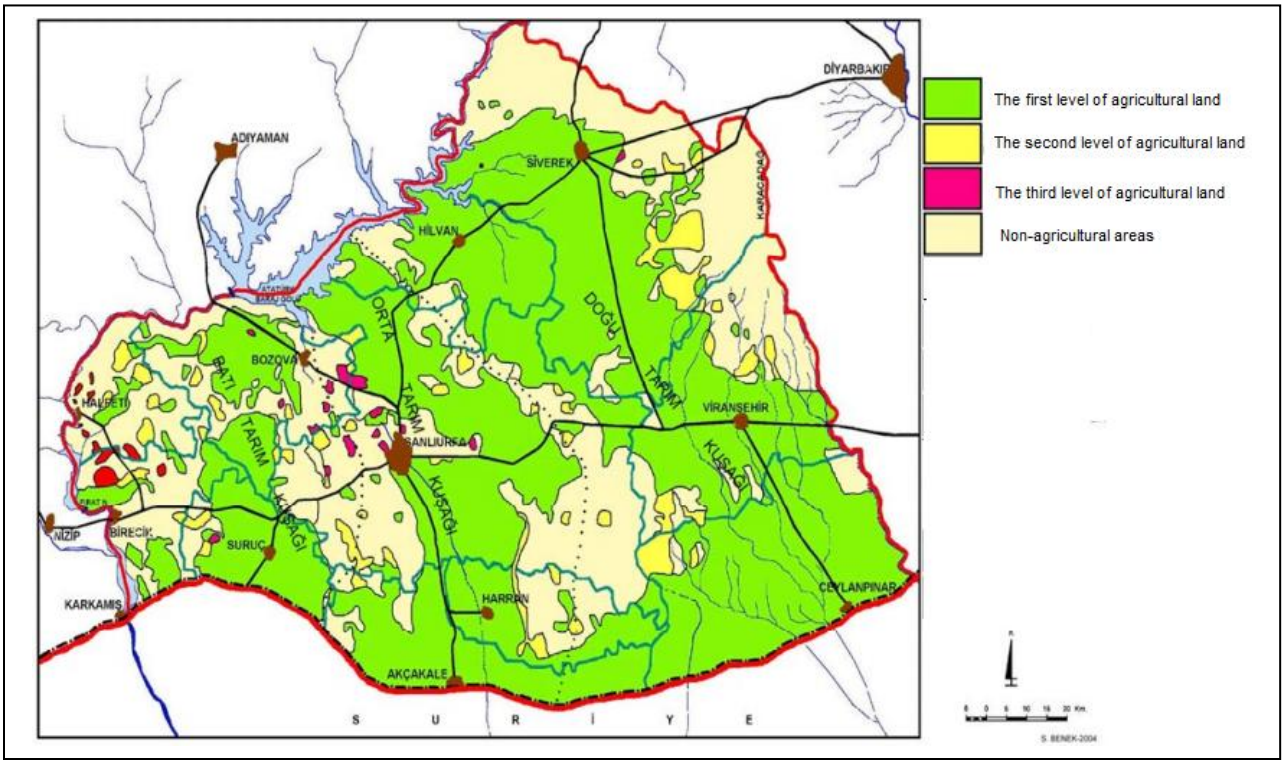

Figure 5.4 : Classified as grade agricultural land in the province of Şanlıurfa.

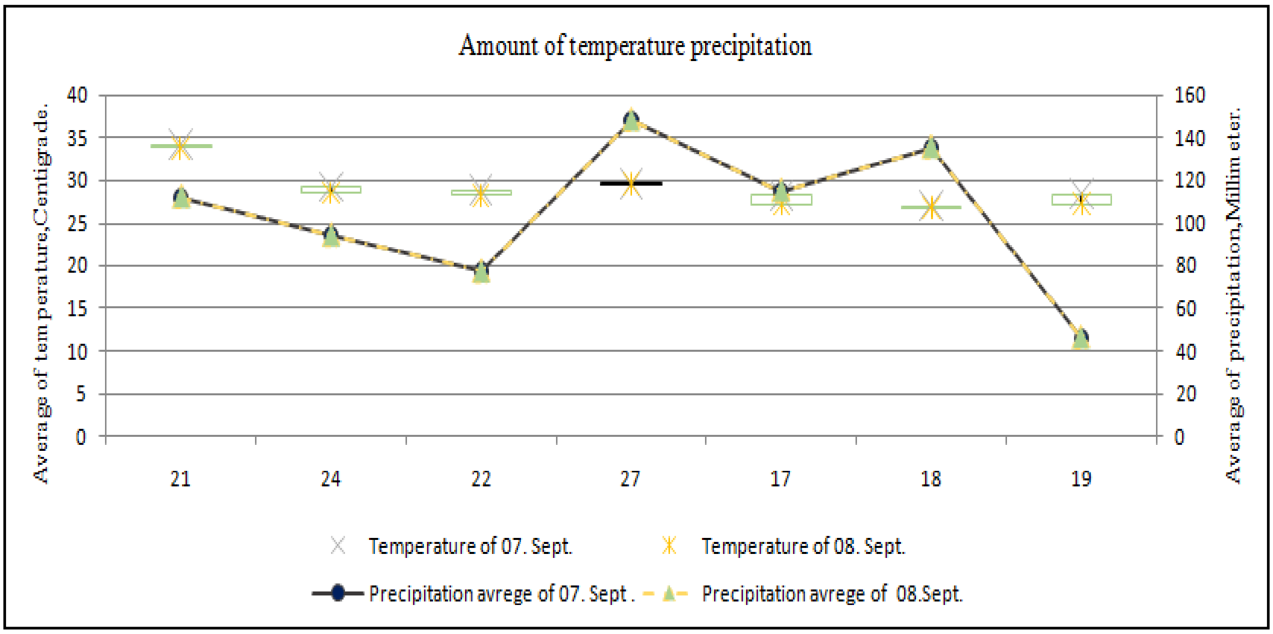

Figure 5.5 : Average of temperature on primary axis of 7th and 8th of September, 2012. Average of precipitation in second axis of 7th and 8th of September 2012. Precipitation values has been collected for each ten minutes in TARBİL.There are not any rainfall in two days.

5.3 Collection Data's Types

5.3.1 Local data collection method

For local study and measurement, data access was collected with TARBİL's(Agricultural Monitoring and Information System) as part of the project. As shown in (Table 5.1), was used, 11 local stations that were located in different coordinate of study area. In these stations,wind direction and speed, precipitation, and soil temperature and soil moisture in two different depths (15Cm and 40Cm) have been measured per 10 minute in each of which the result was shown as a number between 0-200. For showing full soil moisture, '200' was selected and '0' for completelydry areas(Table 5.2& Table 5.3).

Table 5.1 : TARBİL's (agricultural monitoring and ınformation system) station location that was used for collect ground measurements data.

Name	Coordinate	ID	Code
Yakacık	36.9019,38.9229	17	63.15
Rumi	36.9012,38.9207	18	63.16
Aydoğdu	36.9029,38.9198	19	63.17
Demirören	36.9034,38.9159	20	63.18
Tatnar	36.7242,38.9103	21	63.19
Akçatat	36.7222,38.9103	22	63.20
Gündöner	36.7464,38.8081	23	63.21
Akçagün	36.7484,38.8086	24	63.22
Eyyübiye	37.1237,38.8161	25	63.23
Külünçe	37.2116,38.1784	26	63.24
Poyralı	36.9196,38.7542	27	63.25

Table 5.2 : The moisture content (MC) is measured at local stations at different depths(07/09/2012 .15:10).

Name	Coordinate	MC/0-15Cm	MC/0-40Cm
Yakacık	36.9019,38.9229	139	199
Rumi	36.9012,38.9207	200	200
Aydoğdu	36.9029,38.9198	200	200
Demirören	36.9034,38.9159	---	---
Tatnar	36.7242,38.9103	31	75
Akçatat	36.7222,38.9103	127	108
Gündöner	36.7464,38.8081	---	---
Akçagün	36.7484,38.8086	30	36
Eyyübiye	37.1237,38.8161	---	---
Külünçe	37.2116,38.1784	---	---
Poyralı	36.9196,38.7542	200	200

Table 5.3 : The moisture content(MC) is measured at local stations at different depths (08/09/2012 .03:26)

Name	Coordinate	MC/0-15Cm	MC/0-40Cm
Yakacık	36.9019,38.9229	146	200
Rumi	36.9012,38.9207	200	200
Aydoğdu	36.9029,38.9198	200	200
Demirören	36.9034,38.9159	---	---
Tatnar	36.7242,38.9103	33	78
Akçatat	36.7222,38.9103	129	111
Gündöner	36.7464,38.8081	---	---
Akçagün	36.7484,38.8086	28	34
Eyyübiye	37.1237,38.8161	---	---
Külünçe	37.2116,38.1784	---	---
Poyralı	36.9196,38.7542	200	200

5.3.2 RADARSAT-2 data collection

The data used in this study consisted of two RS-2 scenes accompanied by coincident field measurements of soil moisture and surface roughness. Two single-look complex (SLC) fine quad-pol mode RS-2 scenes were acquired over the study area (Table 5.4).The images were taken at low incidence angles, ensuring their suitability for soil moisture detection and maximum penetration depth. In order to acquire the most images in a short time span, the images could not be taken with uniform orbits and incidence angles.Imagery footprints for two different beam modeswere shown in Figure 5.6, in addition raw data was shown in Figure 5.7and Figure 5.8 for 07. September and 08. September sequentially.

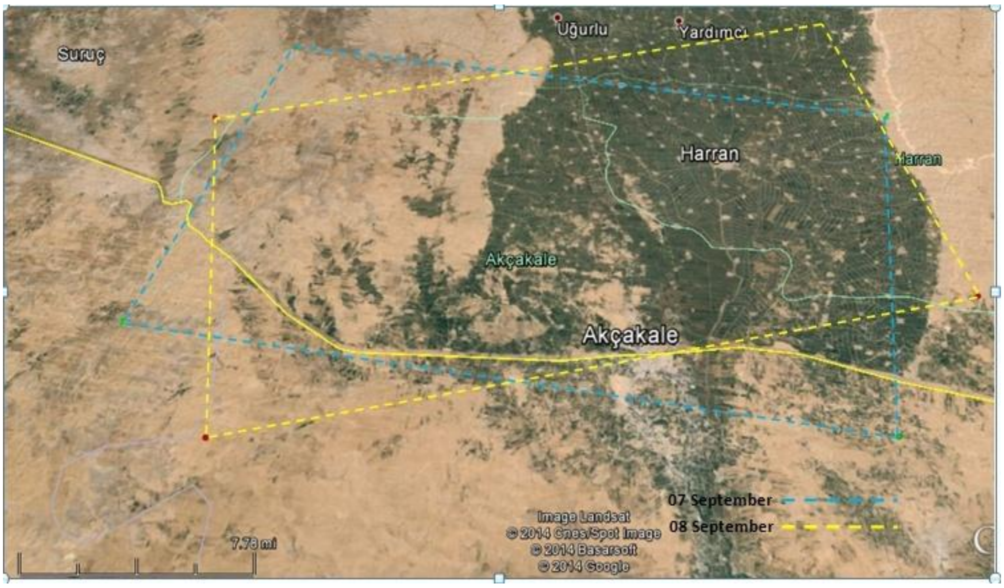

Figure 5.6 : Map of study area, imagery footprints are shown in dasheds line.

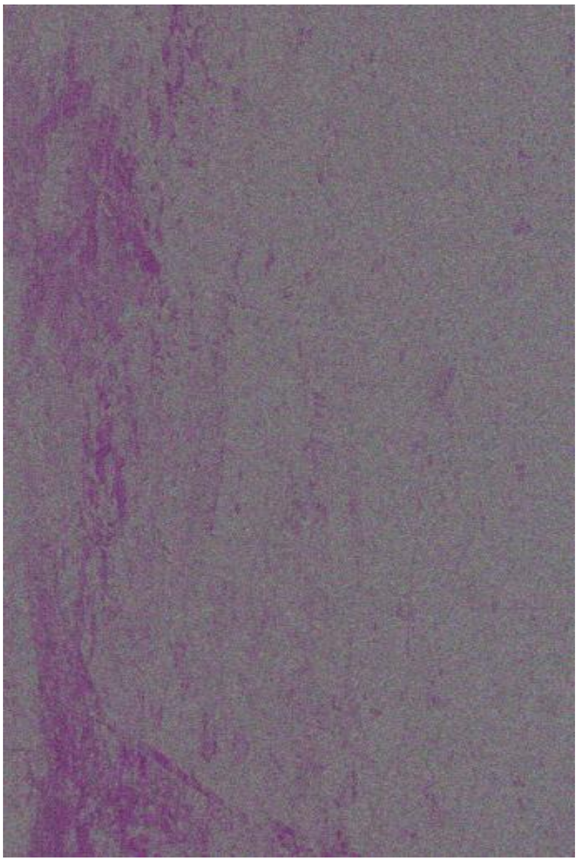

Figure 5.7 : RADARSAT-2 image for 07 September at study area the Harran in Sanliurfa, south-east of Turkey.HH image data on red band, HV image data on green band, VV image data on blue band (3488 × 6164).

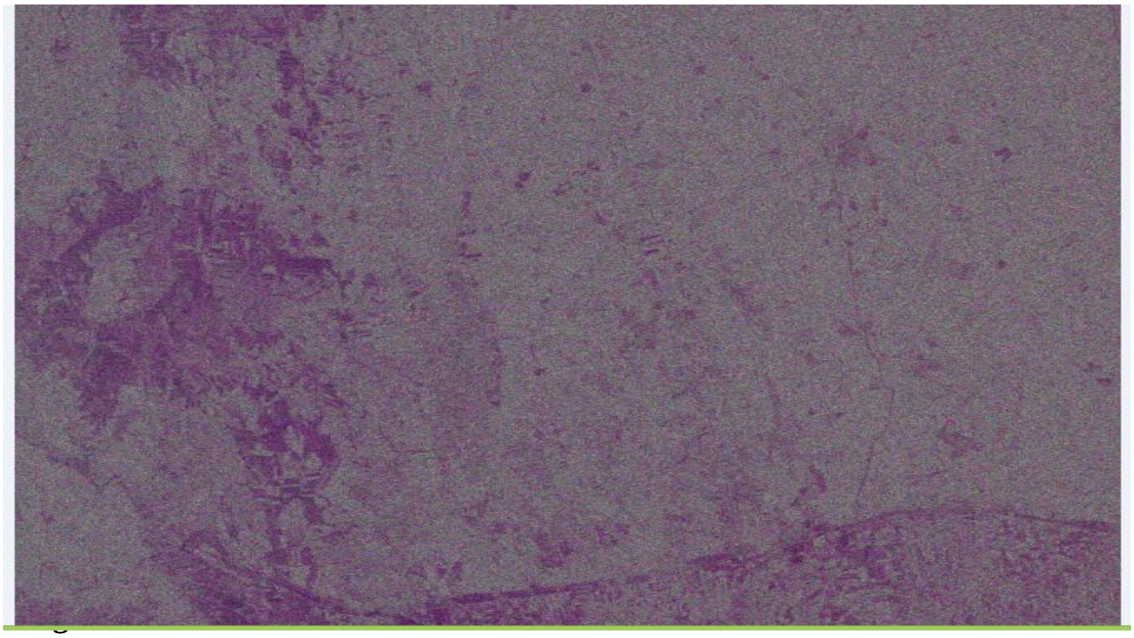

Figure 5.9 : RADARSAT-2 image for 08.September at study area the Harran in Sanliurfa, South-East of Turkey.HH image data on red band, HV image data on green band, VV image data on blue band(6644 ×6218).

Table 5.4 : Summary of Radarsat-2 data (imagery characteristics), DOY: day Of year 2012 (07 September 2012 = 251, 08 September 2012 = 252)

Beam mode	DOY/Time	Incidence angle (degrees)	Orbit	Product type
FQ1	251 /15:11	18.4^{0} -20.4^{0}	Asending	SLC
FQ19	252 /03:26	38.3^{0} -39.8^{0}	Desending	SLC

5.4 Methods

5.4.1 Pre-processing

5.4.1.1 Digital elevation model (DEM) and orthorectification

Data acquired by the SAR containsuncertainties due to variations in altitude, velocity of the sensor platform,relief displacement and non-linearties in sweep of a sensor instantaneousfield of view (IFOV). The datasets need to be properly calibrated/preprocessedto be used it for desired applications. Preprocessing the SAR dataincludes conversion from slant range to ground range, radiometriccalibration, speckle suppression andeneration SAR image georeferencing and orthorectification.

A radar system looks to the side and records the locations of objects using the distance from the sensor to the object along the line of sight, rather than along the surface. An image collected using this geometry is referred to as a slant range image. Slant range radar data have a systematic geometric distortion in the range direction. The true, or ground range, pixel sizes vary across the range direction because of the changing incident angles. This makes the image appear compressed in the near range, relative to what it would look like if all of the pixels covered the same area on the ground.

Digital Elevation Models do play a fundamental role in mapping.But the use of a DEM for orthorectification is also optional, especially in areas of low relief, but was performed in order to increase the radiometric and geometric accuracy of the imagery. Because of error in estimation of area model, DEM can help for correcting the anomaly of surface,sometimes in relatively flat areas, the DEM showed an elevation range of more than some meters, and showing that area that looks flat is not truly flat and can benefit from corrections.

All imagery, whether it is obtained from airborne or space-based sensors, has inherent problems.There are distortions caused by the angle between the camera / sensor and the ground, distortions from the movement of the camera through the air or space, and distortions created from ariations in terrain. The solution is to manipulate imagery through the process of orthorectification. Given the appropriate inputs, a rigorous model can be computed that corrects the distortions introduced by the camera optics, viewing angles, and terrain relief.

Given an accurate calculation of this model, pixel and line locations in unreferenced imagery can be mapped to real world positions on the earth's surface. This results in a planimetrically correct image. The scale of the image is uniform, and usually created to match popular map scales.This means that when you measure a distance between two points on an orthorectified image, the result will be accurate. Put simply, the orthorectification process transforms your imagery from a simple picture into a valuable source of information from which information can be extracted.

In this research, ENVI Classic 5.0.6 (Exelis ENVI 5.0.6) program's additional module, SARscop (A modular set of functions dedicated to the generation of products derived from spaceborne Synthetic Aperture Radar (including JERS-1, ERS-1/2, Radarsat-1/2, ENVISAT/ASAR and ALOS/PALSAR),that was developed by sarmap, a Swiss company) was used for generating the georeferenced image, from RADARSAT-2 raw data. Several process steps are: (i) transforming slant range to ground range, (ii)resampling data by 8m×8m pixels, (iii) projection to UTM coordinates, (iv) selecting standard DEM file (sea level). In this study, selecting the GCP file in geocoding processing steps was ignored; this file can accelerate the process. Finally three different geocoding files in three different polarizations (HH,HV,VV) was created Figure 5.9.Geocoding image for RADARSAT-2 data that was In addition by using PCI Geomatica 2014, georeferenced images in different polarization was merged to show better at Figure 5.10and Figure 5.11.

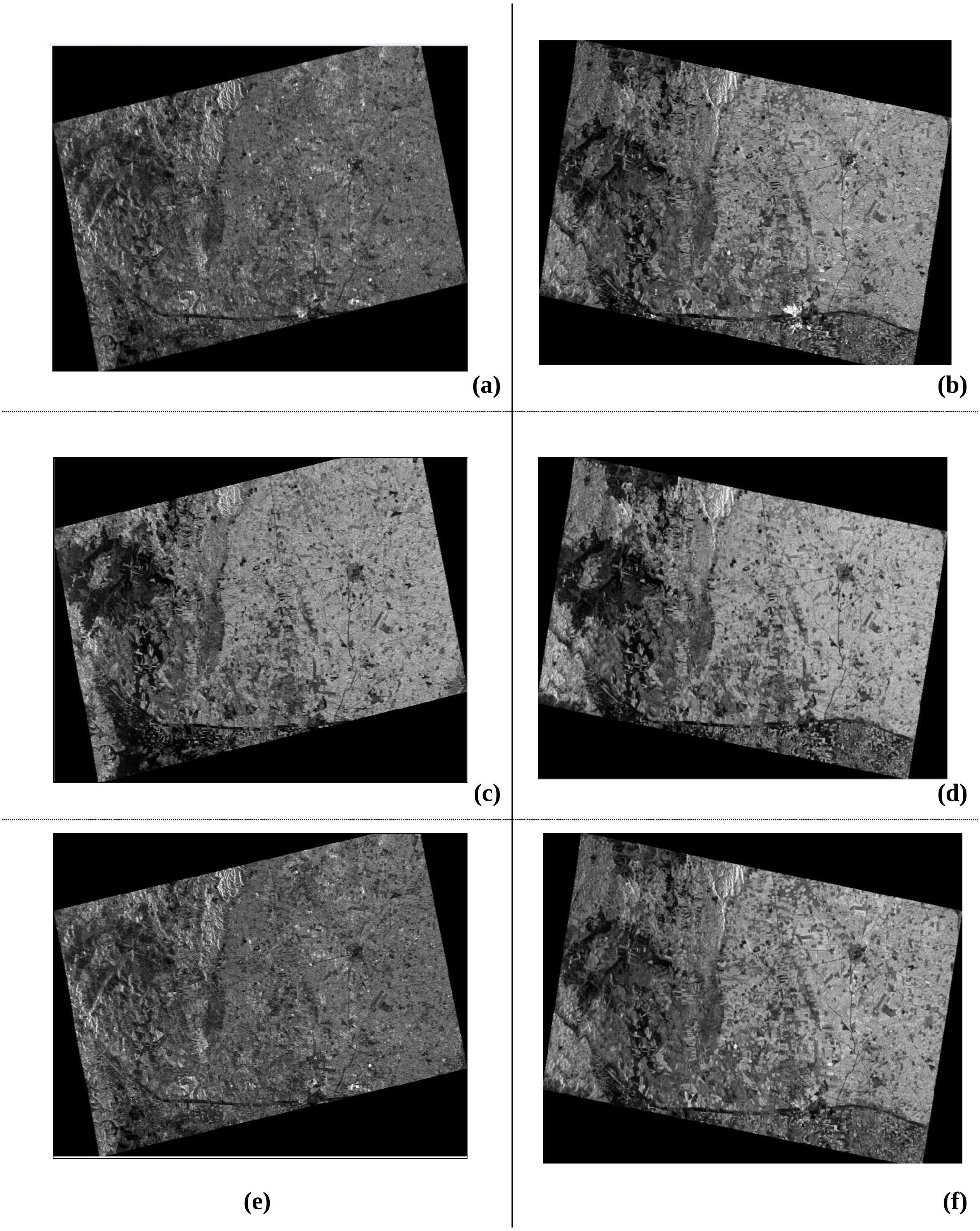

Figure 5.10 : Orthorectified(unfiltered)RS-2Fine-quad SLC scenes acquired on 7th and 8th of September, 2012,(1:250.000). (a) HH,07 Sept. (b)HH ,08 Sept. (c) HV,07 Sept. (d) HV, 08 Sept. (e) VV, 07 Sept. (f)VV, 08 Sept.

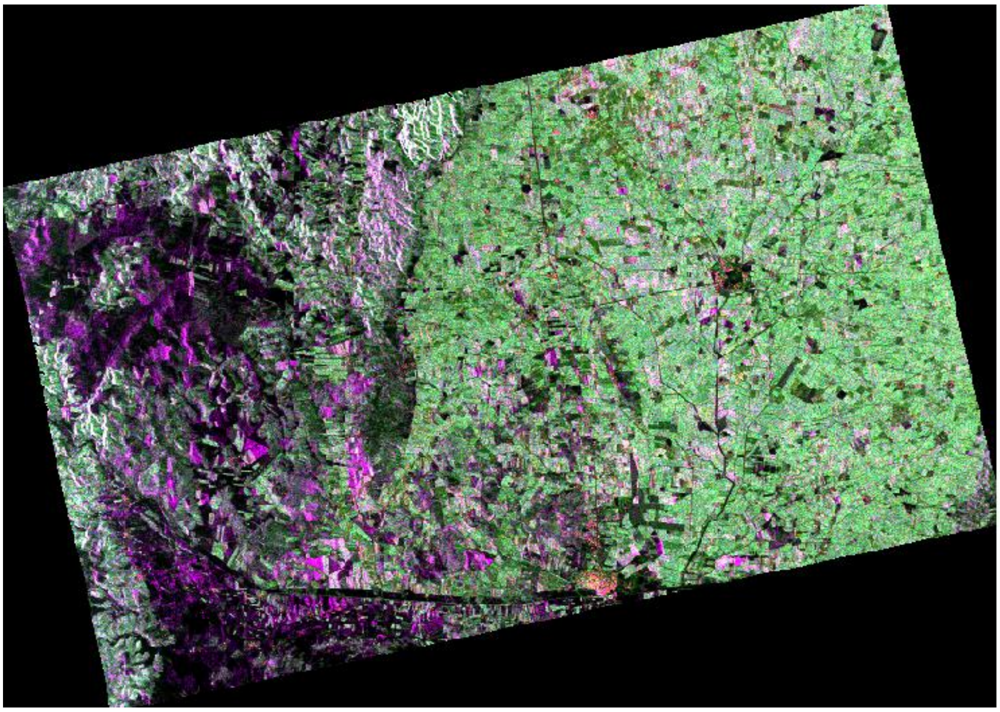

Figure 5.11 : Orthorectified (unfiltered)RS-2 Fine-quad SLC (FQ1) scenes acquired on 07 Sept 2012.The image are presented as R:HH,G:HV and B:VV.

F

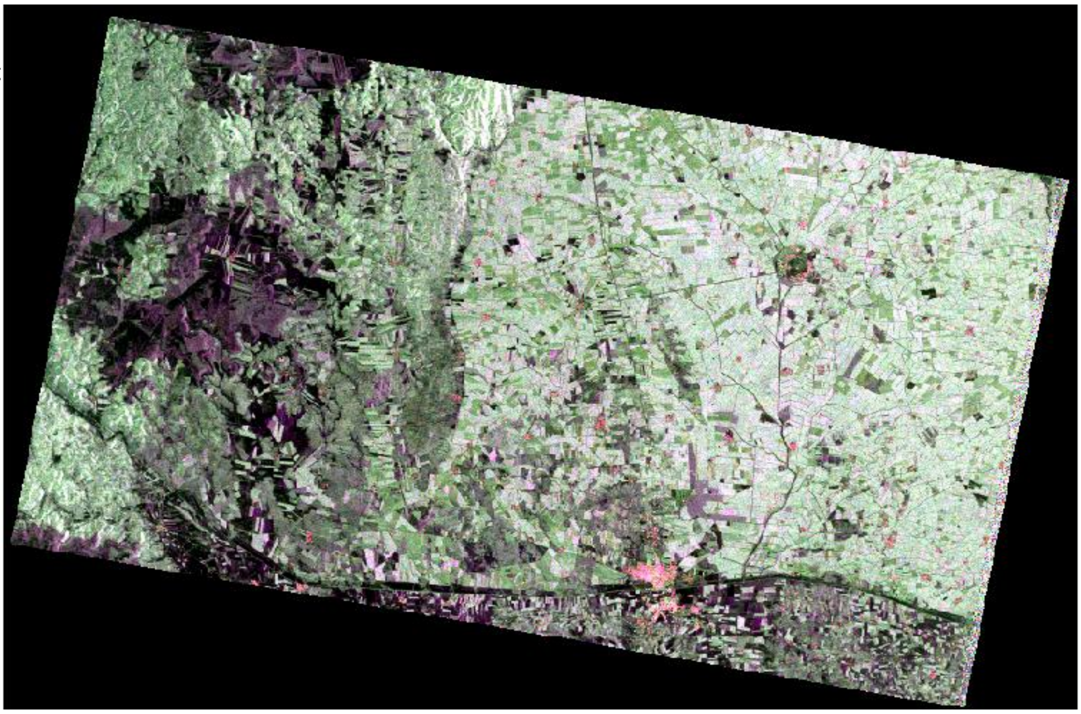

Figure 5.13 : Orthorectified (unfiltered)RS-2 Fine-quad SLC (FQ19) scenes acquired on 08 Sept 2012.The image are presented as R:HH,G:HV and B:VV.

5.4.1.2 Incidence angle image

An incidence angle image was used to generate the soil moisture estimation using semi-empirical models. It is single channel image that was also extracted from the unfiltered imagery. In this resreach, for the extraction of this image, ENVI Classic 5.0.6 (Exelis ENVI 5.0.6) was used.Incidence angle image role in estimated value was examined later.

5.4.2 Application of the soil moisture models

The OH92, OH04 and DU95 soil moisture estimates were calculated based on the georeferenced imagery.These estimations were presented by using a Python version 2.7 (Utrl-2), scripts in two steps. At first scripts (Appendix A): (i) import a georeferenced images that was generated in previous section, (ii) convert to ENVI format, (iii) generated C11,C22,C33 (Equation 2.14) and in next script (Appendix B); (i) call the PolSARpro (PolSARpro (ESA v.5.2.0, 2014) is open-source SAR analysis software created by the European Space Agency (ESA)) (Utrl-1) modules for three surface inversion models forretrieve the estimate of volumetric soil moisture (input files are C11, C22, C33 and incidence angle image was generated in 5.4.1.2 section), (ii) output the result was converted to PCIDSK format for viewing (Figure 5.12 , Figure 5.13).

5.4.3Speckle filtering and determination of optimal speckle filter size

The original maps were estimated by using different empirical soil moisture models that were shown in Figure 5.12 andFigure 5.13. These maps included valid and invalid data and in this part of research, which was carried out to omit the invalid data and subsequently, for the extraction of useful information from polarimetric images and increasing the estimate performance, as shown in section 2.8, Speckle filtering is an essential step in obtaining estimates of soil moisture using semi-empirical models. However, the important issue that should be addressed is the type of filter and filter size.

For estimating and finding optimal filter kind and kernel size, in this research ,three kinds of filters, Lee filter (Lee et al.1994),Enh_Lee, Forst filter (Forst et al. 1982) and Kuan filter(Kuan et al .1985) in seven different sizes 3×3 to 15 ×15 was used.

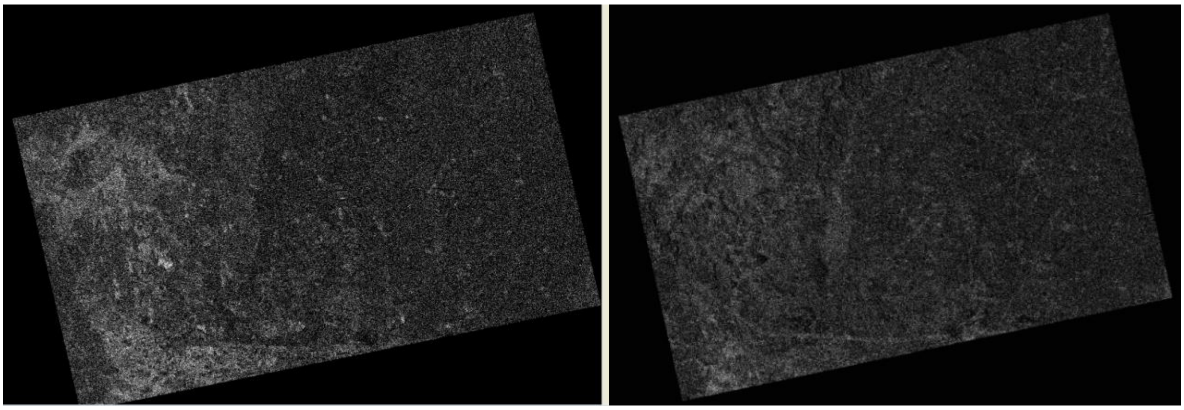

Figure 5.14 : Primary unfiltered images of volumetric soil moisture contentest images from the OH92 model (left),the OH04 model (right), for 07 Sept (DU95 model is not available for this data).

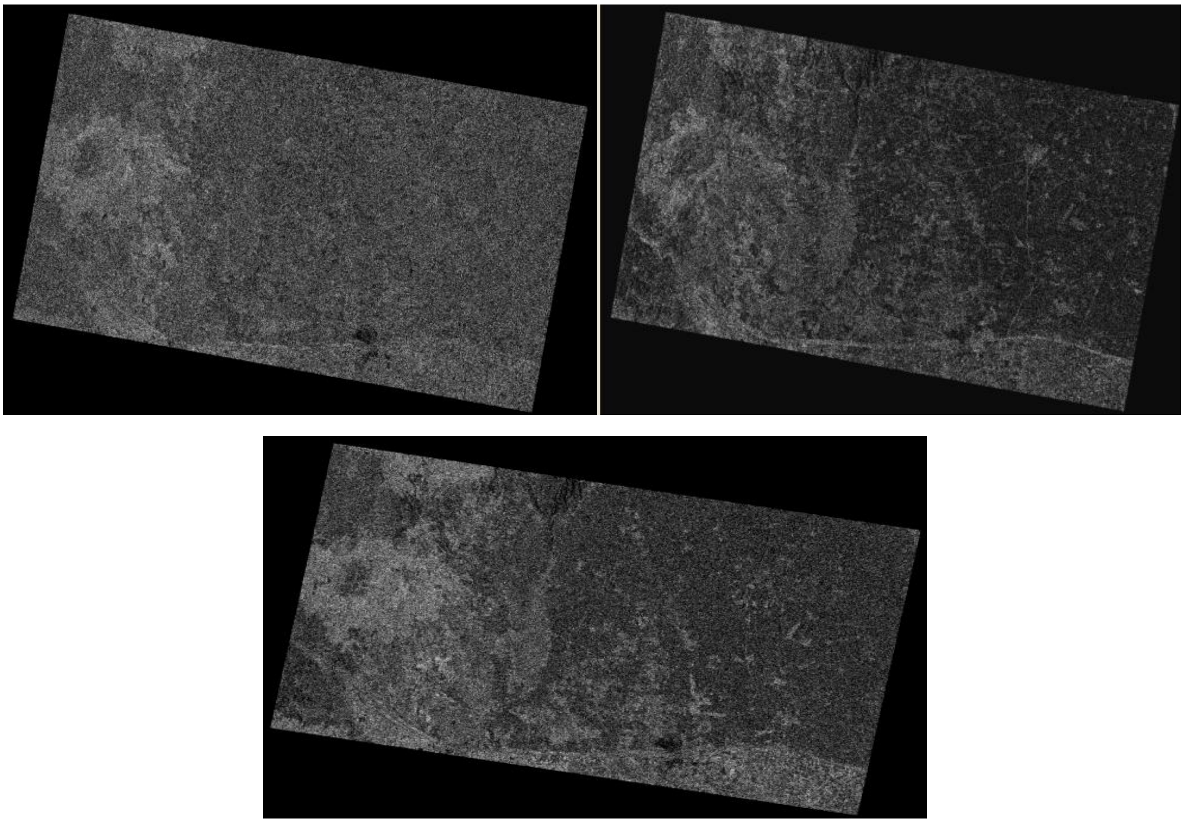

Figure 5.15 : Primary unfiltered images of volumetric soil moisture contentest images from the OH92model (left),the OH04 model (right) and the DU95 model(bottom) for 08 Sept.

For three different soil moisture models which were estimated in the previous section by python script (Appendix B),seven different filter sizes for each model and four different filter kinds for two dates, 140 filtered images were generated. Some statistical definitions like Mean(M), Normalized mean (NM), Standard deviation (Std), and variance value have been used in different papers which help to select suitable filter kind and optimal filter size (Yu and Acton (2002) ;Leeuw et al. (2009)).

Variance value measures how far a set of numbers is spread out. A variance of zero indicates that all the values are identical. Variance is always non-negative: a small variance indicates that the data points tends to be very close to the mean (expected value) and hence to each other, while a high variance indicates that the data points are very spread out around the mean and from each other.Where x is input data and N is the number of cellsvariance was given by:

$$S = \sqrt{\frac{1}{N-1}\sum_{i=1}^{N}(x_{i-}\ x_{mean}\ )^2} \qquad \textbf{(5.1)}$$

Standard deviation (Std) is square root of variance value.The indexes are derived for use, as the evaluation criteria in this thesis are:

(i) Equivalent Number of Looks (ENL) (Gagnon and Jouan, 1997): The value of ENL(mean-to-standard-deviation ratio) a usual way to estimate the speckle noise level in a SAR image over a uniform image area.This value don’t carry information about a resolution degradation. ENL value is given by:

$$\text{ENL}=\left(\frac{mean}{\text{standard \_deviation}}\right)^2 \qquad \textbf{(5.2)}$$

(ii) Speckle Suppression Index (SSI) (Sheng and Xia, 1996): SSI value is given by:

$$\text{SSI}=\frac{\sqrt{var\,(\text{If})}}{mean\ (\text{If})}\times\frac{mean\ (\text{Io})}{\sqrt{var\,(\text{Io})}} \qquad \textbf{(5.3)}$$

Where I_f = filtered image and I_o = noisy image.

(iii) Speckle Suppression and Mean Preservation Index (SSMPI) (Shamsoddini and Trinder, 2010): When the filter overestimates the mean value ENL and SSI indexes are not reliable. According to this index, lower values indicate better performance of the filter in terms of mean preservation and noise reduction. The speckle Suppression and Mean Preservation Index (SMPI) equation's area as follow:

$$\text{SSMPI}=\frac{\sqrt{var\,(\text{If})}}{\sqrt{var\,(\text{Io})}} \times (1 + |\, mean(\text{Io}) - mean(\text{If})\, |) \qquad \textbf{(5.4)}$$

In addition, in Equation 5.4 the mean difference between the speckled and filtered image is not normalized, the result of this equation shows higher values for larger backscattering regions. To address this problem it is usual to use Mean Preservation Speckle Suppression Index (MPSSI), which turns out to be better normalized with respect to SMPI and is better for a comparison of various filters on different images:

$$\text{MPSSI} =|1 - \frac{mean\ (\text{If}))}{mean\ (\text{Io})}| \times \frac{\sqrt{var\,(\text{If})}}{\sqrt{var\,(\text{Io})}} \qquad \textbf{(5.5)}$$

By using Python script (Appendix D) evaluation the optimal filter size ,in this script i) noisy image that filtered by Lee,Enh-Lee, Forst,Kuan filter, ii) statistical value estimate for each filtered image, iii) collected the calculated data to csv file .The results of script are discussion further in Section 6.3.

5.5 Calculation of observed soil moisture at surface soil moisture range

Figure 5.14 (a) and 5.14 (b) show selected fields positions in the study area in 08. September and 07. September.Local measurement of soil moisture value was carried out in 15 cm depth and results were shown between 0 to 200 in volumetric soil moisture dimension. On 08. September for field A, avrage volumetric soil moisture percent (that was collected three 17,18,19 station (Table 5.1 and Table 5.3) is 91% and field A is well-heeled of water; however, for field B average volumetric soil moisture percent (that was collected two 21,22station (Table 5.1 and Table 5.3) is 40 % ; this field is a semi-dry area. Finally, field C (station 24) has 14% of soil moisture which is very poor of water and is a dry area. On 07. September, for field A, the average volumetric soil moisture percentage (that was collected three 17, 18,19 station (Table 5.1 and Table 5.3) was found to be composed of89% and thus field A showed to bemoist, however, for field B, average volumetric soil moisture percent (that was collected two 21,22station (Table 5.1 and Table 5.3) was found as being30 %,this field is Semi-dry area. Finally, field C (station 24) has 15% of soil moisture which is very poor of water and dry area.The moisture content of the soil to a depth of 40 cm was calculated according to the values of the local stations (Table 5.5 and Table 5.6).However, surface soil moisture is the water that is in the upper 10 cm of soil (Verhoest et al.2008),an other hand Semi-empirical soil moisture estimation models that was used in this thesis used RADARSAT-2 data in C-band and for these reasons, observed soil moisture was calculated on valid range (0-5 cm)statistical method and histograms approximately.For these estimations, soil kind,ks values, soil temperature, atmospheric condition during 24 hours and two different soil moisture values in various depth was used (look 3.2.3).The results of calculated observed soil moisture was summarized in Table 5.5 and Table 5.6 .

(a)

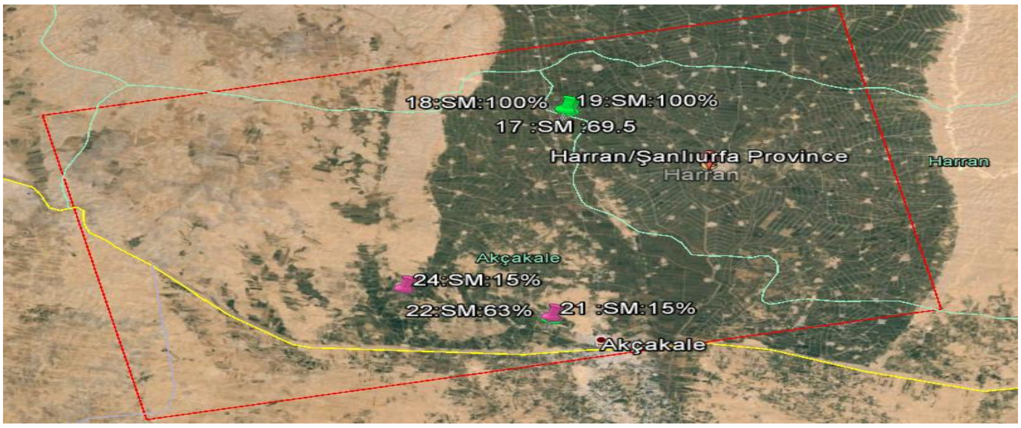

(b)

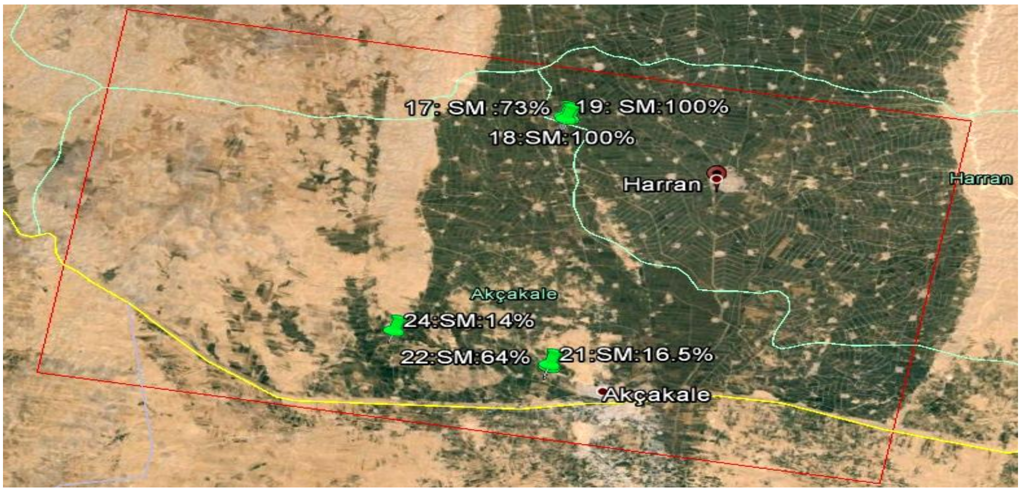

Figure 5.16 : Study area was divided three field. . Field A:stations 17(coordinate: 36.9019, 38.9229), 18(coordinate:36.9012, 38.9207), 19(coordinate: 36. 9029, 38.9198) and field B:stations 21(coordinate: 36.7242 , 38.9103), 22 (coordinate: 36.7222, 38.9103), field C:24(coordinate:36.7484, 38.8086) . (a) 07.Sept.2012 . (b) 08.Sept,2012 .

Table 5.5 : The soil moisture(SM) is calculated at local stations at 0-5cm depths (07/09/2012)

Name	Coordinate	SM%:0-5Cm	SM%:0-15Cm	SM%:0-40Cm
Yakacık	36.9019,38.9229	51.00	69.50	99.50
Rumi	36.9012,38.9207	90.00	100.00	100.00
Aydoğdu	36.9029,38.9198	90.00	100.00	100.00
Demirören	36.9034,38.9159	---	---	---
Tatnar	36.7242,38.9103	10.50	15.50	37.50
Akçatat	36.7222,38.9103	70.00	63.50	54.00
Gündöner	36.7464,38.8081	---	---	---
Akçagün	36.7484,38.8086	12.00	15.00	18.00
Eyyübiye	37.1237,38.8161	---	---	---
Külünçe	37.2116,38.1784	---	---	---
Poyralı	36.9196,38.7542	90.00	100.00	100.00

Table 5.6 : The soil moisture(SM) is calculated at local stations at 0-5cm depths (08/09/2012).

Name	Coordinate	SM%:0-5Cm	SM%:0-15Cm	SM%:0-40Cm
Yakacık	36.9019,38.9229	55.00	73.00	100.00
Rumi	36.9012,38.9207	95.00	100.00	100.00
Aydoğdu	36.9029,38.9198	95.00	100.00	100.00
Demirören	36.9034,38.9159	---	---	---
Tatnar	36.7242,38.9103	9.00	16.50	39.00
Akçatat	36.7222,38.9103	71.06	64.50	55.50
Gündöner	36.7464,38.8081	---	---	---
Akçagün	36.7484,38.8086	10.22	14.00	17.00
Eyyübiye	37.1237,38.8161	---	---	---
Külünçe	37.2116,38.1784	---	---	---
Poyralı	36.9196,38.7542	95.00	100.00	100.00

5.6 Comparing soil moisturevalues on optimal filter maps with local measurements values

The model estimates produced with the “best” combinations of speckle filters were extracted for study area (section 5.5). By using Python script (Appendix C) the value of soil moisture for each site, Figure 5.14(a) and (b), was estimated. In Python script for each site by attention local station' s coordinate closer point in soil moisture maps to local station position was collected as site area. For site A selected point counts are 2750 points,this count is 2100 points in site B and finally 870 points in fsite C.
The soil moisture of selected point in each site for models was collected as CSV format files by using Python script (Appendix C). These values for each models in each sites was investigated. Soil moisture potential was estimated for each site in each model. In addition, by using soil moisture potential dryness level was estimated.

Finally, the local measurement and estimated value was compared. In compression measurement and estimated values the vegetation affect was analyzed by using Pauli RGB image for estimated values. Optimal filtered maps for each model were offered.

6. RESULTS AND DISCUSSION

6.1 Purpose

Mean and Standard deviation (Std) values were computed of selected filter types between 3 × 3 to 15 × 15 filter kernel sizes for each models was calculated. The computed value was evaluated to select the optimal filter kind and windows size. The summary of results and discussion about method was used to select the optimal filter as shown in section 6.3. In addition, the error between estimated value and observed value was estimated.The final discussion about model performance and incidence angle role in estimation is presented in the following sections.

6.2 EstimateThe ModelPermissive Range

The summary of ranges of validity for OH92, OH04 and DU95 models was shown in different sections of chapter 4 seen in Table 6.1.As seen for model DU95, valid incidence angle range is between 30 to 65 degrees. Then by comparing Table 5.4 and Table 6.1, using DU95 model was automatically rejected.On the other hand, ranges of validity for soil moisture and conversion of dielectric permittivity to volumetric soil moisture in soil moisture models (volumetric soil moisture is estimated directly in the OH04 model and independent of dielectric permittivity) as two issues were addressed in analyzing data by PolSARpro modules implementation.

Table 6.1 : Ranges of validity for OH92, OH04 and DU95 models

Model	Source	mv(%)	ks(cm)	θi (degrees)
OH92	Oh et al. (1992)	9 - 31	0.10-6.00	10-70
OH04	Oh (2004)	4 -29.1	0.13-6.98	10-70
DU95	Dubois et al. (1995a,b)	0 -35	0.30-3.00	30-65

The OH92 and DU95 models allowed dielectric permittivity values of 0 to 20, when converted with the Toppetal. (1980) equation equates to a volumetric soil moisture contents of 5.30 to 45.14%, well beyond the originally stated range of 9 to 31% for OH92 and 0 to 35% for the DU95 model (Table 6.1). The OH04 model PolSARpro madule that was used allowed soil moisture contents of 0 to 40%, while the originally stated range is only 4 to 29.1%(Table 6.1).Consideringthese issues in PolSARPro modules running in python script,output of dielectric permittivity was used directly for the OH92 and DU95 models making out values.For giving ranges of validity values when applying the conversion to volumetric soil moisture in Python script, criteria of valid range in Topp et al. (1980) equation(Equation 4.6) was used. It is necessary to add this point that there are some other models for conversion between dielectric permittivity and volumetric soil moisture.The selection of suitable conversion model has an important role to the accuracy of estimates. One of these models is the Hallikainen model(Hallikainen et al. 1985).This model requires information about the soil texture (slit ,sand and clay) and soil type (loam,sandy, Clay) and is thus not the best option for use with remotely sensed data. However, for OH04 range criterion directly for the volumetric soil moisture result was used.

6.3 Models Statics and Effects of Speckle Filter

As discussed in section 5.5, the soil moisture in valid range was generated by using selected suitable criterion for each model. However, for analyzing the best performance in models, the optimal filter size estimate is the important step.Lee, Enhance-Lee, Forst and Kuan filters were used. The noisy soil moisture image that was generated by using DU95, OH92 and OH04 models in section 5.5, (7054×4984-pixel size for 08.September and7173 ×5195-pixel size for 07.September), was selected for comparison. For evaluating the performance of the filters quantitatively, quantities of ENL, SSI, SSMPI, MPSSI were computed and shown in Table 6.2 to Table 6.5 for DU95, Table 6.6 to Table 6.9 for OH92 and Table 6.10 to Table 6.13 for OH04 for 08.Septemberand Table 6.14 to Table 6.17 for OH92 and Table 6.18 to Table 6.21for OH04 for 07. September. In addition, for noisy image in 08 . SeptemberMean and Std were 1.40717 and 6.88089 in DU95 model, 1.644279 and 5.579547 in OH92 and 0.658144 and 3.933535 in OH04 alternatively and for noisy image in 07.SeptemberMean and 1.5074 and 5.4857 in OH92 and 0.6326 and 4.4267 in OH04 alternatively.For noisy images in 07 SeptemberMean and 1.5074 and 5.4857 in OH92 and 0.6326 and 4.4267 in OH04 alternatively.

Table 6.2 :

Table 6.3 : Speckle noise reduction indices values, DU95 model, Lee filter,08.Sept .

Filter type	Kernel size	Mean	Std	ENL	SSI	SSMPI	MPSSI
Lee	3	3.6697	8.4947	0.1866	0.4734	4.0277	1.9850
Lee	5	2.7624	7.6043	0.1320	0.5630	2.6028	1.0643
Lee	7	2.1848	6.9173	0.0998	0.6475	1.7870	0.5555
Lee	9	2.1502	6.8809	0.0976	0.6544	1.7430	0.5280
Lee	11	2.1444	6.8795	0.0972	0.6561	1.7369	0.5238
Lee	13	2.1419	6.8800	0.0969	0.6569	1.7345	0.5221
Lee	15	2.1397	6.8796	0.0967	0.6575	1.7322	0.5205

Table 6.4 : Speckle noise reduction indices values DU95 model, Enh_Lee filter,08.Sept.

Filter type	Kernel size	Mean	Std	ENL	SSI	SSMPI	MPSSI
Enh_Lee	3	1.4062	5.7969	0.0588	0.8430	0.8416	0.0006
Enh_Lee	5	1.4072	5.8364	0.0581	0.8482	0.8482	0.0000
Enh_Lee	7	1.4072	5.8380	0.0581	0.8484	0.8485	0.0000
Enh_Lee	9	1.4072	5.8380	0.0581	0.8484	0.8485	0.0000
Enh_Lee	11	1.4072	5.8380	0.0581	0.8484	0.8485	0.0000
Enh_Lee	13	1.4072	5.8380	0.0581	0.8484	0.8485	0.0000
Enh_Lee	15	1.4072	5.8380	0.0581	0.8484	0.8485	0.0000

Table 6.5 : Speckle noise reduction indices values DU95 model,FORST filter,08.Sept.

Filter type	Kernel size	Mean	Std	ENL	SSI	SSMPI	MPSSI
FORST	3	3.6551	8.2761	0.1951	0.4631	3.9065	1.9214
FORST	5	2.3953	7.2927	0.1079	0.6226	2.1071	0.7442
FORST	7	2.1781	7.0767	0.0947	0.6644	1.8213	0.5634
FORST	9	2.1414	7.0518	0.0922	0.6734	1.7773	0.5347
FORST	11	2.1335	7.0526	0.0915	0.6760	1.7694	0.5290
FORST	13	2.1288	7.0521	0.0911	0.6775	1.7645	0.5256
FORST	15	2.1245	7.0494	0.0908	0.6786	1.7594	0.5223

Table 6.6 : Speckle noise reduction indices values DU95 model,KUAN filter,08,Sept.

Filter type	Kernel size	Mean	Std	ENL	SSI	SSMPI	MPSSI
KUAN	3	1.4071	3.4062	0.1707	0.4950	0.4950	0.0000
KUAN	5	1.4072	3.1292	0.2022	0.4548	0.4548	0.0000
KUAN	7	1.4072	3.0474	0.2132	0.4429	0.4429	0.0000
KUAN	9	1.4072	3.0127	0.2182	0.4378	0.4378	0.0000
KUAN	11	1.4072	2.9948	0.2208	0.4352	0.4352	0.0000
KUAN	13	1.4072	2.9842	0.2224	0.4337	0.4337	0.0000
KUAN	15	1.4072	2.9773	0.2234	0.4327	0.4327	0.0000

Table 6.7 : Speckle noise reduction indices values OH92 model, Lee filter,08.Sept .

Filter type	Kernel size	Mean	Std	ENL	SSI	SSMPI	MPSSI
LEE	3	3.5114	7.2523	0.2344	0.6087	3.7267	1.4760
LEE	5	2.6084	6.5078	0.1607	0.7352	2.2909	0.6839
LEE	7	2.5273	6.4452	0.1538	0.7515	2.1752	0.6204
LEE	9	2.5277	6.4549	0.1533	0.7526	2.1789	0.6215
LEE	11	2.5318	6.4630	0.1535	0.7523	2.1864	0.6252
LEE	13	2.5372	6.4702	0.1538	0.7515	2.1950	0.6297
LEE	15	2.5402	6.4731	0.1540	0.7510	2.1996	0.6321

Table 6.8 : Speckle noise reduction indices values OH92 model, Enh_Lee filter, 08.Sept.

Filter type	Kernel size	Mean	Std	ENL	SSI	SSMPI	MPSSI
Enh_Lee	3	1.6230	5.4640	0.0882	0.9921	1.0001	0.0127
Enh_Lee	**5**	**1.5899**	**5.4871**	**0.0840**	**1.0171**	**1.0369**	**0.0325**
Enh_Lee	**7**	**1.5344**	**5.4035**	**0.0806**	**1.0378**	**1.0749**	**0.0647**
Enh_Lee	**9**	**1.4595**	**5.2799**	**0.0764**	**1.0661**	**1.1212**	**0.1063**
Enh_Lee	**11**	**1.3632**	**5.1149**	**0.0710**	**1.1057**	**1.1744**	**0.1567**
Enh_Lee	**13**	**1.2469**	**4.9060**	**0.0646**	**1.1595**	**1.2287**	**0.2125**
Enh_Lee	**15**	**1.2376**	**4.8009**	**0.0665**	**1.1432**	**1.2104**	**0.2128**

Table 6.9 : Speckle noise reduction indices values OH92 model, FORST filter, 08.Sept.

Filter type	Kernel size	Mean	Std	ENL	SSI	SSMPI	MPSSI
FORST	3	3.4913	6.8180	0.2622	0.5755	3.4790	1.3726
FORST	5	2.6025	6.4958	0.1605	0.7356	2.2798	0.6785
FORST	7	2.5180	6.5525	0.1477	0.7669	2.2005	0.6240
FORST	9	2.5133	6.6061	0.1447	0.7746	2.2129	0.6258
FORST	11	2.5106	6.6302	0.1434	0.7783	2.2178	0.6261
FORST	13	2.5064	6.6396	0.1425	0.7807	2.2159	0.6239
FORST	15	2.4921	6.6430	0.1407	0.7856	2.2000	0.6139

Table 6.10 : Speckle noise reduction indices values OH92 model, KUAN filter, 08.Sept.

Filter type	Kernel size	Mean	Std	ENL	SSI	SSMPI	MPSSI
KUAN	3	1.6256	3.2659	0.2478	0.5921	0.5963	0.0066
KUAN	5	1.5899	2.9787	0.2849	0.5521	0.5629	0.0177
KUAN	7	1.5345	2.8665	0.2866	0.5505	0.5702	0.0343
KUAN	9	1.4594	2.7856	0.2745	0.5625	0.5916	0.0561
KUAN	11	1.3630	2.7026	0.2543	0.5843	0.6206	0.0829
KUAN	13	1.2465	2.6059	0.2288	0.6161	0.6528	0.1130
KUAN	15	1.1112	2.4874	0.1996	0.6597	0.6835	0.1445

Table 6.11 : Speckle noise reduction indices values OH04 model, Lee filter, 08.Sept.

Filter type	Kernel size	Mean	Std	ENL	SSI	SSMPI	MPSSI
LEE	3	2.9799	7.5542	0.1556	0.4242	6.3793	6.7749
LEE	5	1.6213	5.8364	0.0772	0.6023	2.9129	2.1715
LEE	7	1.3403	5.3413	0.0630	0.6668	2.2841	1.4073
LEE	9	2.9799	7.5542	0.1556	0.4242	6.3793	6.7749
LEE	11	1.0741	4.7893	0.0503	0.7460	1.7241	0.7696
LEE	13	0.6420	3.7305	0.0296	0.9723	0.9637	0.0233
LEE	**15**	**0.2689**	**2.4349**	**0.0122**	**1.5150**	**0.8600**	**0.3661**

Table 6.12 : Speckle noise reduction indices values OH04 model,Enh_Lee filter,08.Sept.

Filter type	Kernel size	Mean	Std	ENL	SSI	SSMPI	MPSSI
Enh_LEE	**3**	**0.5159**	**3.4741**	**0.0221**	**1.1267**	**1.0088**	**0.1909**
Enh_LEE	**5**	**0.3116**	**2.7098**	**0.0132**	**1.4550**	**0.9276**	**0.3627**
Enh_LEE	**7**	**0.1210**	**1.6890**	**0.0051**	**2.3355**	**0.6600**	**0.3504**
Enh_LEE	**9**	**0.0345**	**0.8991**	**0.0015**	**4.3604**	**0.3711**	**0.2166**
Enh_LEE	**11**	**0.0086**	**0.4490**	**0.0004**	**8.7355**	**0.1883**	**0.1127**
Enh_LEE	**13**	**0.0019**	**0.2082**	**0.0001**	**18.3343**	**0.0877**	**0.0528**
Enh_LEE	**15**	**0.0004**	**0.1011**	**0.0000**	**42.2892**	**0.0426**	**0.0257**

Table 6.13 : Speckle noise reduction indices values OH04 model, FORST filter,08.Sept.

Filter type	Kernel size	Mean	Std	ENL	SSI	SSMPI	MPSSI
FORST	3	2.9582	7.5513	0.1535	0.4271	6.3352	6.7090
FORST	5	1.5978	5.9244	0.0727	0.6204	2.9214	2.1504
FORST	7	1.2654	5.3166	0.0566	0.7030	2.1724	1.2471
FORST	9	0.9762	4.6847	0.0434	0.8029	1.5698	0.5755
FORST	**11**	**0.4820**	**3.3206**	**0.0211**	**1.1527**	**0.9929**	**0.2259**
FORST	**13**	**0.1256**	**1.7046**	**0.0054**	**2.2708**	**0.6641**	**0.3507**
FORST	**15**	**0.0282**	**0.8093**	**0.0012**	**4.7947**	**0.3353**	**0.1969**

Table 6.14 : Speckle noise reduction indices values OH04 model, KUAN filter,08.Sept.

Filter type	Kernel size	Mean	Std	ENL	SSI	SSMPI	MPSSI
KUAN	3	0.5222	2.0214	0.0667	0.6477	0.5838	0.1061
KUAN	5	0.3126	1.4628	0.0457	0.7829	0.5004	0.1952
KUAN	**7**	**0.1200**	**0.9017**	**0.0177**	**1.2572**	**0.3526**	**0.1874**
KUAN	**9**	**0.0348**	**0.4784**	**0.0053**	**2.2974**	**0.1974**	**0.1152**
KUAN	**11**	**0.0088**	**0.2379**	**0.0014**	**4.5025**	**0.0997**	**0.0597**
KUAN	**13**	**0.0021**	**0.1101**	**0.0004**	**8.8734**	**0.0464**	**0.0279**
KUAN	**15**	**0.0006**	**0.0533**	**0.0001**	**15.9630**	**0.0225**	**0.0135**

Table 6.15 : Speckle noise reduction indices valuesOH92 model, Lee filter,07. Sept.

Filter type	Kernel size	Mean	Std	ENL	SSI	SSMPI	MPSSI
LEE	3	3.5673	7.5006	0.2262	0.5778	4.1838	1.8685
LEE	5	2.4444	6.5064	0.1411	0.7314	2.2973	0.7372
LEE	7	2.2901	6.3543	0.1299	0.7624	2.0650	0.6015
LEE	9	2.2740	6.3474	0.1283	0.7670	2.0441	0.5884
LEE	11	2.2710	6.3506	0.1279	0.7684	2.0417	0.5864
LEE	13	2.2687	6.3519	0.1276	0.7693	2.0395	0.5848
LEE	15	2.2665	6.3518	0.1273	0.7701	2.0368	0.5831

Table 6.16 : Speckle noise reduction indices valuesOH92 model, Enh_Lee filter,07.Sept.

Filter type	Kernel size	Mean	Std	ENL	SSI	SSMPI	MPSSI
ENH_LEE	3	**1.5074**	**5.4857**	**0.0755**	**1.0000**	**1.0000**	**0.0000**
ENH_LEE	5	1.5067	5.4570	0.0762	0.9952	0.9955	0.0005
ENH_LEE	7	1.5073	5.4838	0.0756	0.9997	0.9997	0.0000
ENH_LEE	9	1.5074	5.4852	0.0755	0.9999	0.9999	0.0000
ENH_LEE	11	**1.5074**	**5.4855**	**0.0755**	**1.0000**	**1.0000**	**0.0000**
ENH_LEE	13	**1.5074**	**5.4856**	**0.0755**	**1.0000**	**1.0000**	**0.0000**
ENH_LEE	15	**1.5074**	**5.4857**	**0.0755**	**1.0000**	**1.0000**	**0.0000**

Table 6.17 : Speckle noise reduction indices valuesOH92 model, FORST filter,07.Sept.

Filter type	Kernel size	Mean	Std	ENL	SSI	SSMPI	MPSSI
FORST	3	3.5348	7.0808	0.2492	0.5504	3.9076	1.7360
FORST	5	2.4385	6.5130	0.1402	0.7339	2.2927	0.7334
FORST	7	2.2836	6.4642	0.1248	0.7778	2.0930	0.6067
FORST	9	2.2649	6.4930	0.1217	0.7877	2.0802	0.5948
FORST	11	2.2596	6.5110	0.1204	0.7918	2.0797	0.5923
FORST	13	2.2550	6.5189	0.1197	0.7944	2.0768	0.5894
FORST	15	2.2505	6.5217	0.1191	0.7963	2.0723	0.5861

Table 6.18 : Speckle noise reduction indices valuesOH92 model, KUAN filter,07.Sept.

Filter type	Kernel size	Mean	Std	ENL	SSI	SSMPI	MPSSI
KUAN	3	1.5069	3.2538	0.2145	0.5933	0.5934	0.0002
KUAN	5	1.5073	2.9734	0.2570	0.5421	0.5421	0.0000
KUAN	7	1.5074	2.8866	0.2727	0.5262	0.5262	0.0000
KUAN	9	1.5074	2.8497	0.2798	0.5195	0.5195	0.0000
KUAN	11	1.5074	2.8305	0.2836	0.5160	0.5160	0.0000
KUAN	13	1.5074	2.8191	0.2859	0.5139	0.5139	0.0000
KUAN	15	1.5074	2.8118	0.2874	0.5126	0.5126	0.0000

Table 6.19 : Speckle noise reduction indices valuesOH04 model, Lee filter,07.Sept.

Filter type	Kernel size	Mean	Std	ENL	SSI	SSMPI	MPSSI
LEE	3	3.8992	9.9973	0.1521	0.3664	9.6359	11.6629
LEE	5	1.8881	7.3589	0.0658	0.5569	1.0000	0.0000
LEE	7	1.4087	6.4544	0.0476	0.6547	1.2976	0.2227
LEE	9	1.2418	6.1011	0.0414	0.7021	1.3649	0.2838
LEE	11	1.1456	5.8839	0.0379	0.7340	1.3933	0.3144
LEE	13	1.0612	5.6810	0.0349	0.7650	1.4104	0.3381
LEE	15	0.9582	5.4147	0.0313	0.8075	1.4200	0.3624

Table 6.20 : Speckle noise reduction indices valuesOH04 model, Enh_Lee filter,07.Sept.

Filter type	Kernel size	Mean	Std	ENL	SSI	SSMPI	MPSSI
Enh_LEE	3	**0.4671**	**3.8275**	**0.0149**	**1.1710**	**1.2592**	**0.3915**
Enh_LEE	5	**0.3141**	**3.1551**	**0.0099**	**1.4356**	**1.1036**	**0.3574**
Enh_LEE	7	**0.1781**	**2.3857**	**0.0056**	**1.9140**	**0.8786**	**0.2936**
Enh_LEE	9	**0.0957**	**1.7539**	**0.0030**	**2.6195**	**0.6655**	**0.2263**
Enh_LEE	11	**0.0512**	**1.2856**	**0.0016**	**3.5866**	**0.4956**	**0.1700**
Enh_LEE	13	**0.0274**	**0.9419**	**0.0008**	**4.9057**	**0.3662**	**0.1261**
Enh_LEE	15	**0.0144**	**0.6835**	**0.0004**	**6.7706**	**0.2669**	**0.0922**

Table 6.21 : Speckle noise reduction indices valuesOH04 model, FORST filter,07.Sept.

Filter type	Kernel size	Mean	Std	ENL	SSI	SSMPI	MPSSI
FORST	3	3.8580	10.0550	0.1472	0.3724	4.0580	1.4256
FORST	5	1.8601	7.4629	0.0621	0.5733	1.0426	0.0151
FORST	7	1.3607	6.4667	0.0443	0.6791	1.3422	0.2455
FORST	9	1.1453	5.9672	0.0368	0.7446	1.4133	0.3190
FORST	11	0.9631	5.4951	0.0307	0.8153	1.4374	0.3658
FORST	13	0.8720	5.0230	0.0301	0.8231	1.3761	0.3673
FORST	15	0.8289	4.9850	0.0277	0.8593	1.3949	0.3800

Table 6.22 : Speckle noise reduction indices valuesOH04 model, KUAN filter,07.Sept.

Filter type	Kernel size	Mean	Std	ENL	SSI	SSMPI	MPSSI
KUAN	3	0.4784	2.2316	0.0459	0.6666	0.7307	0.2264
KUAN	5	0.3187	1.6931	0.0354	0.7590	0.5911	0.1912
KUAN	7	**0.1797**	**1.2559**	**0.0205**	**0.9987**	**0.4622**	**0.1544**
KUAN	9	**0.0965**	**0.9168**	**0.0111**	**1.3573**	**0.3478**	**0.1182**
KUAN	11	**0.0518**	**0.6690**	**0.0060**	**1.8453**	**0.2578**	**0.0884**
KUAN	13	**0.0278**	**0.4883**	**0.0033**	**2.5057**	**0.1898**	**0.0654**
KUAN	15	**0.0148**	**0.3531**	**0.0018**	**3.4095**	**0.1379**	**0.0476**

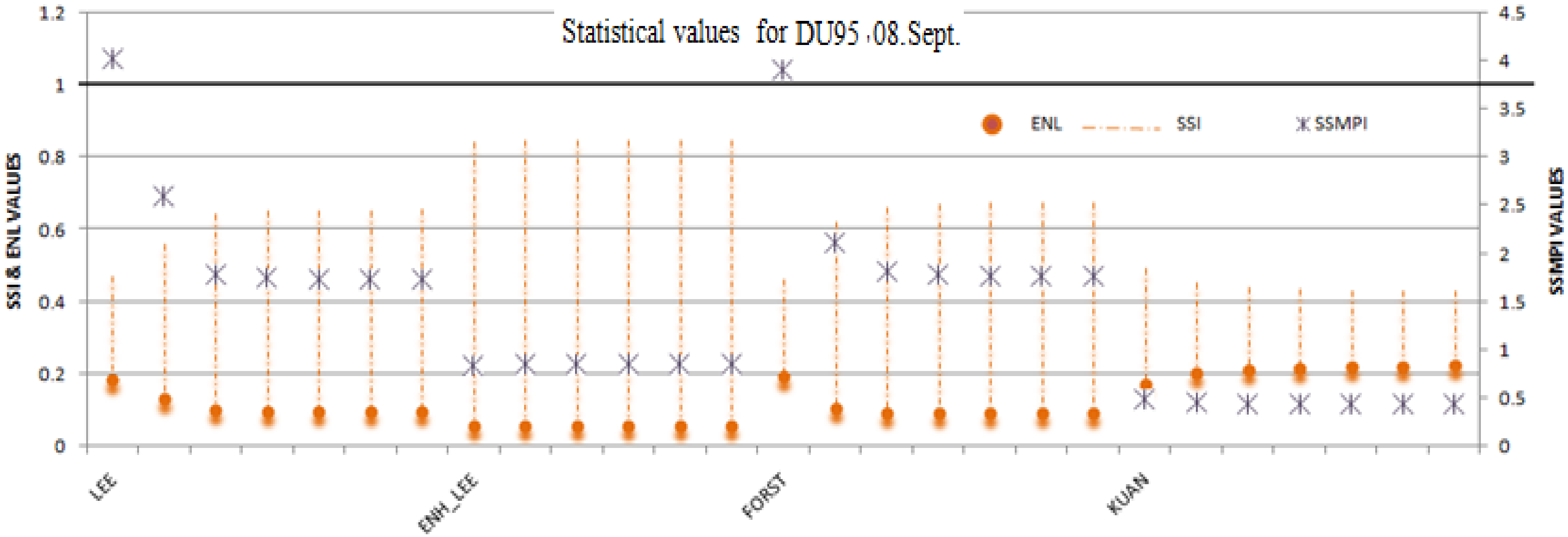

Figure 6.2 : Statistical values comparing for semi empirical models DU95,(a) 08.Sept.

(a)

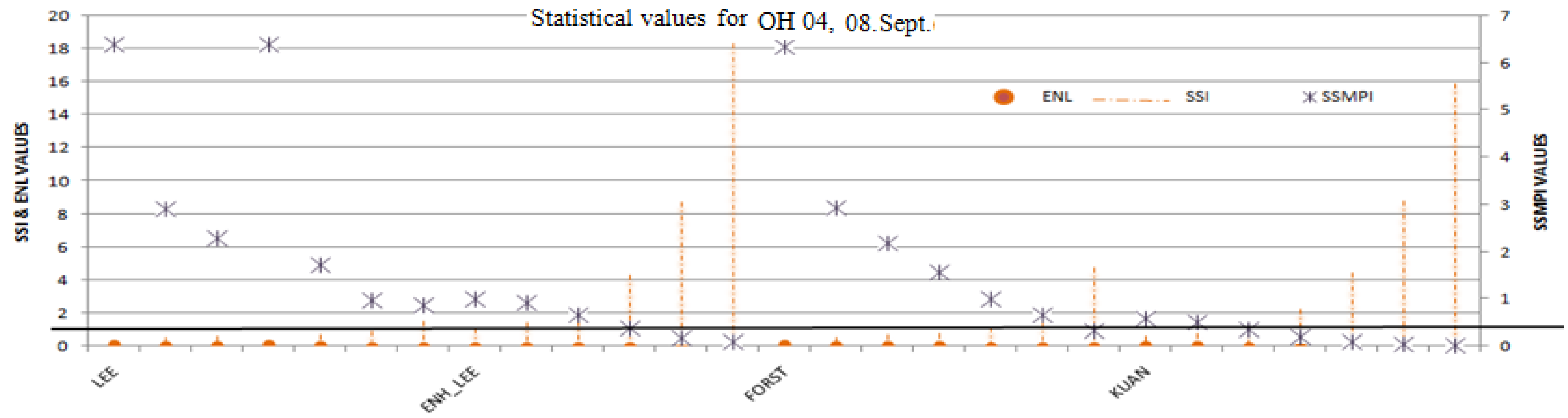

(b)

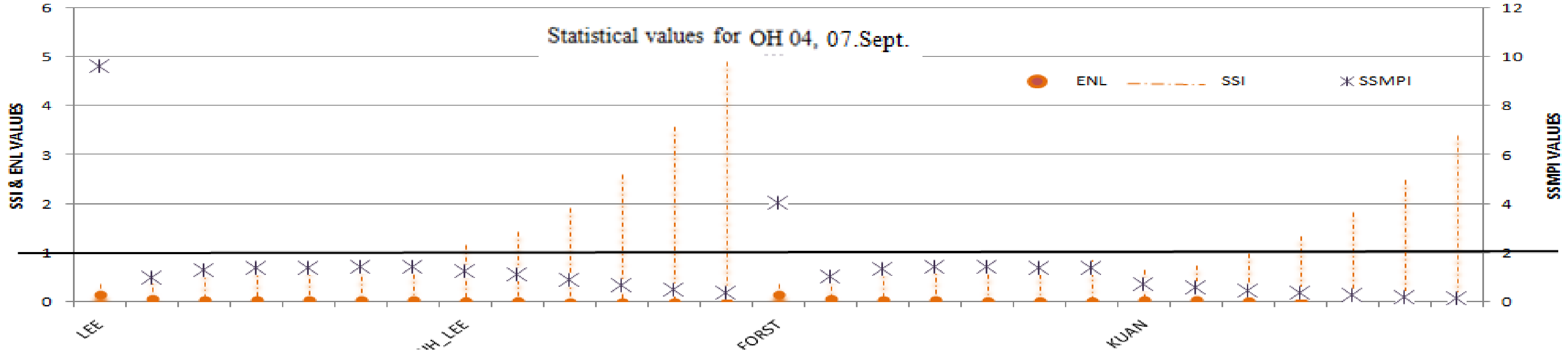

Figure 6.3 : Statistical values comparing for semi empirical models OH 04,(a) 08.Sept. (b) 07.Sept.

(a)

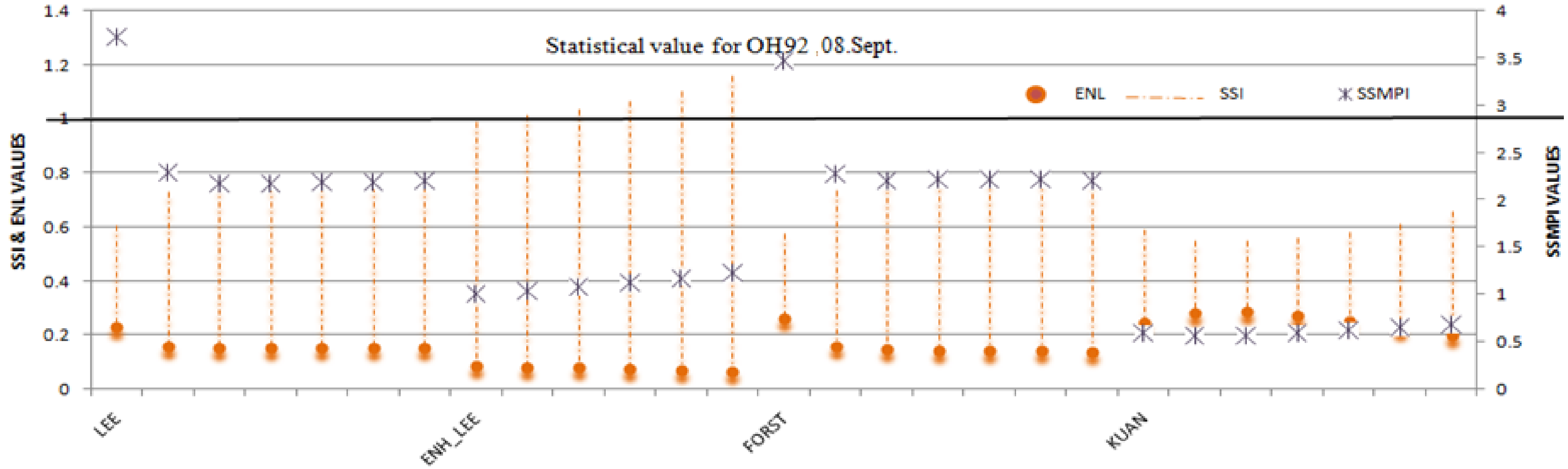

(b)

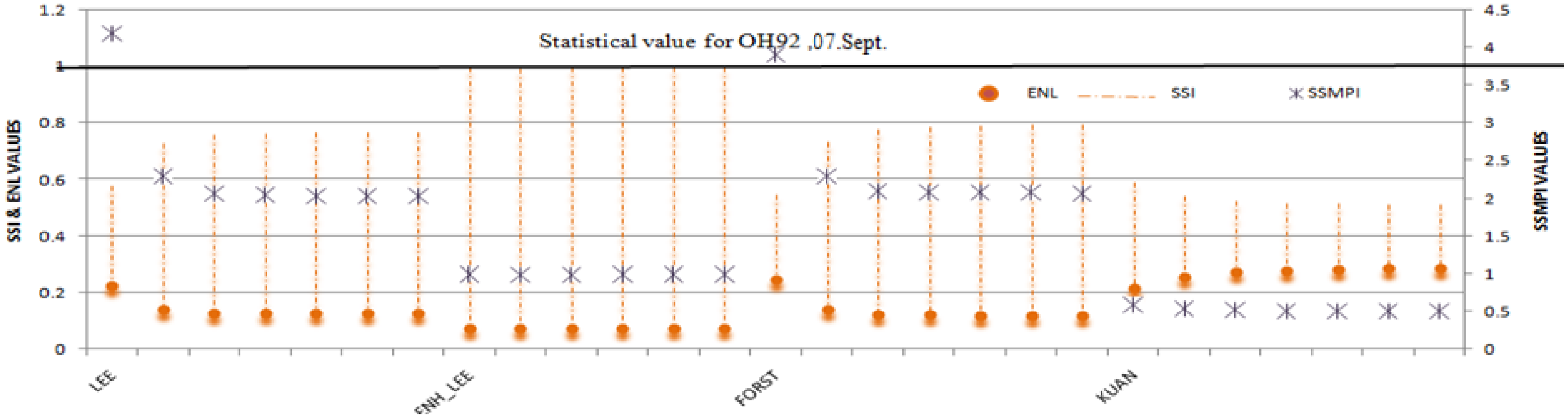

Figure 6.4 : Statistical values comparing for semi empirical models OH 92,(a) 08.Sept, . (b) 07. Sept.

6.4 Statistical Analysis of Filtered Image and Optimal Flter Selection

An assessment of the ability of filters to reduce speckle noise over different model results and find best filter size and type that was calculated five indices (Mean, Std,ENL, SSI, SSMPI and MPSSI) is shown in Tables 6.2 to 6.21.

Filter performance assessment (FPA) methods via the use of statistical indices show that, when the mean of the filtered image is close to the original image while the Std of filtered image has the minimum value (Mansourpour et al(n.d), The higher ENL value for a filtered images, SSI indice values less then1(in Tables 6.2 to 6.21 the values are not valid for SSI indices shown bold on corresponding row) (Sheng and Xia, 1996) and lower values on SSMPI indice usually indicate better performance of the filter to reduce speckle noise in homogeneous areas. However,studying the whole of the calculated indices is necessary in order tobest find the performance of the filter (Gagnon and Jouan, (1997); Shamsoddini et al. (2010); Dellepiane. (2014);Wang et al. (2012)).

Studying statistical indicevalues for DU95 model on 08 September which was shown in the previous section and attention to summarized maindata in Figure 6.1,SSI values for all of the used filter is less than one then all of the filters are in valid range,therefore, all of the filter can be used to reduce the speckle noise.However, by comparing the other statistical values, ENL values in Kuan filter are higher than other filters, but it is not enoughreason to select this filter type as optimal filter. By comparing other filters'SSI and SSMPI values,Kuan filter images have the lowestSSI and SSMPI values,and it is enough to prove this type of filter as an optimal filter type.By citing ENL and SSMPI values,the highest ENL value is equal to 0.2234 and the lowest SSMPI value is equal to 0.4327, then kuan filter with 15×15 kernel size has best performance and was selected as an optimal filter for this model.

Upon analyzing the statistical values for OH92 modelon 08 Septembershow that SSI values for Enh-Lee filtered images is greater than 1(Table 6.7),it is good reason to emit this type of filter for optimal filter selection. For selecting optimal filter,statistical values sort by ENL and SSMPI values, maximum ENL value find 0.2866 and minimum SSMPI find 0.5629.According to Table 6.9,these values in order of different5×5 kernel size. Then, the Kuan filter with a 15×15 kernel size was found to perform bestand was selected as the optimal filter for this model (Figure 6.3(a)).In addition, like OH92 model 08 September optimal filter selection process was repeated for OH 92 model for 07. September. Results shown that maximum ENL value is 0.2874 and minimum SSMPI and SSI values are 0.5126 and 0.5126 alternatively, then Kuan filter with 15×15 kernel size has best performance and was selected as an optimal filter for this model (Figure 6.3 (b)).

Processing for OH04 model for 08.September, resultes that Kuan filter with 5×5 kernel size has best performance and was selected as an optimal filter for this model (SSMPI=0.5004 and SSI=0.7829<1) (Figure 6.2(a)). For OH04 model on 07.September at first glance 7×7 kernel size in Kuan filter looks as optimal filter.The SSMPI value is the lowest in this size(SSMPI=0.8449). However, SSI value is very near to one (SSI=0,9987) and it is enough to emit this filter from optimal filter list .Then, kuan filter with 5×5 kennel size was selected as optimal filter (SSMPI=1.000 & SSI=0.7590<1)(Figure 6.2(b)).

Optimal soil moisture maps (soil moisture maps by using optimal filter) as shown Figure 6.7, Figure 6.8, Figure 6.9.

6.5 Estimation Soil Moisture Values on Optimal Filter Maps, Comparison Estimated and Local Values

7 SeptemberFor OH92 model:at fieldA,B andC,387,136 and 65 points was obtained for soil moisture respectively(Figures 6.4,6.5,6.6 (a)). By statistical evaluation, around selected points for each field ,dryness level and humidity level was calculated.

Instance for field B in OH92 models in beyond values for soil moisture (9%-31%), 19.85% of points have volumetric soil moisture values less than 10%,14.7% have volumetric soil moisture values less than 12%, 40% have volumetric soil moisture values less than 14%, 23.52% have volumetric soil moisture values less than 16% and 1.47% have volumetric soil moisture values less than 18%.Using R-squared value for estimating the level percentage shows that 86% of estimated value is in dryness range.It points out that this area has little water potential and it could be set in dry or semi-dry level .

In addition, for OH04 model ;at field A,B and C,49,18 and 3 points were obtained for soil moisture respectively(Figures 6.4,6.5,6.6 (b)).At field B, results of OH92 and OH04 at first review is an opposite but by studying the local measurement and valid point location in same field at different models, it was obtained in OH92 model potential of estimated value which is near the station 21. Then, the estimated values were separated in to two parts in field B (Figures 6.5 (b)).Part A shows the data near station 21 (because OH92 model in this field only estimated value near station 21,this part of field B was selected).In part A of field B,only 7 points were obtained for soil moisture and results show that71.42% of estimated points is in dryness level.

8 SeptemberFor OH92 model;at field A,B andC,54,247 and 69 points were obtained for soil moisture respectively(Figures 6.4,6.5,6.6 (a)), also for OH04 model: at field A,B andC,75,12 and 17 points (Figures 6.4,6.5,6.6 (b)) and for DU95 model: at field A,B andC, 2651, 1960 and 870 points(Figures 6.4,6.5,6.6 (c))were obtained for soil moisture.

The instance for field B,at selected points for OH92 model 18.25% have volumetric soil moisture values less than 10% of soil moisture value,13.49 % have volumetric soil moisture values less than 12%,34.92 % havevolumetric soil moisture of values less than14%, 25.39 % and have volumetric soil moisture values of less than16%. Mean while 7.95 % have volumetric soil moisture values less than18%.Subsequently, in this model results show that 93.13% of point located in dryness level and 7.95 in humidity level. On other hand, for OH04 model only 12 points were given.98% of the selected located between 12% volumetric soil moisture to 14% volumetric soil moisture and located in dryness level values and 2% of points in humidity level .Finally, for DU95 model 88.3% between 0% to 10% volumetric soil moisture valuesand located in dryness leveland 11.7% between 10% to 20%volumetric soil moisture values and located in semi-dry level.

All of the results were obtained for estimating soil moisture on 07.September and 08.September for two different beam modes that were implemented in field A ,B,C, shown in Table 6.22 (limit of Dubois validity domain (incidence should be > 30◦) then for 07.Septemberthe soil moisture values didn't calculate).

Table 6.23 : Summarize of dryness and humidity on field A,B,C at 07.Sept and 08.Sept.

Statistics	Models For Field A					
	OH92(9%-31%)		OH04(4%-29.1%)		DU95(0%-35%)	
	07.Sept	08.Sept	07.Sept	08.Sept	07.Sept	08.Sept
Dryness level (%)	61.66	64.91	59.14	52.34	- - -	81
Humidity level (%)	38.34	35.61	40.85	48.66	- - -	19
Number of vaild test (point)	387	54	49	75	- - -	2651
Optimal Filtering	15×15	5×5	5×5	5×5	- - -	15×15
Statistics	**Models For Field B**					
	OH92(9%-31%)		OH04(4%-29.1%)		DU95(0%-35%)	
	07.Sept	08.Sept	07.Sept	08.Sept	07.Sept	08.Sept
Dryness level (%)	86	89.13	71.42	91.67	- - -	88.3
Humidity level (%)	14	10.27	28.58	8.33	- - -	11.7
Number of vaild test (point)	136	247	18	12	- - -	1960
Optimal Filtering	15×15	5×5	5×5	5×5	- - -	15×15
Statistics	**Models For Field C**					
	OH92(9%-31%)		OH04(4%-29.1%)		DU95(0%-35%)	
	07.Sept	08.Sept	07.Sept	08.Sept	07.Sept	08.Sept
Dryness level (%)	90.64	90.86	- - -	85	- - -	92
Humidity level (%)	9.36	9.14	- - -	15	- - -	8
Number of vaild test (point)	65	69	3	17	- - -	870
Optimal Filtering	15×15	5×5	5×5	5×5	- - -	15×15

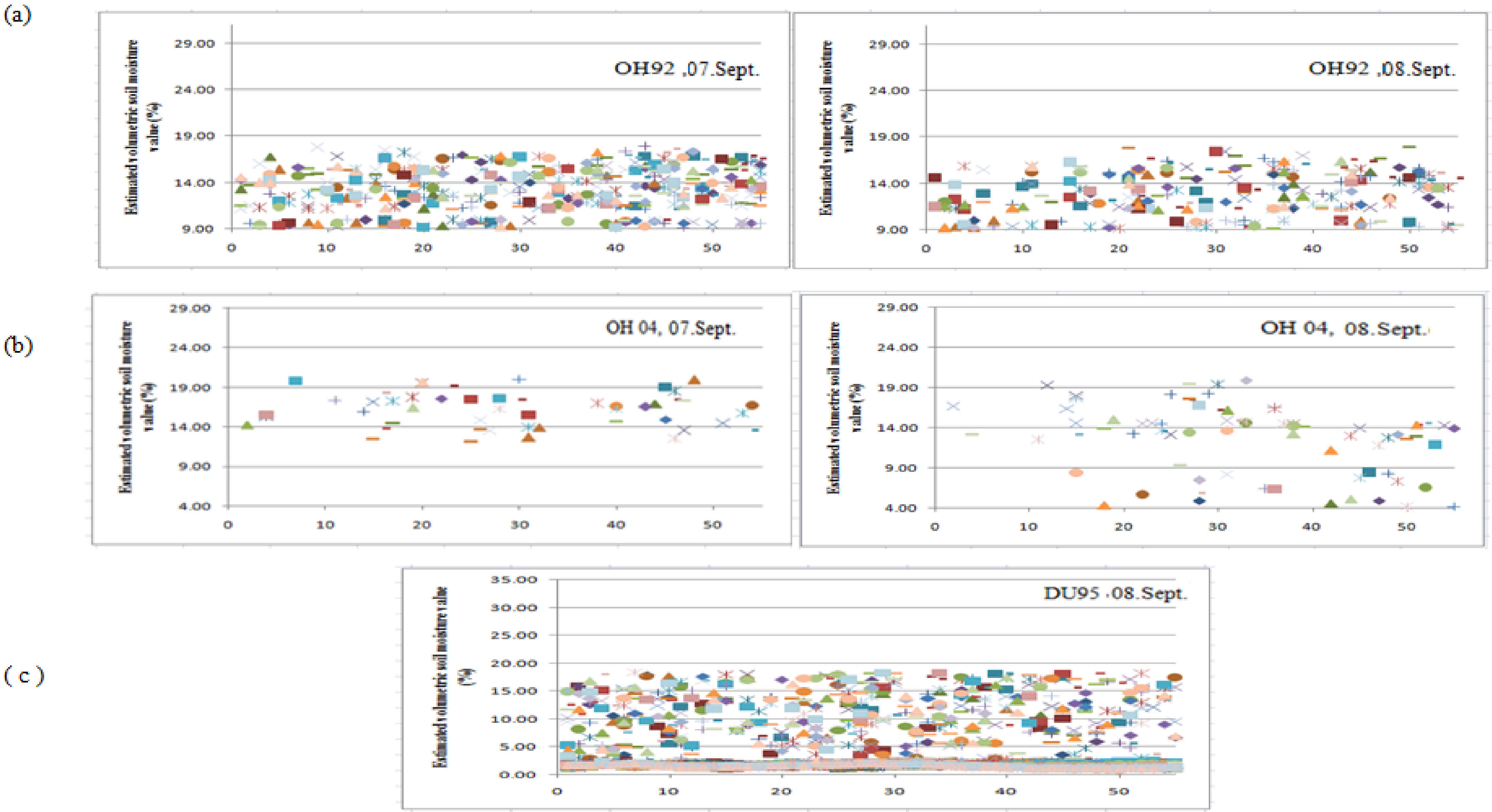

Figure 6.5 : Estimated volumetric soil moisture value (%) , field A. (a) OH92, (b) OH04, (C)DU95. Array size for field A is 50×55. Vertical axis show column number.

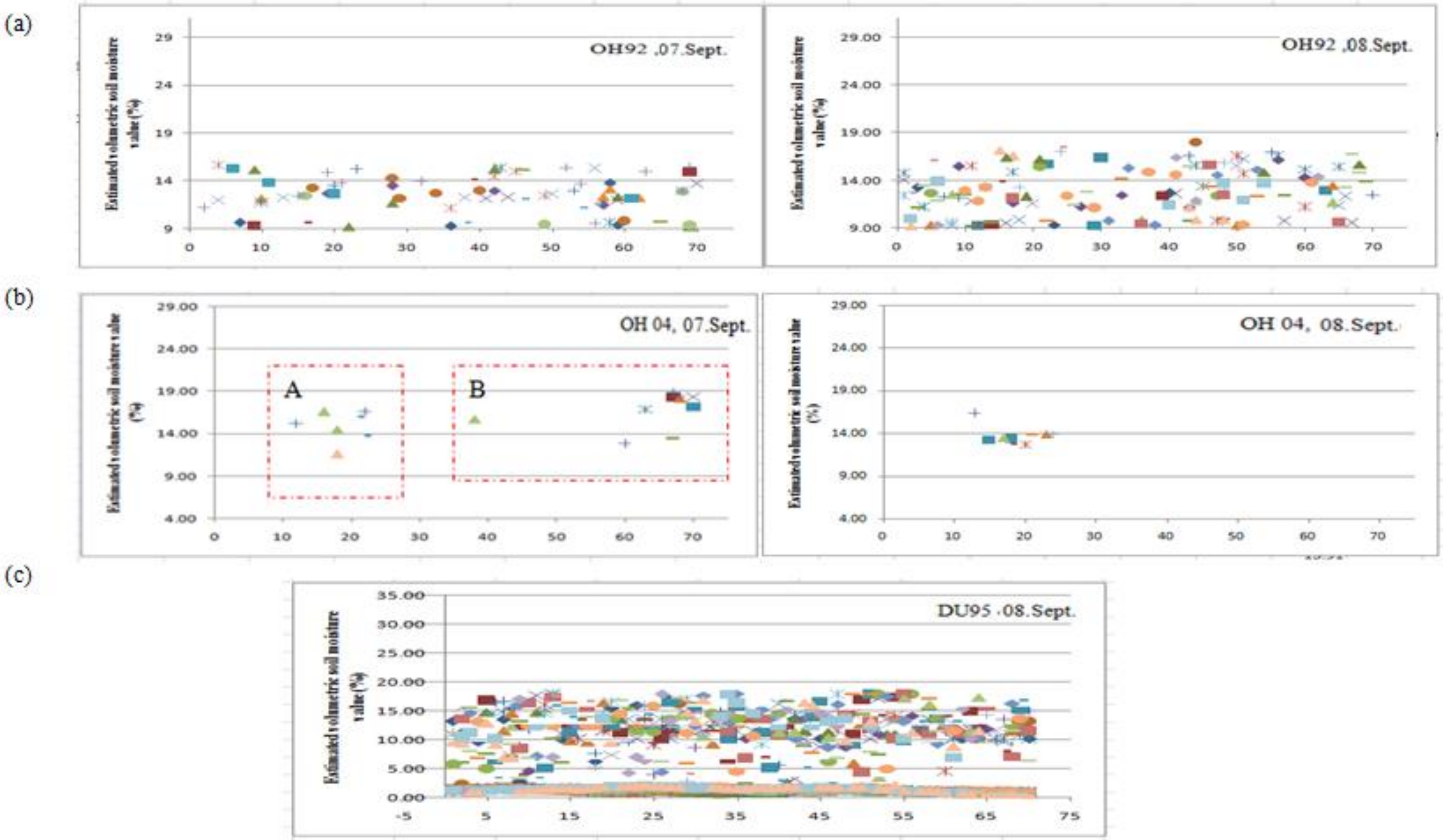

Figure 6.6 : Estimated volumetric soil moisture value (%) , Field B. (a) OH92, (b)OH04, (C)DU95. Array size for field B is 70x30. Vertical axis show column number.

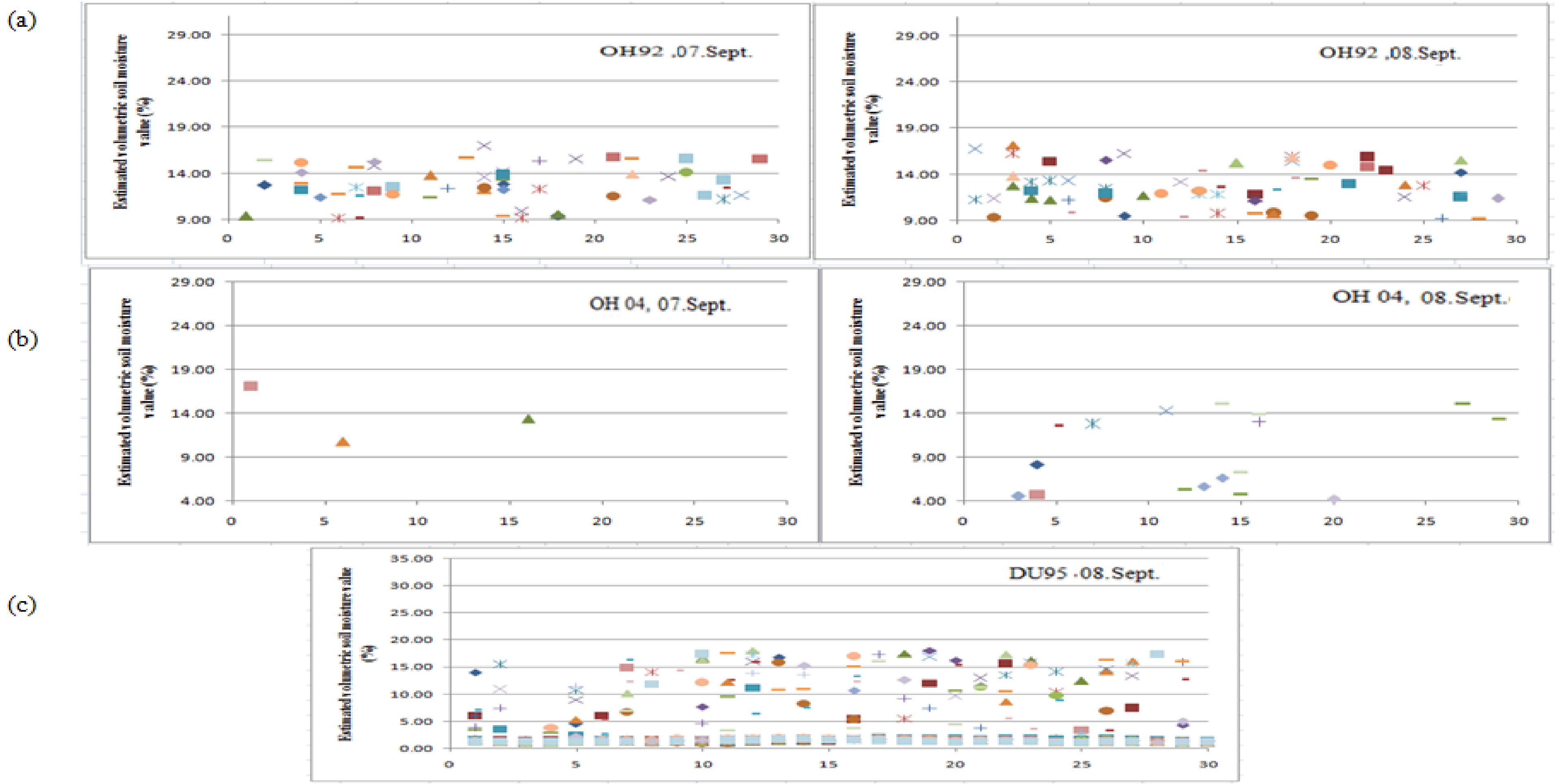

Figure 6.7 : Estimated volumetric soil moisture value (%),Field C. (a) OH92,(b)OH04,(C)DU95. Array size for field C is 29×30 . Vertical axis show column number.

By investigation and studying by selected points on selected fields over study area, some of the selected points have not a number (NAN values) (Figure 6.7, Figure 6.8, Figure 6.9).There are several reason to explain NAN values in soil moisture maps, that was generated by using semi- emprical models. Land surface conditions is another factor that was pointed out in many studies (Dubois et al. 1995 , Khabazan et al 2013, Zribi and Dechambre, 2003).The mostly used indexes are the normalized difference vegetation index (NDVI) to explain the land surface coverage. In soil moisture modeling semi-empirical model surface coverage is important. OH92,DU95 was suggested for bare soil (NDVI<0.2) and moderate vegetation cover ($0.2 < NDVI \leq 0.4$) on band -C. It is to be noted that in this study have not done field work to know crop pattern exactly, but Figure 5.4 shows that these fields are on first level agricultural area and as shown in section 5.2, September is harvest time in study area and farmland covered by various type of crops. Crop height, tillage methods and soil type have adifferent whole over the study area.Perhapsin highly moist areas vegetation coverage is compressed.As shown in the study sample, vegetation has various heights and types(there are height differences between cotton,corn and lentils, for example). The Pauli RGB image for study area by using PolSARpro was generated. Pauli RGB image for 07 September and 08 September was shown on Figure 6.10 (a) and Figure 6.10 (b)respectively. In Figure 6.10 (a) and Figure 6.10 (b), the bare agricultural areas has been shown blue to violet color tons, dense vegetation areas has been shown light yellow and villages has been shown medium white color (Raoet al. 2011).It can effect the results and during soil moisture estimation process, created gaps or NAN values points on generated soil moisture maps. On the other hand, beyond values was limited by using python script at section 6.2.Omitted values appear as NAN values on soil moisture maps too.

At field A, 2750 points for test soil moisture values was selected. However, for OH92 model on 07.September only 387 points, for OH92 model on 08 September only 54 points, OH04 model on 07.September only 49 points, for OH04 model on 08 September only 75 points and finally for DU95 model on 08 September 2651points have valid values.By study around the valid selected points in different models it was found that all of these points near the station 17 in field A. As shown Figure 6.10 (a) and Figure 6.10 (b), Stations 18 and 19 are located in dense vegetation areas (light yellow).

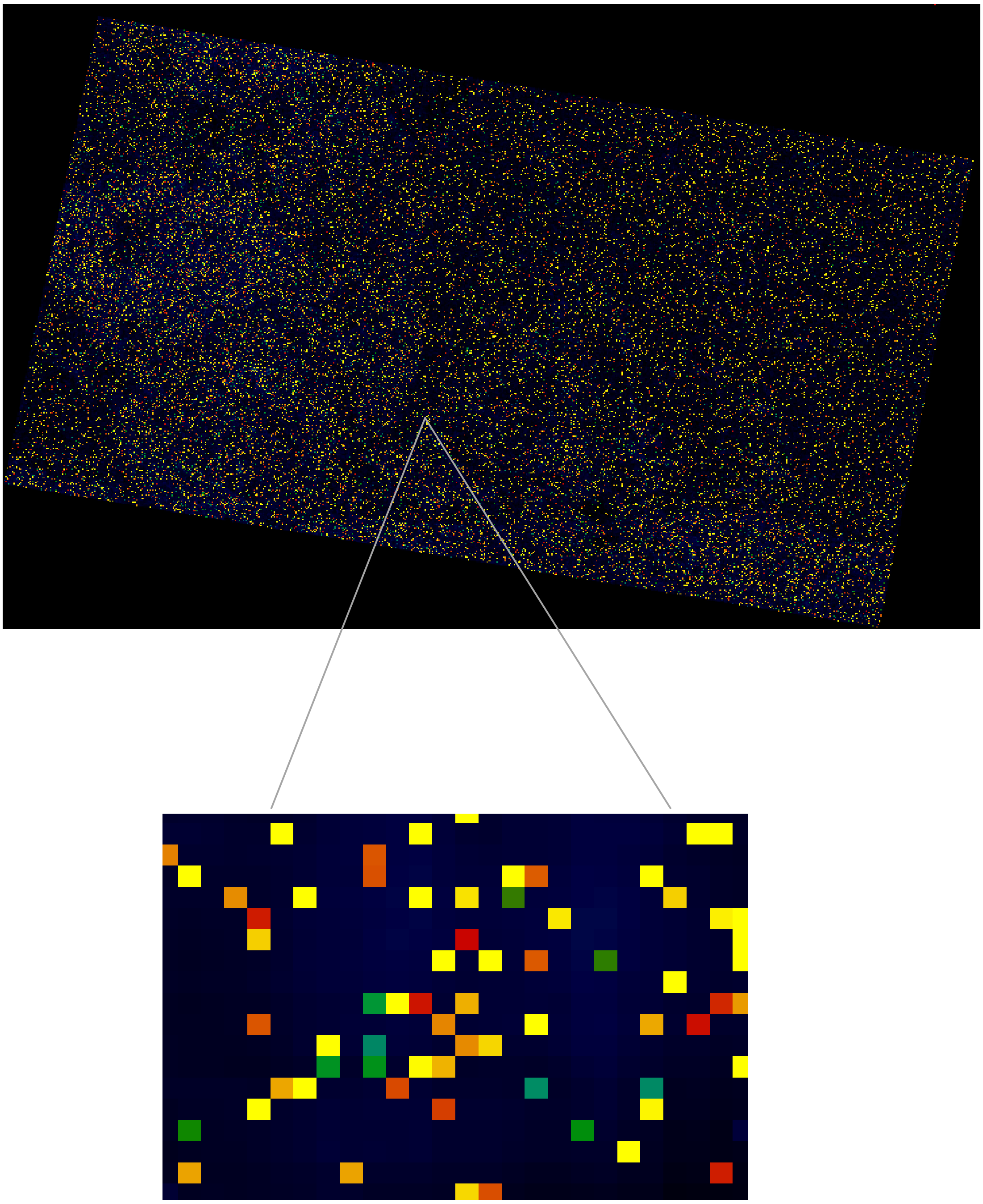

Figure 6.8 : Optimal soil moisture map, Harran, Sanliurfa, southeast of Turkey by using DU95 model for 08.Sept.2012.Black areas are pixels outside model's of range validity (NAN values). Pixels vary from blue (dry conditions 0%) to green (wet conditions 20%).

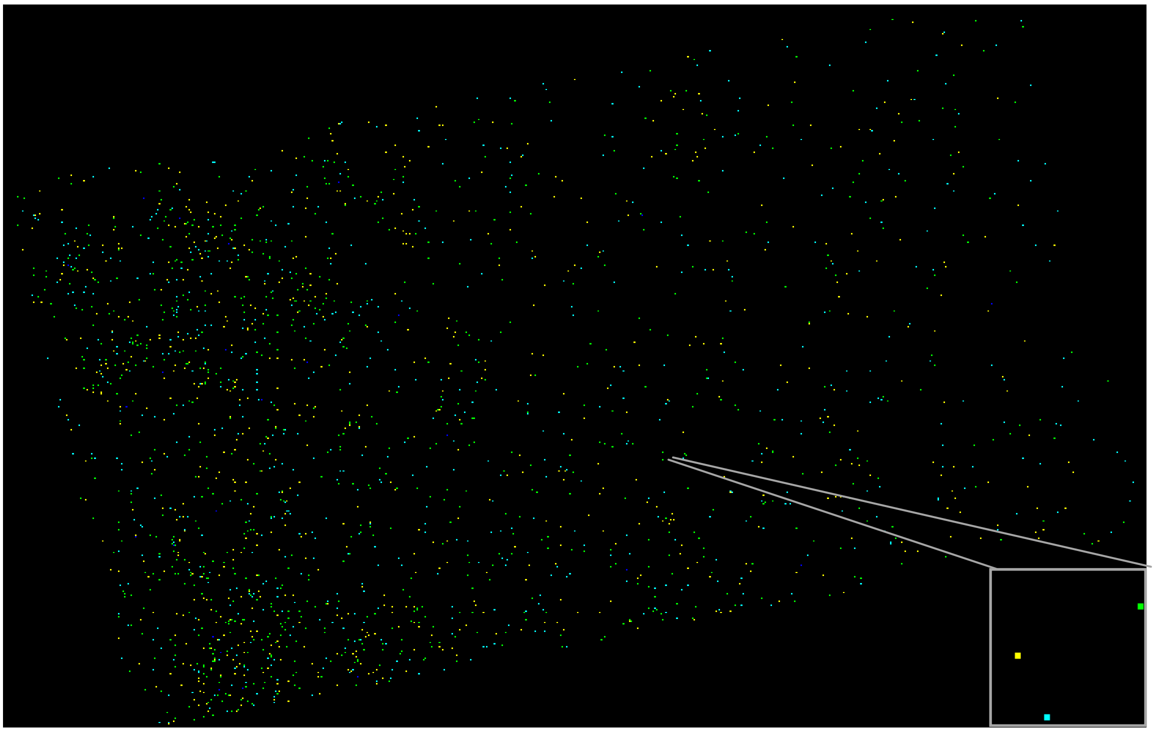

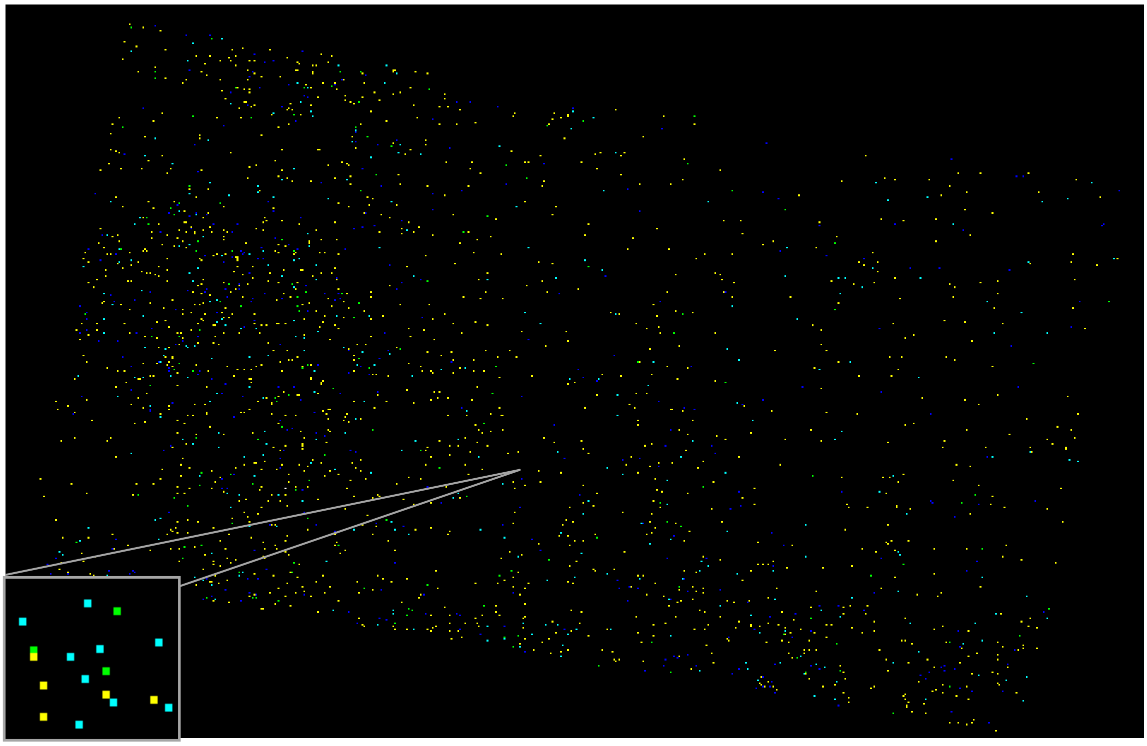

Figure 6.9 : Optimal soil moisture map, Harran, Sanliurfa, South-East of Turkey by using OH04 model for: (a) 07.Sept.2012, (b) 08.Sept.2012.Blackareas are pixels outside model's of range validity (NAN values). Pixels vary from very blue (dry conditions 4%) to green (wet conditions 23.18%).

Figure 6.10 : Optimal soil moisture map, Harran, Sanliurfa, South-East of Turkey by using OH92 model for: (a) 07.Sept.2012, (b) 08.Sept.2012.White areas are pixels outside model's of range validity (NAN values). Pixels vary from red (dry conditions 9%) to green (wet conditions 20%).

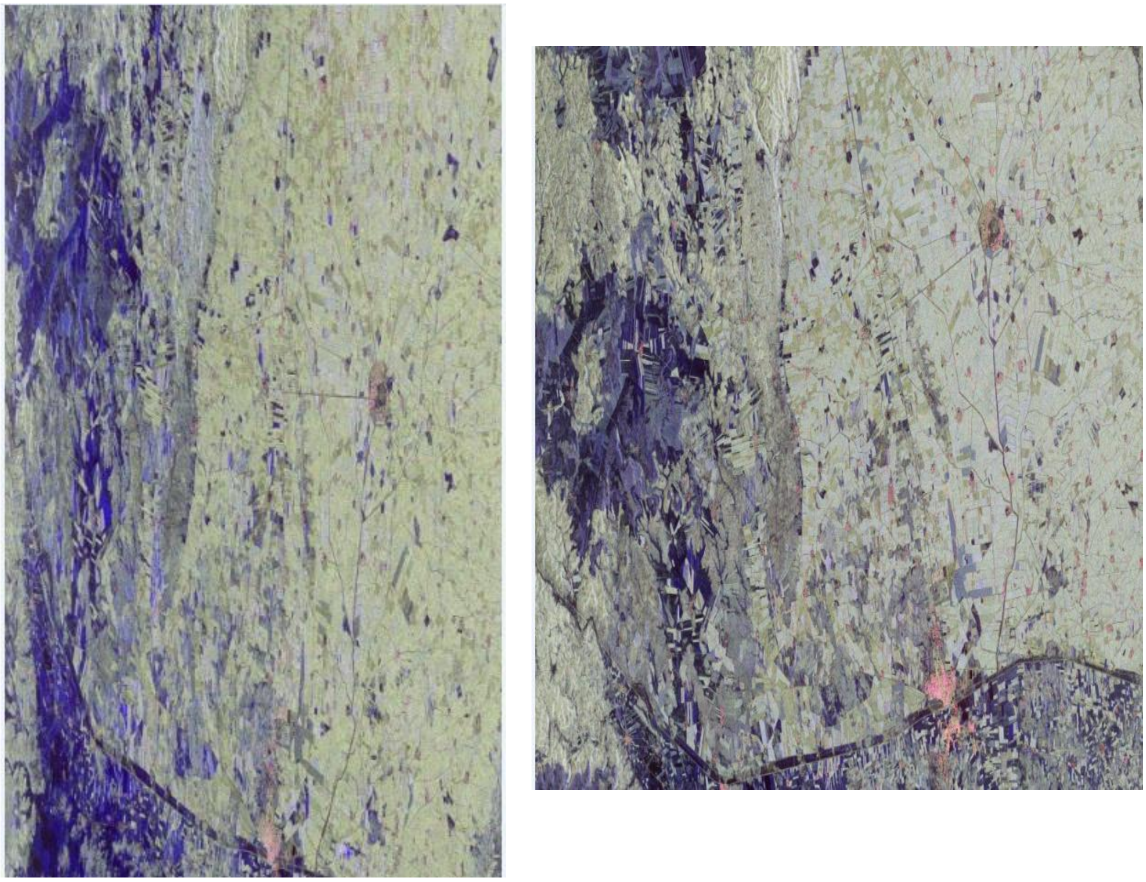

Figure 6.11 : Pauli -RGB image of Harran, Sanliurfa, south-east of Turkey. (a) 07. Sep t (left), (b) 08.Sept (right). Color Codes: (i) blue to violet, bare agr- ricultural area, (ii) light yellow, dense vegetation areas, (iii) medium white, villages.

Also at field B, 2100 points for test soil moisture values was selected. However, for OH92 model on 07.September only 136 points,for OH92 model on 08 September only 247 points, OH04 model on 07.September only 18 points,for OH04 model on 08 September only 12 points and finally for DU95 model on 08 September 1960 points have valid values.By studying around the valid selected points with different models it was discovered that a lot of these points near the station 21 in field B. As shown Figure 6.10 (a) and Figure 6.10 (b), this station is located in moderate vegetation cover area.

Finally,at field C,870 points for test soil moisture values was selected. However,for OH92 model on 07.September only 65 points,for OH92 model on 08 Septebr only 69 points, OH04 model on 07.September only 3 points,for OH04 model on 08

September only 17 points and finally for DU95 model on 08 September 870 points have valid values.

By attention thecount of valid points in different fields and models,can seen that, unfortunately,surface roughness is an important factor that could affect semi -empirical model's performance (Baghdadi et al.,2002; Verhoest et al., 2000).Comparing the models in this field shows that OH92 model on 07.September is not as successful as other models.However, estimated soil moisture valuesnear station 17 in field A and estimated soil moisture values near station 21 in field B was shown that this area is semi –dry and estimated values for field C results was shown that this field is dry area.

The difference between surface and deeper layers moisture trends can be explained by the fact that surface soil moisture is more strongly affected by atmospheric conditions than deeper layers moisture. On the other hand, no exact information about roughness, soil kind and tillage method was obtained, making it difficult to attach the absolute value for the surface soil moisture. However, the soil moisture for surface layer of soil, estimated approximately in section 5.6 (Table 5.5 and Table 5.6). As shown in these results, the potential of water is high near station 18 and 19 in field A, medium for staion 17 at field A and whole of field B and low whole of field C. Then field A was called semi-humid (soil moisture ~85%) field near the stations 18 and 19. In continue area around station 17(soil moisture ~51 %) on field A and field B(soil moisture ~40 %), was labeled semi -dry and field C, dry(soil moisture ~10 %).

Comparison of local measured and calculated Soil moisture values, expose alignment of the results on the bare soil and moderate coverage soil.

6.6 Incidence Angle Effect in Estimated Soil MoistureValues

It is a fact that the models are not highly sensitive to incidence angle, compared to their sensitivity to roughness (Baghdadi and Zribi , 2006).But it does not reduce incidence angle role and effect in soil moisture estimation, because the sensitivity of microwave sensors to soil moisture decreases when incidence angle increases(Mo et al. 1984),the energy backscattered by vegetation reduces the contribution of soil to the total backscattering (Ghedira et al .2000; Mo et al .1984) and the optimal soil moisture can be derived using a steeper incidence angle (30^0 -50^0)because it increases the vegetation depth and minimizes the effect of vegetation and surface roughness on the backscatter signal (Ulaby et al .1986b).

The results in Table 6.2 for three site and three different models for two beams was offered. As shown in this table, OH92 models on 08. September have better results than 07.September of fields A, B and C; also OH04 models on models on 08. September have better results than 07.September of fields A, B and C (this model failed in field C). The results presented here suggest that incidence angles of approximately40 (steeper incidence angle) degrees give the best result for soil moisture estimation in the OH92 and OH04 (Ulaby et al. (1982)).

A´ lvarez-Mozos et al (2007)show that for DU95 model better efficiency is at large incidence angles. For roughness class as smooth (s=0.7 cmand l=2.5 cm) and medium(s=1.5 cmand l=4.0 cm) they have suggested incidence angle equal to 40 ^{0}.Used beam (FQ19) has incidence angle range near 40 ^{0}. In model estimate in field C all of the selected points contain soil moisture values and results showed good performance in this model for field C.Results on field A and B also were supported this idea.

6.7 Limitation

The most important limitation of this study is the difference between estimated and observed soil depth. Observed soil moisture was estimated in 5 cm depth by using approximate formula because kind of soil and tillage methods information are not available;therefore, the results were not exact soil moisture in this depth for observed data. For solving this problem for future studies, it is suggested to use RADAR data In L-band.

Incidence angle range that was used for FQ1 is less than 30 degrees.This range is valid for OH models but Dubois validity domain for incidence angle should be greater than 30 degrees.In future work by using valid range of incidence angle DU 95 model performance can be investigated.

In georeference image processing, the DEM was not calculated and the calibration was ignored for backscatter . These factors can also affect the results and generate the error during the estimation.

CONCLUSIONS

Three SAR surface scattering models (OH92, OH04 and DU95) were implementedusing two RADARSAT-2, C-band data for estimation of soil moisture, and their outputswere compared with field measurements of soil moisture over agricultural soil surfaces in sought east of Turkey.

The local data that had been collected on 15Cm and 40Cm confirmed Darcy law (Vincent at el., 2014), by using this law soil moisture was calculated in surface level for ground measurement part.

Because of invalid incidence angle for 07.September DU95 model didn't run for this data. In order to improve the accuracy of the RADARSAT-2 soil moisture maps, speckle noise effect was decreasedon soil moisture maps by using Lee, Enh-Lee,Forst and Kuan filters in different sizes (3×3 -15×15). The Kuan filter was selected as optimal filter for all of the models results. The optimal filters sizes are 5×5 kernel size for OH04 model at 07 and 08 September and OH92 on 08.Sepember, also optimal filters sizes are 15×15 kernel size for Oh92 at 07 September and DU95 on 08 September. The semi-empirical inverse models that were used in this study have close relation with surface roughness, vegetation coverage, vegetation dense and height, and tillage methods. Negative influence of these factors on soil moisture applications (NAN values) by using Pauli RGB image has been explained. By using the sampling point in three different fields of study area estimated value and ground measurement was compared.Future research should consider the detailed evaluation of vegetation and roughness parameters of the study sites.

This research supports the idea of incidence angle effect on the performance of the models (Baghdadi et al. 2008;Mo et al. 1984; Ulaby et al .1986b) as well as the idea of surface roughness havingan important effect on the estimation ofsoil moisture values (Baghdadi et al.,2002; Verhoest et al., 2000; S.Khabazan et al., 2013; Zribi and Dechambre, 2003).

REFERENCES

A´ lvarez-Mozos J, Casalı´ J, aGonza´ lez-Audı´cana M, Verhoes N.E.C. (2005).Neural Correlation between Ground Measured Soil Moisture and RADARSAT-1 derived Backscattering Coefficient over an Agricultural Catchment of Navarre (North of Spain). Biosystems Engineering (2005) 92 (1), 119–133

A´ lvarez-Mozos J,Gonzalez-Audicana.M and Casali.J. (2007). Evalutiob of empirical and semi-empirical backscattering models for surface soil moisture estimation.*Can.J.Remote sensing ,Vol33,No3,pp:176-188.*

Bond, J. J. & WillisW. O. (1971).Soil-Water Evaporation - Long-Term Drying as Influenced bySurface Residue and Evaporation Potentia. Soil Science Society of America Proceedings, vol. 35, no. 6, p. 984.

Boerner, W.-M. & M.B. El-Arini.(1981).Polarization dependence in electromagnetic inverse problem.IEEE Transactions on Antennas and Propagation, 29(2), 262–271.

Born, M. & Wolf, E. (1999). *Principles of Optics: Electromagnetic Theory of Prop agation, Interference and Di raction of Light. Cambridge University Press, 7 edition, October 1999.*

Baltzer, H. (2001). Forest mapping and monitoring with interferometric synthetic aperture radar (InSAR). *Progress in Physical Geography, 25: 159-177.*

Blumberg, D.G, and Freilikher, V. (2001). Semi empirical calibration of the IEM backscattering model using radar images and moistture and roughness field meaurments.J *Indian soc Remote Sens vol 25(18):3593-3623*

Baghdadi, N., King .C, Chanzy, A. and J. P. Wigneron, J. P. (2002).An empirical calibration of the integral equation model based on SAR data, soil moisture and surface roughness measurement over bare soils. *Int. J. Remote Sens., 23(20), 4325 – 4340.*

Baghdadi, N., Holah, N. and Zribi, M. (2006).Soil moisture estimation using multiincidence and multi-polarization ASAR - data.*International Journal of Remote Sensing, 27(10):1907–1920*

Baghdadi., N., Gherbudj,M., Zribi, M.,Sahebi,F. and C.king. (2004). Polarization dependence in electromagnetic inverse problem . *Journal of Arid Environments, 49, (3), pp: 449-464.*

Baghdadi, N., Holah, N. and Zribi, M. (2006).Evaluation of radar backscatter models IEM, OH - and Dubois using experimental observations. *International Journal of Remote Sensing, 27(18):3831–3852.*

Baup, F., Mougin, E., de Rosnay, P., Timouk, F. and Chenérie, I. (2007).Surface soil moisture estimation over the AMMA Sahelian site in Mali using ENVISAT/ASAR data.*Remote Sensing of Environment, 109, (4), pp: 473-481*.

Baghdadi, N., Chaaya J.A.and Zribi, M. (2011**)**.Semi empirical calibrations of the Integral Equation Model for SAR data in c-band crosspolarization using radar images and field measurement. *IEEE Transactions on Geoscience and Remote Sensing, vol.8 no. 1, pp:14-18.*

Cumming, I. G. and F. H. Wong. (2005). Digital Processing of Synthetic Aperture Radar Data Algorithms and Implementation, Artech House, Norwood, p. 633.

Cracolice, Mark S. and Edward Peters I. (2006). *Basics of Introductory Chemistry*. Thompson, Brooks/Cole Publishing Company

Campbell, J. (2007). Introduction to remote sensing .Third edition. New York: Guilford Publications, pp: 626.

Chan Y.K and Koo V.C. (2008). An introduction to synthetic aperture radar (SAR).Progress In Electromagnatics Research B,vol2,p.27-60

Chudinova, S. M. (2009). Dielectric characteristics of soils and categories of soil water. *Eurasian Soil Science 42.4, pp: 405-414.*

Debye, P. J. W. (1929). Polar Molecules, Dover Publications Inc., New York, p. 172.

Dubois, P., van Zyl, J.and Engman, T. (1995 a). Measuring soil moisture with imaging radars. *IEEE Transactions on Geoscience and Remote Sensing, 33(4):915– 926*

Dubois, P., van Zyl, J.and Engman, T. (1995 b). Corrections to "Measuring soil moisture with imaging radars". *IEEE Transactions on Geoscience and Remote Sensing, 33(6):13-40.*

D'Urso, G. and Minacapilli, M. (2006). A semi-empirical approach for surface soil water content estimation from radar data without a-priori information on surface roughness. Journal of Hydrology, 321, (1-4), pp: 297-310.

Engman, E.T. and Chauhan, N. (1995). Status of Microwave Soil Moisture Measurements with Remote Sensing.Remote Sensing of Environment., 51(1): pp:189-198

Eom K. B. (2008). Speckle noise removal by rebuts modeling.IEEE Transactions on Antennas and Propagation ,vol(2):pp:165-168.

Foody .G.M. (1991). *Soil moistute content ground data for remote sensing investigation of agriculture region.Int. J.Remote sensing 1991 ,pp:1461-1469*

Fung, A.K., Li, Z. and Chen, K.S. (1992). Backscattering from a randomly rough dielectric surface.*IEEE Transactions on Geoscience and Remote Sensing, 30, pp:356–369.*

Fannin, P., S. Charles, D. Vincent and A. Giannitsis. (2002). Measurement of the highfrequency complex permittivity and conductivity of magnetic uids. Journal of Magnetism and Magnetic Materials 252.1, pp: 80-82.

Foucher S and Martinez C.L. (2009). An evaluation of PolSAR speckle filters. *IEEE Transactions on Geoscience and Remote Sensing,IV-845 - IV-848.*

Gardner, W. H. (1986). Water Content, in Methods of Soil Analysis Part1: Physical and Mineralogical Methods,*2nd ed. A. Klute, Ed., American Society of Agronomy, Soil Science Society of America, Madison, pp: 493-544.*

Gaskin, G. J. and J. D. Miller.(1996). Measurement of soil water content using a simplified impedance measuring technique.*Journal of Agricultural Engineering Research, vol. 63, no. 2, pp: 153-159*.

Ghedira,H , Bernier.M and OUARDA ,T.B.M.J. (2000). Application of Neural Networks for Wetland Classification in RADARSAT SAR Imagery.*IEEE Transactions on Geoscience and Remote Sensing,vol2, pp:675-677*.

Gherboudj. I , Magagi .R,Berg A.A ,Toth B. (2011). Soil moisture retrieval over agricultural fields from multi-polarized and multi-angular RADARSAT-2 SAR data.*Remote Sensing of Environment 115 (2011) 33–43*.

Heimovaara, T. J., E. J. G. deWinter, W. K. P. vanLoon and D. C. Esveld. (1996). Frequencydependent dielectric permittivity from 0 to 1 GHz: Time domain reflectometry measurements compared with frequency domain network analyzer measurements.*Water Resources Research, vol. 32, no. 12, pp: 3603-3610.*

Huynen J.R. (1970). Phenomenological Theory of Radar Targets, PhD Thesis, University of Technology, Delft, The Netherlands.

Heilman, J.L, Kanemasu, E.T., Bagley, J.O. and Rasmussen, V.P. (1977). Evaluating soil moisture and yield of winter wheat in the Great Plains using Landsat data.*Remote Sensing of Environment, 6, (4), pp: 315-326*.

Hanks ,R.G. and Aahcroft ,G.L. (1980). Applied soil physics :soil water and temperature applications.Springer-Verlag Berlin Heidelberg 1980.ISBN-13: 978-0-387-90927-1,chapter 3 :pp 62:66.

Hallikainen, M., Ulaby, F., Dobson, M., El-Rayes, M. and Wu, L. (1985). Microwave Dielectric Behavior of Wet Soil-Part 1: Empirical Models and Experimental Observations.*IEEE Transactions on Geoscience and Remote Sensing, vol. GE-23, no. 1.*

Henderson, F. M. and A. J. Lewis. (1998). Manual of Remote Sensing Vol. 2: Principles and Applications of Imaging Radar, *3rd ed., R. A. Ryerson, Ed., John Wiley & Sons, New York.*

Huynen J.R. (1990). The Stokes parameters and their interpretation in terms of physical target properties, Proceedings of the International Workshop on Radar Polarimetry, JIPR-90, 20–22 March .

Huisman, J. A., Sperl, C., Bouten, W. and Verstraten, J. M. (2001). Soil water content measurements at different scales: accuracy of time domain reflectometry and ground-penetrating radar. *Journal of Hydrology, 245, (1-4), pp: 48-58.*

Jensen, J.R. (1996). Introductory Digital Image Processing: A Remote Sensing Perspective. *Second Edition, Upper Saddle River, NJ, Prentice Hall. 318pp:*

Jackson, T. J., H. McNairn, M. A. Weltz, B. Brisco and R. Brown,. (1997). First order surface roughness correction of active microwave observations for estimating soil moisture.*IEEE Transactions on Geoscience and Remote Sensing, vol. 35, no. 4, pp: 1065-1069.*

Jensen, J.R. (2000). Remote Sensing of the Environment: An Earth Resource Perspective. Prentice Hall, Saddle River. 544 p.

Jester W, Klik A. (2005). Soil surface roughness measurement methods,applicability and surface representation.*CATENAVolume 64, Issues 2–3, 30 December 2005, Pages 174–192*

Kostinski, A.B. and W.M. Boerner. (1981). On foundations of radar polarimetry.*IEEE Transactions on Antennas and Propagation,34, 1395–1404.*

Khabazan S , Motagh M. , Hosseini M. (2013). Evaluation of Radar Backscattering Models IEM, OH and Dubois using L and C-Bands SAR Data over different vegetation canopy covers and soil depths .*International Archives of the Photogrammetry, Remote Sensing and Spatial Information Sciences, Volume XL-1/W3, 2013 SMPR 2013, 5 – 8 October 2013, Tehran, Iran.*

Low, A. J. (1954). The Study of Soil Structure in the Field and the Laboratory. Journal of Soil Science, vol. 5, no. 1, pp: 57-79.

Lewis, A.J. and Henderson, F.M. (1997). Radar fundamentals: the geoscience perspective. In: F. M. a. Henderson and A. J. Lewis (Eds.). Principles and Applications of Imaging Radar, *John Wiley, New York, pp: 131-181.*

L. Gagnon and A. Jouan.(1977). *Speckle filtering of SAR images: A comparative study between complex- wavelet-based and standard filters.SPIE proceedings series 3169, 80-91.*

Le Hégarat-Mascle, S., M. Zribi, F. Alem, A. Weisse and C. Loumagne. (2002).Soil moisture estimation from ERS/SAR data: Toward an operational methodology .*IEEE Transactions on Geoscience and Remote Sensing, vol. 40, no. 12, pp: 2647-2658.*

Leconte, R., F. Brissette, M. Galarneau and J. Rousselle. (2004). Mapping near-surface soil moisture with RADARSAT-1 synthetic aperture radar data .*Water Resources Research, vol. 40, no. 1.*

Livingstone, C.E., Sikaneta, I., Gierull, C., Chiu, S. and Beaulne, P. (2005).Radarsat-2 System and Mode Description. In Integration of Space-Based Assets within Full Spectrum Operations (pp: 15-1 – 15-22). Meeting Proceedings RTO-MP SCI-150,Paper 15. Neuilly-sur-Seine, France: RTO.

Lopez-Martinez ,c . Pottier ,E. and S.R Cloude. (2005).Statistical assessment of eigenvector based target decomposition theorems in radar polarimetry.

.IEEE Transaction on Geoscience and Remote Sensing, 43(9):2058 - 2074.

Lunt, I.A., Hubbard, S.S. and Rubin, Y. (2005). Soil moisture content estimation using ground-penetrating radar reflection data.*Journal of Hydrology, 307, (1-4), pp:254-269.*

Loew, A., R. Ludwig and W. Mauser. (2006).Derivation of surface soil moisture from ENVISAT ASAR wide swath and image mode data in agricultural areas *.IEEE Transactions on Geoscience and Remote Sensing, vol. 44, no. 4, pp: 889-899.*

Li, Z., Wang, Y., Zhou, Q., Wu, J., Peng, J. and Chang, H. (2008).Spatiotemporal variability of land surface moisture based on vegetation and temperature characteristics in Northern Shaanxi Loess Plateau, China *.Journal of Arid Environments, 72, (6), pp: 974-985.*

Lakhankaar, T., Ghedira, H., Temimi, M., Azar, A. and Khanbilvardi, R. (2009).Effect of land cover heterogeneity on soil moisture retrieval using active microwave remote sensing dataRemote sensing, 1, pp: 80-91.

Lee, J.S and E.Pottier. (2009).Polarimetric RADAR imaging :from basic to applicatins .Bocca Raton ,FL,USA:CRC Press.

MO T , SCHMUGGE T. J,JACKSON T. J. (1984). Calculations of Radar Backscattering Coefficient of Vegetation-Covered Soils. Remote sensing of enviroment *15:119-133.*

Marshall, T. J., J. W. Holmes and C. W. Rose. (1999).Soil Physics, 3rd Ed., Cambridge University Press, Cambridge, p. 457.

Mohanty, B. P. and Skaggs, T. H. W. Rose. (2001).patio-temporal evolution and time-stable characteristics of soil moisture within remote sensing footprints with varying soil,slope and vegetation.*Advances in Water Resources, 24, (9-10), pp: 1051-1067*

Moran, M. S., C. D. Peters-Lidard, J. M. Watts and S. McElroy. *(*2004). Estimating soil moisture at the watershed scale with satellite-based radar and land surface models. *Canadian Journal of Remote Sensing 30.5, pp: 805--826.*

Mattia, F., G. Satalino, L. Dente and G. Pasquariello. (2006). Using a priori information to improve soil moisture retrieval from ENVISAT ASAR AP data in semiarid regions.*IEEE Transactions on Geoscience and Remote Sensing, vol. 44, no. 4, pp: 900-912.*

Merzouki. A, McNairn.H and Pacheco .A. (2010).Evaluation of the Dubois, Oh and IEM radar backscatter models over agricultural fields using C-band RADARSAT-2 SAR image data.*Can. J. Remote Sensing, Vol. 36, Suppl. 2, pp: S274–S286.*

Mishra.P,Goel.SH and Singh .D. (2013). An impedance based approach to determine soil moisture using RADARSAT-2 data.*IEEE Transactions on Geoscience and Remote Sensing, vol. 13:pp:2724-2727.*

Némethy, G .(1966). Structure of water and of aqueous solutions.*Cryobiology, vol. 3, no. 1, pp19-26.*

Oh, Y., Sarabandi, K. and Ulaby, F. (1992). An empirical model and an inversion technique for radar scattering from bare soil surfaces.*IEEE Transactions on Geoscience and Remote Sensing,30(2):370–381.*

Oh, Y., Sarabandi, K. and Ulaby, F. (1994). An inversion algorithm for retrieving soil moisture and surface roughness from polarimetric radar observation.*In Proceedings of the Geoscience and Remote Sensing Symposium, volume 3, pages 1582–1584.*

Oh, Y., Sarabandi, K. and Ulaby, F. (2002). Semi-empirical model of the ensemble-averaged differential Mueller matrix for microwave backscattering from bare soil surfaces IEEE Transactions on Geoscience and Remote Sensing,40(6):1348–1355.

Oh, Y. (2004). Quantitative retrieval of soil moisture content and surface roughness from multipolarized radar observations of bare soil surfaces.*IEEE Transactions on Geoscience and Remote Sensing,42(3):596–601.*

Paloscia, S., P. Pampaloni, S. Pettinato and E. Santi. (2008). A Comparison of Algorithms for Retrieving Soil Moisture from ENVISAT/ASAR Images.*IEEE Transactions on Geoscience and Remote Sensing, vol. 46, no. 10, pp: 3274-3284.*

Quesney, A., Le Hégarat-Mascle, S., Taconet, O., Vidal-Madjar, D., Wigneron, J.P., Loumagne, C. and Normand, M.(2000). Estimation of Watershed Soil Moisture Index from ERS/SAR Data.*Remote Sensing of Environment, 72, (3), pp: 290-303.*

Rao Y.S and Venkataraman G. (2011). Soil moisture mapping using ALOS PALSAR and ENVISATASAR data over India.Synthetic Aperture Radar (APSAR), 2011 3rd International Asia-Pacific Conference on, *pp1-4.*

Rho S. H, . Song W. Y, Kim J and Kwag Y. K. (2011). Geolocation Error Correction Method For SAR Image Using Ground Control.*IEEE Transactions on Geoscience and Remote Sensing.*

Stratton, J.A. (1941). Electromagnetic Theory, McGraw-Hill, New York, 1941.

Snell, F. D., C. T. Snell and I. Reich. (1950). The Nature of Soil to be Deterged and Its Bonding to the Surface.*Journal of the American Oil Chemists Society, vol. 27, no. 2, pp: 62-68.*

Sherwin.C.W,Ruina J.P and Rawcliffe R.D. (1961). Some earlydevelopments in synthetic aperture radar systemIRE Transctions on military electronics ,1962,pp:111-115.

Schuler D.L., Lee J.-S. and Grandi G. De. (1996). Measurement of topography using polarimetric SAR images.*IEEE Transactions on Geoscience and Remote Sensing, (5), 1266–1277, 1996.*

Sheng, Y. & Xia, Z. (1996). A comprehensive evaluation of filters for radar speckle suppression. Geoscience and Remote sensing Symposium, 1996.*IGARSS'96. 'Remote sensing for a Sustainable Future.',International.*

Sherwin, C. W., J. P. Ruina and R. D. Rawcliffe. (1962). Some Early Developments in Synthetic Aperture Radar Systems.*Military Electronics, IRE Transactions on, vol. MIL-6, no. 2, pp: 111-115.*

Schmugge, T. *(1985).* Hydrological Forecasting. *New York, NY, USA: John Wiley*

Schmugge, T. (1998). Applications of passive microwave observations of surface soil moisture.*Journal of Hydrology, 212-213, pp: 188-197.*

Satalino, G., G. Pasquariello, F. Mattia, M. Davidson, T. Le Toan and M. Borgeaud. (2001). Soil moisture retrieval using SAR data and a priori roughness information.*Proceedings of IGARSS '01: Scanning the Present, Resolving the Future, pp: 3111-3113.*

Scheffer, F. and P. Schachtschabel. (2002). Lehrbuch der Bodenkunde, 15. Aufl. / neubearb. und erw von H.-P. Blume, Spectrum Akad. Verlag, Heidelberg, p. 593.

Shaver, T. M., G. A. Peterson, L. R. Ahuja, D. G. Westfall, L. A. Sherrod and G. Dunn. (2002). Surface soil physical properties after twelve years of dryland no-till management.*Soil Sci Soc Am J, vol. 66, no. 4, pp: 1296-1303.*

Sahebi, M. R., Bonn, F. and Gwyn, Q. H. J. (2003). Estimation of the moisture content of bare soil from RADARSAT-1 SAR using simple empirical modelsInternational Journal of Remote Sensing 24, (12), pp: 2575.

Sanli F.B ,Kurucu .Y, Esetlili M.T ,Abdikan s. (2008). Soilmoisture estimation from RADARSAT -1, ASAR AND PALSAR data in agricultural fields of Menemen planeof western WESTERN Turkey.*The International Archives of the Photogrammetry, Remote Sensing and Spatial Information Sciences. Vol. XXXVII. Part B7. Beijing.*

Sahebi, M.R., Angles, J. (2009). An inversion method based on multi-angular approaches for estimating bare soil surface parameters from RADARSAT-1.*Hydrology and Earth System Sciences Discussions, 6, pp: 207-241.*

Srivastava, H.S., Patel, P., Sharma, Y., Navalgund, R.R. (2009). Large-Area Soil moisture estimation using multi_incidence _angle Radarsat-1 SAR data.*Geoscience and Remote Sensing, IEEE Transactions, 47(8), 2528 – 2535.*

Shamsoddini, A., Trinder, J.C. (2010). Image texture presevation in speckle noise suppression *.In: Wagner W., Székely, B. (eds.): ISPRS TC VII Symposium – 100 Years ISPRS, Vienna, Austria, July 5–7, 2010, IAPRS, Vol. XXXVIII, Part 7A.*

Singh .J, Soccorsi M, Datcu M. (2010). SAR complex image analysis: A Gauss Markov and a multiple subaperture based target characteration.*IEEE Transactions on Geoscience and Remote Sensing, pp: 1585-1588.*

Srinvasa Rao S, Dinesh Kumar S, Das S,N,Nagaraju M.S.Svenugopal M.V.,Rajankar P,Laghate P,Reddy M.S,Joshi A.K,Sharma J.R. (2013). modified the Dubois model for estimating soil moisture with dual polarized SAR data.*J Indian soe Remote Sens vol 41(4):865-872.*

Touzi. R.(2004). Target scattering decomposition of one-look and multi-look SAR data using a new coherent scattering model.*In International Geoscienc and Remote Sensing Symposium, IGARSS, pages 2491-2494.*

Tromp-van Meerveld,H.J & McDonnell J.J. (2005)On the interrelations between topography, soil depth, soil moisture, transpiration rates and species distribution at the hillslope scale.*Advances in Water Resources 29 (2006) 293–310.*

Touzi. R. (2007). Speckle effect on polarimetric target scattering decomposition of SAR imagery.*Canadian Journal of Remote Sensing, 33(1):60-66.*

Ticconi .F, Pulvirenti. L and Pierdicca.l . (2011). Electromagnetic Waves. Vitaliy Zhurbenko (Ed.), ISBN: 978-953-307-304-0, InTech, Available from: http://www.intechopen.com/books/electromagnetic-waves/models-for-scattering-from-rough-surfaces

Ulaby, F. T., P. P. Batlivala and M. C. Dobson. (1978). Microwave Backscatter Dependence on Surface Roughness, Soil Moisture and Soil Texture: Part I-Bare Soil.*IEEE Transactions on Geoscience Electronics, vol. 16, no. 4, pp: 286-295*.

Ulaby, F. T., F. Kouyate, A. K. Fung and A. J. Sieber. (1982). A backscatter Mmodel for a randomly perturbed periodic surface.*IEEE Transactions on Geoscience and Remote Sensing,vol. GE-20, no. 4, pp: 518-528.*

Ulaby, F. T., R. K. Moore and A. K. Fung. (1981b). Microwave remote sensing active and passive volume I - fundamentals and radiometry.*1st Edition, D. S. Simonett, Ed., Addison-Wesley Publishing Company, Inc., Reading, Massachusetts 01867, USA, p. 456.*

Ulaby, F. T, R. K. Moore and FungA. K. (1981b). Microwave remote sensing active and passive volume I - Surface Scattering and Emission Theory, 1st Edition, D. S. Simonett, Ed., AddisonWesley Publishing Company, Inc.

von Hippel, A.(1995). Dielectrics and Waves, New ed., A. S. Labounsky, Ed., Artech House, Boston, p. 284.

Verhoest, N. E. C., R. Hoeben, F. P. De Troch and P. A. Troch. (2000). Soil moisture inversion from ERS and SIR-C imagery at the Zwalm catchment, Belgium.*In Proceedings of IGARSS '00:Taking the Pulse of the Planet, pp: 2041-2043.*

Vincent, K.K, Muthama, M.N, Muoki,S.N. (2014) Darcy's Law Equation with Application to Underground Seepage in Earth Dams in Calculation of the Amount of Seepage.*American Journal of Applied Mathematics and Statistics. Vol. 2 No. 3, 143-149*.

Wang, J. R. and Schmugge,T. J. (1980). An empirical model for the complex dielectric permittivity of soils as a function of water content. *IEEE Transactions on Geoscience and Remote Sensing GE-18.4, pp: 288 - 295.*

Wensink. W. A.(1993). Dielectric properties of wet soils in the frequency range 1-3000 MHz, Geophysical Prospecting, 41, 671–696 (1993).

Waring, R.H., Way, J., Hunt Jr., E.R., Morrissey, L., Ranson, K.J., Weishampel, J.F., Orem, R. and Franklin, S.E. (1995). Imaging radar for ecosystems studies. *BioScience, 45: 715-723*.

Wickel, A. J., Jackson, T. J. and Wood, E. F. (2001). Multitemporal monitoring of soil moisture with RADARSAT SAR during the 1997 Southern Great Plains hydrology experiment .*International Journal of Remote Sensing, 22, (8), pp: 1571-1583.*

Wang H,Ouchi K,Watanabe M,Shimada M,Tadono T,Rosenqvist A,Romshoo A ,S,Matsuoka M,Moriyama,T,Uratsuka ,S. (2006). In Search of the Statistical Properties of High-Resolution Polarimetric SAR Data for the Measurements of Forest Biomass Beyond the RCS Saturation Limits.*IEEE Transactions on Geoscience and Remote Sensing leters, vol, no. 4.*

Wang, L. (2008). Remote sensing techniques for soil moisture and agricultural drought monitoring. PhD thesis. George Mason University, Fairfax, VA, USA.

Xiao.W ,Zengxiang .Z. (2005). A Review :Theories methods and development of soil moisture monitoring by remote sensing.Geoscience and Remote Sensing Symposium, 2005. IGARSS '05. Proceedings. 2005 IEEE International ,Vol 6: pp:4505-4507.

Zribi, M. and Dechambre, M. (2003). A new empirical model to retrieve soil moisture and roughness from C-band radar data.Remote Sensing of Environment, 84(1):42-52.

Zheng, X. and K. Zhao. (2010). A method for surface roughness parameter estimation in passive microwave remote sensing. Chinese Geographical Science 20.4, pp: 345-352.

Url-1 <*https://earth.esa.int/web/polsarpro/home* >, date retrieved05.01.2015.

Url-2 <*https://www.python.org/downloads*>,date retrieved 10.11.2014.

Url,3<*http://gs.mdacorporation.com/products/sensor/radarsat2/RS2_Product_Description.pdf*>,date retrieved05.11.2014.

Utrl-4<*http://pyradar-tools.readthedocs.org/en/latest*>,dateretrieved 10.11.2014.

APPENDICES

APPENDIX A: Script for GeneratingSome of Covariance Matrix Elements.
APPENDIX B: Script for Model Estimates.
APPENDIX C: Script for Soil Moisture Models Image Filtering and Calculated Statistical Value.
APPENDIX D : Part of Product File of RS2_OK40034_PK385312_DK338797_ FQ1W_20120907_151121_HH_VV_HV_VH_SLC.
APPENDIX E : Part of Product File of RS2_OK40034_PK385313_DK338798_ FQ19W_20120908_032638_HH_VV_HV_VH_SLC.

APPENDIXA :Script for Generating Some of Covariance Matrix Elements

In this script by using Python (2,7) programing ,C11, C22,C33 was generated . Attention that the “++” plass plass character at the end of a line indicates that a command is continued on the following line.

```
import os,csv,math,subprocess
from osgeo import gdal
from gdalconst import *
import numpy as np
#current directory
os.chdir(r'"D:')
###############################################
def geofile ( beamno , polarizationmode  ):
    fn = 'FQ'+str(beamno)+'_'++str(polarizationmode)+'_scl_geo'
    ds = gdal.Open(fn,GA_ReadOnly)
    ## get image size
    rows = ds.RasterYSize
    cols = ds.RasterXSize
    print rows,cols
    # Set NoData Value
    c11 = ds.GetRasterBand(1)
    data1 = c11.ReadAsArray(0, 0, cols, rows)
    c11=pow(data1,2)
    # Delete the band and dataset objects
    ds = None
    data1 = None
    # Write the files to ENVI format
    driver = gdal.GetDriverByName('ENVI')
    ds = driver.Create('c11.bin', cols, rows, 1, GDT_Float32,['SUFFIX=ADD'++
    , 'INTERLEAVE=BSQ'])
    ds.GetRasterBand(1).WriteArray(c11, 0, 0)
    ds = None
    # Write the accompanying config.txt file
    file = open('config.txt', 'w')
    text = "Nrow\n" + str(rows) + "\n ---------\nNcol\n" +str(cols) + "\n ++
    ---------\nPolarCase\nmonostatic\n ---------\nPolarType\nfull\n"
    file.write(text)
    file = None
################################################
def geofile2 ( beamno , polarizationmode  ):
    fn = 'FQ'+str(beamno)+'_'+str(polarizationmode)+'_scl_geo'
    ds = gdal.Open(fn,GA_ReadOnly)
    # get image size
    rows = ds.RasterYSize
    cols = ds.RasterXSize
    # Set NoData Value
    c22Band = ds.GetRasterBand(1)
    data2 = c22Band.ReadAsArray(0, 0, cols, rows)
    # Delete the band and dataset objects
    ds = None
    data1 = None
    # Write the files to ENVI format
    driver = gdal.GetDriverByName('ENVI')
    ds = driver.Create('c22.bin', cols, rows, 1, GDT_Float32,['SUFFIX=ADD'++
    , 'INTERLEAVE=BSQ'])
    ds.GetRasterBand(1).WriteArray(c22, 0, 0)
    ds = None
```

```
################################################################
def geofile3 ( beamno , polarizationmode  ):
    fn = 'FQ'+str(beamno)+'_'+str(polarizationmode)+'_scl_geo'
    ds = gdal.Open(fn,GA_ReadOnly)
    ds = gdal.Open('FQ1_PK385312_product_VV_slc_geo', GA_ReadOnly)
    # get image size
    rows = ds.RasterYSize
    cols = ds.RasterXSize
    # Set NoData Value
    c33Band = ds.GetRasterBand(1)
    data3 = c33Band.ReadAsArray(0, 0, cols, rows)
    c33=pow(data3,2)
    print c33
    # Delete the band and dataset objects
    ds = None
    data1 = None
    # Write the files to ENVI format
    driver = gdal.GetDriverByName('ENVI')
    ds = driver.Create('c33.bin', cols, rows, 1, GDT_Float32,['SUFFIX=ADD',++
    'INTERLEAVE=BSQ'])
    ds.GetRasterBand(1).WriteArray(c33, 0, 0)
    ds = None
```

APPENDIX B : Script for Model Estimates

In this script by using Python (2,7) programing and surface inversion models modules,that was run from PolSARpro (ESA v.4.2.0, 2011), was evaluated dielectric permittivity and volumetric soil moisture. Attention that the “++” plass plass character at the end of a line indicates that a command is continued on the following line.

```
import scipy
from scipy import ndimage
import os, subprocess, csv, math
import numpy as np
from osgeo import gdal
from gdalconst import *
def inputdate(date ):
    #xsize and ysize by using config file data
    xsize = 7054
    ysize = 4984
    # Run the OH92 module in PolSARpro to generate .bin files : mv and er
    cwd1 = 'C:\Program Files (x86)\PolSARpro_v4.2.0\Soft\data_process_sngl'
    cmd1 = ['surface_inversion_oh_C3.exe', "D:/eren","D:/eren", "D:/eren/8.bin",++
    '0', '0', '4984', '7054', '0']
    process = subprocess.Popen(cmd1, shell=True, stdout=subprocess.PIPE,cwd=cwd1)
    process.wait()
    # Write the .bin.hdr file for the mv layer
    file = open('oh_er.bin.hdr', 'w')
    text = "ENVI\ndescription={\n File Imported into ENVI.}\nsamples = " + str(xsize)++
    + "\nlines = " + str(ysize) + "\nbands = 1\nheaderoffset = 0\nfile type = ENVI  ++
    Standard\ndata type = 4\ninterleave =\bsq\nsensor type = Unknown\nbyte order = ++
    0\nband names ={\n oh_mv.bin}\n"
    file.write(text)
    file = None
    # Re-import the ENVI mv file and write to array
    driver = gdal.GetDriverByName('ENVI')
    ds = gdal.Open('oh_er.bin', GA_ReadOnly)
    erdata = ds.GetRasterBand(1)
    er = erdata.ReadAsArray(0, 0, xsize, ysize)
    # Conversion using good version of Topp model
    mv = (-0.053 + 0.0292*er - 0.00055*pow(er,2) +0.0000043*pow(er, 3)) * 100
    mv = ((mv>=9)*1)*((mv<=31)*1)*mv
    # Filter out out of bounds values
```

```
erdata = None
er= None
ds = None
# Export the estimates to PCIDSK format
driver = gdal.GetDriverByName('PCIDSK')
fn = str(date) + "_OH92.pix"
ds = driver.Create(fn, xsize, ysize, 1, GDT_Float32)
ds.GetRasterBand(1).WriteArray(mv, 0, 0)
ds = None
mv= None

# Run the DUBOIS95 module in PolSARpro to generate .bin files
cwd1 = 'C:\Program Files (x86)\PolSARpro_v4.2.0\Soft\data_process_sngl'
cmd1 = ['surface_inversion_dubois_C3.exe', "D:/eren","D:/eren", "D:/eren/8.bin",++
'0', '0', '4984', '7054', '5.404999242769673','0', '0', '1.0']
subprocess.Popen(cmd1, shell=True, stdout=subprocess.PIPE,cwd=cwd1).wait()
# Write the .bin.hdr file for the mv layer
file = open('dubois_er.bin.hdr', 'w')
text = "ENVI\ndescription={\n File Imported into ENVI.}\nsamples= " + str(xsize) +++
"\nlines = " + str(ysize) + "\nbands = 1\nheader offset = 0\nfile type = ENVI Standard\ndata ++
type = 4\ninterleave = bsq\nsensor type = Unknown\nbyte order = 0\nband names = {\n dubois_er.bin}\n"
file.write(text)
file = None
# Re-import the ENVI mv file and write to array
driver = gdal.GetDriverByName('ENVI')
ds = gdal.Open('dubois_er.bin', GA_ReadOnly)
erdata = ds.GetRasterBand(1)
er = erdata.ReadAsArray(0, 0, xsize, ysize)
# Conversion using good version of Topp model
mv = (-0.053 + 0.0292*er - 0.00055*pow(er,2) +0.0000043*pow(er, 3)) * 100
# Filter out negative values
mv = (mv>0)*1*mv
erdata = None
er= None
ds = None
# Export the estimates to PCIDSK format
driver = gdal.GetDriverByName('PCIDSK')
fn = str(date) + "_DU95.pix"
ds = driver.Create(fn, xsize, ysize, 1, GDT_Float32)
ds.GetRasterBand(1).WriteArray(mv, 0, 0)
ds = None
mv= None
#Run the OH04 module in PolSARpro to generate .bin files : mv and er
```

```
cwd1 = 'C:\Program Files (x86)\PolSARpro_v4.2.0\Soft\data_process_sngl'
cmd1 = ['surface_inversion_oh2004_C3.exe', "D:/eren","D:/eren", "D:/eren/8.bin"++
,'0','0', '4984', '7054', '0', '5.404999242769673']
subprocess.Popen(cmd1, shell=True, stdout=subprocess.PIPE,cwd=cwd1).wait()
# Write the .bin.hdr file for the mv layer
file = open('oh2004_mv.bin.hdr', 'w')
text = "ENVI\ndescription={\n File Imported into ENVI.}\nsamples = " ++
+ str(xsize) + "\nlines = " + str(ysize) + "\nbands =1\nheader offset = ++
0\nfile type = ENVI Standard\ndata type =4\ninterleave = bsq\nsensor type = ++
Unknown\nbyte order = 0\nband names = {\n oh2004_mv.bin}\n"
file.write(text)
file = None
# Re-import the ENVI mv file and write to array
driver = gdal.GetDriverByName('ENVI')
ds = gdal.Open('oh2004_mv.bin', GA_ReadOnly)
mvdata = ds.GetRasterBand(1)
mvdata = mvdata[np.logical_not(np.isnan(mvdata))]
mv = mvdata.ReadAsArray(0, 0, xsize, ysize)
mv = ((mv>=4)*1)*((mv<=29.1)*1)*mv
print mv
mvdata = None
ds = None
# Export the estimates to PCIDSK format
driver = gdal.GetDriverByName('PCIDSK')
fn = str(date) + "_OH04.pix"
ds = driver.Create(fn, xsize, ysize, 1, GDT_Float32)
ds.GetRasterBand(1).WriteArray(mv, 0, 0)
ds = None
mv= None
```

APPENDIX C : Script for Soil Moisture Models Image Filtering and Calculated Statistical Value

In this script by using Python (2,7) programing run four kind of filtering for soil moisture file on each model and calculated statistical value for fine optimal filter . Attention that the “++” plass plass character at the end of a line indicates that a command is continued on the following line.

For filtering part was used pyradar codes [Utrl-4].

```
import scipy
from scipy import ndimage
import os, subprocess, csv, math
import numpy as np
from osgeo import gdal
from gdalconst import *
import numpy
os.chdir(r'"D:\elena\answer\results final')
#open original file
def orgfile (date , model ,filttype ,filtsize ):
    # open orginal soil moisture .pix file and write to array
    driver = gdal.GetDriverByName('PCIDSK')
    fn = str(date) + "_" + str(model) + ".pix"
    ds = gdal.Open(fn, GA_ReadOnly)
    RAW = ds.GetRasterBand(1)
    xsize = ds.RasterXSize
    ysize = ds.RasterYSize
    RAW = RAW.ReadAsArray(0, 0, xsize, ysize)
ds = None
#open filterd file
def Filtfile (date , model ,filtsize ):
# open optimom soil moisture .pix file and write to array
    driver = gdal.GetDriverByName('PCIDSK')
    fn = str(date) + "_" + str(model)+"Kuan"+str(filsize) + ".pix"
    ds = gdal.Open(fn, GA_ReadOnly)
    erdata = ds.GetRasterBand(1)
    xsize = ds.RasterXSize
    ysize = ds.RasterYSize
    FILT= erdata.ReadAsArray(0, 0, xsize, ysize)
```

```
#Calculate normalized mean ( NM )
    FILT_mean = SA.mean()
    RAW_mean = RAW.mean()
    NM = FILT_mean/RAW_mean
#Calculate  Standard deviation to mean (STM)
    RAW_std = RAW.std()
    FILT_std = SA.std()
    STM = FILT.std()/FILT.mean()
#Calculate    mean to Standard deviation (ENL)
    ENL= FILT.mean()/FILT.std()
#Calculate    mean to Standard deviation (SSI)
    SSI=(RAW.std()/RAw.mean())*ENL
#Calculate filterd file  Standard deviation to orignal file Std (SSMPI)
    STDFO= FILT.std()/RAW.std()
    SSMPI=STDFO*(1+abs(FILT.men()-RAW.mean())
 #Write out a .csv file with the locations and values
    fn = str(date) + "_"+ str(model) + str(filttype )+++
                 str(filtsize) + "x" +str(filtsize) + ".csv"
    file = open(fn, 'w')
    firstrow = "FILT_mean ,FILT_std, \n"
    file.write(firstrow)
    row = str(FILT_mean) + ", " +str(FILT_std )+", " +str(ENL) +++
                 ", " + str(SSI)+","+str(SSMPI)+ "\n"
    file.write(row)
file=None
   file = open(fn, 'w')
   firstrow = "FILT men,FILT std,ENL,SSI,SSMPI, n\n"

#coordinate for site A
    SA=mv[3760:3830,3805:3835]
    where_are_NaNs = np.isnan(SA)
    SA[where_are_NaNs] = 0
        if model == 'OH92':
            # Filter out out of bounds values
            SA = ((SA>=9)*1)*((SA<=31)*1)*SA
        elif model == 'OH04':
            # Filter out out of bounds values
            SA = ((SA>=4)*1)*((SA<=29)*1)*SA
        else:
        # Filter out out of bounds values
        SA = ((SA>0)*1)*((SA<35)*1)*SA
#write site A values to CSV file
    fn = fn = str(date) + "_" + str(model)+str(filsize)+"csv"
    numpy.savetxt(fn,SA, delimiter=",")
ds = None
```

```
#coordinate for site B
    SB=mv[3760:3830,3805:3835]
    where_are_NaNs = np.isnan(SB)
    SB[where_are_NaNs] = 0
        if model == 'OH92':
            # Filter out out of bounds values
            SB = ((SB>=9)*1)*((SB<=31)*1)*SB
        elif model == 'OH04':
            # Filter out out of bounds values
            SB = ((SB>=4)*1)*((SB<=29)*1)*SB
        else:
        # Filter out out of bounds values
        SB = ((SB>0)*1)*((SB<35)*1)*SB
#write site C values to CSV file
    fn = fn = str(date) + "_" + str(model)+str(filsize)+"SB"+"csv"
    numpy.savetxt(fn,SB, delimiter=",")
ds = None
#coordinate for site C it is example
    SC=mv[3760:3830,3805:3835]
    where_are_NaNs = np.isnan(SC)
    SC[where_are_NaNs] = 0
        if model == 'OH92':
            # Filter out out of bounds values
            SC = ((SC>=9)*1)*((SC<=31)*1)*SC
        elif model == 'OH04':
            # Filter out out of bounds values
            SC= ((SC>=4)*1)*((SC<=29)*1)*SC
        else:
        # Filter out out of bounds values
        SC = ((SC>0)*1)*((SC<35)*1)*SC
#write site A values to CSV file
    fn = fn = str(date) + "_" + str(model)+str(filsize)+"SC"+"csv"
    numpy.savetxt(fn,SC, delimiter=",")
ds = None
```

APPENDIX D:Part of Product File ofRS2_OK40034_PK385312_DK338797_ FQ1W_20120907_151121_HH_VV_HV_VH_SLC.

Part of product file of FQ1 is shown below, this file ix html format ,continue of file and other details are presented in CD.


```
<?xmlversion="1.0"encoding="UTF-8"standalone="yes"?>
<productxmlns="http://www.rsi.ca/rs2/prod/xml/schemas"copyright="RADARSAT-2 Data and Products (c) MacDonald, Dettwiler and Associates Ltd., 2012 - All Rights Reserved."xmlns:xsi="http://www.w3.org/2001/XMLSchema-instance"xsi:schemaLocation="http://www.rsi.ca/rs2/prod/xml/schemas schemas/rs2prod_product.xsd">
	<productId>PDS_02926160</productId>
	<documentIdentifier>RN-RP-51-2713, Issue 1/11</documentIdentifier>
	<sourceAttributes>
		<satellite>RADARSAT-2</satellite>
		<sensor>SAR</sensor>
		<inputDatasetId>/Fred/RSAT-2/336012G</inputDatasetId>
		<imageId>217238</imageId>
		<inputDatasetFacilityId>Not Specified</inputDatasetFacilityId>
		<beamModeId>8600</beamModeId>
		<beamModeMnemonic>FQ1W</beamModeMnemonic>
		<rawDataStartTime>2012-09-07T15:11:21.352417Z</rawDataStartTime>
		<radarParameters>
			<acquisitionType>Fine Quad Polarization</acquisitionType>
			<beams>Q1</beams>
			<polarizations>HH VV HV VH</polarizations>
			<pulses>30short</pulses>
			<rankbeam="Q1">15</rank>

	<settableGainbeam="Q1"pole="HH"wing="Combined"units="dB">-1.299999917804813e+01</settableGain>

	<settableGainbeam="Q1"pole="HV"wing="Combined"units="dB">-1.299999917804813e+01</settableGain>

	<settableGainbeam="Q1"pole="VH"wing="Combined"units="dB">-1.299999917804813e+01</settableGain>

	<settableGainbeam="Q1"pole="VV"wing="Combined"units="dB">-1.299999917804813e+01</settableGain>

	<radarCenterFrequencyunits="Hz">5.404999242769673e+09</radarCenterFrequency>

	<pulseRepetitionFrequencybeam="Q1"units="Hz">2.772227050781250e+03</pulseRepetitionFrequency>

	<pulseLengthpulse="30short"units="s">2.080838775634766e-05</pulseLength>

	<pulseBandwidthpulse="30short"units="Hz">3.002442203000000e+07</pulseBandwidth>
			<antennaPointing>Right</antennaPointing>
```

<adcSamplingRatepulse="30short"units="Hz">3.166992187500000e+07</adc
SamplingRate>
<yawSteeringFlag>YawSteeringOn</yawSteeringFlag>
<geodeticFlag>Off-Geocentric</geodeticFlag>
<rawBitsPerSample>3</rawBitsPerSample>
<samplesPerEchoLinebeam="Q1">4164</samplesPerEchoLine>
<referenceNoiseLevelincidenceAngleCorrection="Beta
Nought">
<pixelFirstNoiseValue>0</pixelFirstNoiseValue>
<stepSize>36</stepSize>

<numberOfNoiseLevelValues>97</numberOfNoiseLevelValues>
<noiseLevelValuesunits="dB">-1.97959099e+01 -
2.05202103e+01 -2.12424793e+01 -2.19223995e+01 -2.25573006e+01 -
2.31904602e+01 -2.37630692e+01 -2.43239193e+01 -2.48713493e+01 -
2.53703709e+01 -2.58680401e+01 -2.63369904e+01 -2.67807198e+01 -
2.72232704e+01 -2.76260204e+01 -2.80206108e+01 -2.84084892e+01 -
2.87596703e+01 -2.91099396e+01 -2.94437199e+01 -2.97542992e+01 -
3.00640697e+01 -3.03496609e+01 -3.06227493e+01 -3.08951397e+01 -
3.11371994e+01 -3.13753510e+01 -3.16093102e+01 -3.18151398e+01 -
3.20204582e+01 -3.22160416e+01 -3.23907204e+01 -3.25649605e+01 -
3.27249107e+01 -3.28699188e+01 -3.30145607e+01 -3.31411591e+01 -
3.32577095e+01 -3.33739700e+01 -3.34691200e+01 -3.35582390e+01 -
3.36471291e+01 -3.37124290e+01 -3.37749405e+01 -3.38373108e+01 -
3.38740692e+01 -3.39106712e+01 -3.39452782e+01 -3.39565201e+01 -
3.39677315e+01 -3.39755707e+01 -3.39617386e+01 -3.39479408e+01 -
3.39298897e+01 -3.38912582e+01 -3.38527107e+01 -3.38095093e+01 -
3.37461891e+01 -3.36830215e+01 -3.36152496e+01 -3.35272484e+01 -
3.34394417e+01 -3.33475914e+01 -3.32347488e+01 -3.31221504e+01 -
3.30065689e+01 -3.28685799e+01 -3.27308998e+01 -3.25918503e+01 -
3.24282608e+01 -3.22650108e+01 -3.21021118e+01 -3.19128094e+01 -
3.17233391e+01 -3.15342808e+01 -3.13207607e+01 -3.11041908e+01 -
3.08880806e+01 -3.06500797e+01 -3.04052792e+01 -3.01609707e+01 -
2.98980999e+01 -2.96235695e+01 -2.93495998e+01 -2.90613403e+01 -
2.87551899e+01 -2.84496708e+01 -2.81354008e+01 -2.77952194e+01 -
2.74556999e+01 -2.71147308e+01 -2.67373295e+01 -2.63606892e+01 -
2.59847908e+01 -2.55735397e+01 -2.51556206e+01 -
2.47385292e+01</noiseLevelValues>
</referenceNoiseLevel>
<referenceNoiseLevelincidenceAngleCorrection="Sigma
Nought">
<pixelFirstNoiseValue>0</pixelFirstNoiseValue>
<stepSize>36</stepSize>

<numberOfNoiseLevelValues>97</numberOfNoiseLevelValues> …

APPENDIX E :Part of Product File of RS2_OK40034_PK385313_DK338798_ FQ19W_20120908_032638_HH_VV_HV_VH_SLC.

Part of product file of FQ19 is shown below, this file ix html format ,continue of file and other details are presented in CD


```
<?xmlversion="1.0"encoding="UTF-8"standalone="yes"?>
<productxmlns="http://www.rsi.ca/rs2/prod/xml/schemas"copyright="RADARSAT-
2 Data and Products (c) MacDonald, Dettwiler and Associates Ltd., 2012 -
All Rights Reserved."xmlns:xsi="http://www.w3.org/2001/XMLSchema-
instance"xsi:schemaLocation="http://www.rsi.ca/rs2/prod/xml/schemas
schemas/rs2prod_product.xsd">
	<productId>PDS_02926180</productId>
	<documentIdentifier>RN-RP-51-2713, Issue 1/11</documentIdentifier>
	<sourceAttributes>
		<satellite>RADARSAT-2</satellite>
		<sensor>SAR</sensor>
		<inputDatasetId>/Fred/RSAT-2/336116G</inputDatasetId>
		<imageId>217323</imageId>
		<inputDatasetFacilityId>Not
Specified</inputDatasetFacilityId>
		<beamModeId>8636</beamModeId>
		<beamModeMnemonic>FQ19W</beamModeMnemonic>
		<rawDataStartTime>2012-09-
08T03:26:38.416199Z</rawDataStartTime>
		<radarParameters>
			<acquisitionType>Fine Quad
Polarization</acquisitionType>
			<beams>Q19</beams>
			<polarizations>HH VV HV VH</polarizations>
			<pulses>30short</pulses>
			<rankbeam="Q19">18</rank>

	<settableGainbeam="Q19"pole="HH"wing="Combined"units="dB">-
9.000000145386835e+00</settableGain>

	<settableGainbeam="Q19"pole="HV"wing="Combined"units="dB">-
9.000000145386835e+00</settableGain>

	<settableGainbeam="Q19"pole="VH"wing="Combined"units="dB">-
9.000000145386835e+00</settableGain>

	<settableGainbeam="Q19"pole="VV"wing="Combined"units="dB">-
9.000000145386835e+00</settableGain>

	<radarCenterFrequencyunits="Hz">5.404999242769673e+09</radarCenterFr
equency>

	<pulseRepetitionFrequencybeam="Q19"units="Hz">2.800169921875000e+03<
/pulseRepetitionFrequency>

	<pulseLengthpulse="30short"units="s">2.080838775634766e-
05</pulseLength>

	<pulseBandwidthpulse="30short"units="Hz">3.002442203000000e+07</puls
eBandwidth>
			<antennaPointing>Right</antennaPointing>
```

```
<adcSamplingRatepulse="30short"units="Hz">3.166992187500000e+07</adc
SamplingRate>
<yawSteeringFlag>YawSteeringOn</yawSteeringFlag>
<geodeticFlag>Off-Geocentric</geodeticFlag>
<rawBitsPerSample>3</rawBitsPerSample>
<samplesPerEchoLinebeam="Q19">7320</samplesPerEchoLine>
<referenceNoiseLevelincidenceAngleCorrection="Beta
Nought">
<pixelFirstNoiseValue>47</pixelFirstNoiseValue>
<stepSize>68</stepSize>

<numberOfNoiseLevelValues>98</numberOfNoiseLevelValues>
<noiseLevelValuesunits="dB">-2.71197109e+01 -
2.73498993e+01 -2.75630703e+01 -2.77756805e+01 -2.79885597e+01 -
2.81874199e+01 -2.83834591e+01 -2.85797596e+01 -2.87645397e+01 -
2.89446297e+01 -2.91249504e+01 -2.92958603e+01 -2.94605198e+01 -
2.96253796e+01 -2.97825794e+01 -2.99322300e+01 -3.00820694e+01 -
3.02256908e+01 -3.03607006e+01 -3.04958801e+01 -3.06260204e+01 -
3.07466908e+01 -3.08675003e+01 -3.09842091e+01 -3.10907707e+01 -
3.11974602e+01 -3.13007908e+01 -3.13934307e+01 -3.14861908e+01 -
3.15760994e+01 -3.16549797e+01 -3.17339401e+01 -3.18104191e+01 -
3.18756104e+01 -3.19408894e+01 -3.20038414e+01 -3.20554199e+01 -
3.21070595e+01 -3.21563797e+01 -3.21943703e+01 -3.22323990e+01 -
3.22679291e+01 -3.22923012e+01 -3.23167000e+01 -3.23382683e+01 -
3.23489685e+01 -3.23596802e+01 -3.23670616e+01 -3.23639984e+01 -
3.23609200e+01 -3.23538513e+01 -3.23368912e+01 -3.23199005e+01 -
3.22980690e+01 -3.22670403e+01 -3.22359695e+01 -3.21990089e+01 -
3.21537018e+01 -3.21083412e+01 -3.20558395e+01 -3.19960098e+01 -
3.19360905e+01 -3.18675995e+01 -3.17929401e+01 -3.17181892e+01 -
3.16331406e+01 -3.15433197e+01 -3.14533691e+01 -3.13511696e+01 -
3.12457905e+01 -3.11402607e+01 -3.10202103e+01 -3.08987999e+01 -
3.07762909e+01 -3.06385403e+01 -3.05006008e+01 -3.03590698e+01 -
3.02042198e+01 -3.00491505e+01 -2.98876591e+01 -2.97150402e+01 -
2.95421696e+01 -2.93596191e+01 -2.91684494e+01 -2.89770107e+01 -
2.87721195e+01 -2.85615292e+01 -2.83506603e+01 -2.81219292e+01 -
2.78909397e+01 -2.76575603e+01 -2.74053402e+01 -2.71527691e+01 -
2.68930492e+01 -2.66179600e+01 -2.63424892e+01 -2.60542297e+01 -
2.57546997e+01</noiseLevelValues>
</referenceNoiseLevel>
<referenceNoiseLevelincidenceAngleCorrection="Sigma
Nought">
<pixelFirstNoiseValue>47</pixelFirstNoiseValue>
<stepSize>68</stepSize>
```

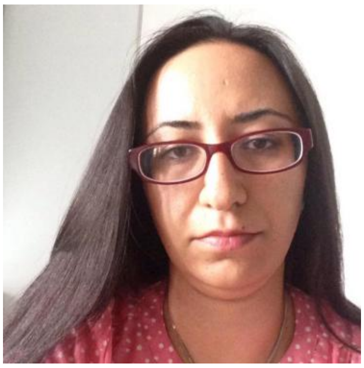

CURRICULUM ITAE

Name Surname: Elnaz BEHNAM MAKOEI

Place and Date of Birth: South Azerbayjan, Orumieh, 1980

E-Mail: Elena.behnam@gmail.com

B.Sc.:Telecommunication Engineering, Orumieh university, 2000.

Professional Experience and Rewards:

……

List of Publications and Patents:

……